CANADIAN THESES

THÈSES CANADIENNES

NOTICE

The quality of this microfiche is heavily dependent upon the quality of the original thesis submitted for microfilming. Every effort has been made to ensure the highest quality of reproduction possible.

If pages are missing, contact the university which granted the degree.

Some pages may have indistinct print especially if the original pages were typed with a poor typewriter ribbon or if the university sent us an inferior photocopy.

Previously copyrighted materials (journal articles, published tests, etc.) are not filmed.

Reproduction in full or in part of this film is governed by the Canadian Copyright Act, R.S.C. 1970, c. C-30.

AVIS

La qualité de cette microfiche dépend grandement de la qualité de la thèse soumise au microfilmage. Nous avons tout fait pour assurer une qualité supérieure de reproduction.

S'il manque des pages, veuillez communiquer avec l'université qui a conféré le grade.

La qualité d'impression de certaines pages peut laisser à désirer, surtout si les pages originales ont été dactylographiées à l'aide d'un ruban usé ou si l'université nous a fait parvenir une photocopie de qualité inférieure.

Les documents qui font déjà l'objet d'un droit d'auteur (articles de revue, examens publiés, etc.) ne sont pas microfilmés.

La reproduction, même partielle, de ce microfilm est soumise à la Loi canadienne sur le droit d'auteur, SRC 1970, c. C-30.

THIS DISSERTATION HAS BEEN MICROFILMED EXACTLY AS RECEIVED

LA THÈSE A ÉTÉ MICROFILMÉE TELLE QUE NOUS L'AVONS REÇUE

A Computer-aided Methodology for the Calibration of Industrial Robots Employing Optical Metrology

Ramesh Rajagopalan

A Thesis

in

The Department

of

Mechanical Engineering

Presented in Partial Fulfillment of the Requirements
for the Degree of Master of Engineering at
Concordia University
Montréal, Quebéc, Canada

December 1986

ISBN 0-315-35526-3

ABSTRACT

A Computer-aided Methodology for the Calibration of Industrial Robots Employing Optical Metrology

Ramesh Rajagopalan

Repeatability and accuracy of robots are two important factors when the robots are considered for a specific application. Robots can be controlled using on-line and off-line programming techniques. For off-line applications, accuracy is more important than repeatability. Hence, a calibration technique is essential to improve the accuracy of robots. However in the case of on-line applications using teach mode programming, repeatability is more important than accuracy and hence calibration is not mandatory.

The errors in robots are attributed to errors resulting from manufacturing, assembling, servo-positioning, and designing errors. The effect of some of these errors mostly appear at the joint end instead of at the actuator end. Hence it is necessary to measure these errors and provide compensation to improve accuracy.

It has been emphasized in this thesis that the experimental technique itself introduce additional errors referred to as the estimation errors in this thesis onto the computed robot errors. Error analysis is included to evaluate these errors. This analysis indicates the confidence

level that can be placed on the evaluated robot errors. The resulting tool location errors should be within the repeatability of the robot itself. Hence it is imperative to minimize the estimation errors.

It has been observed here that by changing the geometrical parameters of the experimental setup, the estimation error can be controlled. A mathematical search technique is used to establish an appropriate experimental setup consisting of the robot, calibration instruments, and a reference tool that will result in minimum estimation errors. Experiments are performed using the Puma 560 robot to test the suitability of the methodology for industrial robots.

ACKNOWLEDGEMENT

The author wish to express his sincere gratitude to the thesis supervisors Prof. R.M.H. Cheng and Prof. Y. Stepanenko for their constant guidance, invaluable criticism and financial support during the course of this work. The author also acknowledges the financial support from numerous sources, especially the Concordia University Graduate Fellowship, 1985 - 86.

Special thanks to Professors. M. Douglass and A. Hanna of the Civil Engineering Department for the extended loan of 2 theodolites. This research project is financed by the Natural Sciences and Engineering Research Council of Canada and FCAR of the Ministry of Education of the Province of Quebéc, Canada in the form of Personal Operating Grants awarded to Prof. R.M.H. Cheng.

The author wish to acknowledge the provision of assistance of the staff at Mechanical Engineering Department. The author thank the Computer center staff at the Computer Research and Interactive Graphics Laboratory(CRIGL) for their assistance.

TABLE OF CONTENTS

TABLE OF FIGURES

TABLE OF NOTATIONS

A	Theodolite 1 Center
B	Theodolite 2 Center
C;D,E	Reference points on the reference ruler
R_f	Reference Coordinate frame with the origin at A
t_{fj}	Coordinate frame centered at A and parallel to the Coordinate frame of the joint j for the TE analysis
S_{fj}	Coordinate frame centered at A and parallel to the Coordinate frame of the joint j
C_{fj}	Coordinate frame of the joint j
L	Center distance between A & B measured along X_{R_f}
a_j, d_j	Link parameters : lengths and offset distances.
N	Number of degrees of freedom.
P	Translation joint.
j	Joint under consideration.
R	Reference distance between C & E for pre-calibration
X_1	Distance between A & C
r_1	Distance between C & D
r_2	Distance between D & E.
Y_1	Distance between A & C.

Y_2	Distance between B & E.
α_i	Theodolite A Azimuth angle.
β_i	Theodolite B Azimuth angle.
ϕ_i	Theodolite A elevation angle.
γ_1	Offset angle for the theodolite A with respect to X_{R_f}.
γ_2	Offset angle for the theodolite B with respect to X_{R_f}.
α_i	$\alpha_i - \gamma_1$.
β_i	$\beta_i - \gamma_2$.
M_j	Bending moment for the link j.
E_j	Modulus of Elasticity of the link j material.
I_j	Moment of inertia of the link j.
$\frac{d^2Y_j}{dX_j^2}$	Curvature of the beam for the link j.
L_j	Location of the load from the j^{th} joint center.
R_x, R_y, R_z	Position vector of the tool with respect to the world frame.
R_ϕ, R_θ, R_ψ	Roll, pitch, and yaw - rotations of the tool with respect to the world frame.
θ_j	Joint angle of the j^{th} joint.
α_j	The twist of the link.
d_j	The distance of the link.

a_j	The length of the link.
θ_j, α_j, d_j, a_j	Link parameters of the j^{th} link.
C_{θ_j}, S_{θ_j}, S_{α_j}, C_{α_j}	$Cos\theta_j$, $Sin\theta_j$, $Sin\alpha_j$, $Cos\alpha_j$.
θ_1 to θ_6	Joints 1 to 6 angles.
A_j	The A - matrix for the j^{th} link.
${}^{w}T_6$	The transformation relating the 6^{th} link and the world coordinate frame.
${}^{6}E$	The transformation relating the 6^{th} link and the end effector.
P_j	Reference point for the Denawit-Hartenberg parameters.
R_{pj}	Distance between P_j and the joint center of the j^{th} joint.
X_{cj}, Y_{cj}, Z_{cj}	Joint j center coordinates with respect to the reference frame R_f.
Q_j, S_j, T_j, V_j	The locations of the reference point P_j for joint j.
$R_{f_{\delta_z}}$	Orientation of the world frame with respect to R_f in the XY-plane.
θ_{xj}, θ_{yj}, θ_{zj}	Orientations of the j^{th} joint coordinate frame with respect to R_f.
$\Delta\theta_{xj}$, $\Delta\theta_{yj}$, $\Delta\theta_{zj}$	Joint misalignments between joints j and (j-1) with respect to C_{fj}.
$\Lambda\theta_{xj}$, $\Lambda\theta_{yj}$, $\Lambda\theta_{zj}$	Joint orientations between joints j and (j-1)

	with respect to C_{fj}.
$\delta\theta_{xj}$, $\delta\theta_{yj}$, $\delta\theta_{zj}$	Differential rotations about the three principle axes.
X_{pj}, Y_{pj}, Z_{pj}	Coordinates of the point P_j with respect to R_f.
${}^{S_{fj}}(X_{pj}, Y_{pj}, Z_{pj})$	Coordinates of the point P_j with respect to S_{fj}.
${}^{C_{fj}}(X_{pj}, Y_{pj}, Z_{pj})$	Coordinates of the point P_j with respect to C_{fj}.
X_{dj}, Y_{dj}, Z_{dj}	Joint j center coordinates with respect to R_f for the TE analysis.
A_{1j}, A_{2j}	Reference points for the TE analysis for the joint j.
R_{dj}	Distance between A_{1j} and A_{2j}.
X_{a1}, Y_{a1}, Z_{a1}	Coordinates of A_{1j} with respect to R_f.
X_{a2}, Y_{a2}, Z_{a2}	Coordinates of A_{2j} with respect to R_f.
${}^{t_{fj}}(X_{a1}, Y_{a1}, Z_{a1})$	Coordinates of A_{1j} with respect to t_{fj}.
${}^{t_{fj}}(X_{a2}, Y_{a2}, Z_{a2})$	Coordinates of A_{2j} with respect to t_{fj}.
${}^{t_{fj}}\theta_{mj}$	Measured instantaneous joint angle for TE analysis for joint j.
${}^{t_{fj}}\theta_{ij}$	Measured initial joint angle for TE analysis for joint j.
${}^{t_{fj}}\theta_{rj}$	Measured resultant joint angle for TE

	analysis for joint j.
θ_{cj}	Controller reading for TE analysis for joint j.
${}^{t_{fj}}\theta_{dj}$	Desired joint angle for TE analysis for joint j.
T_j	Twisting moment for the joint j due to a load N_j.
K_j	Joint stiffness of the joint j.
N_j	External load for the j^{th} joint.
$\frac{1}{K_j}$	Angular deflection/unit torque.
σ_{jk}	Cross coupling factor between joints j and k.
S_k	Resolution of the joint k encoder(deg/per count).
θ_k	Joint angle of the joint k.
ξ_k	Encoder counts for the joint k.
θ'_k	Actual joint angle of the joint k including cross coupling effects between joints j and k.
X_{c1}, Y_{c1}, Z_{c1}	Location of the world coordinate frame with respect to R_f.
X_t, Y_t, Z_t	Tool dimensions.
(X_e, Y_e, Z_e)	Location of the tool with respect to R_f.
dA_j	The differential value of the A_j matrix.
δA_j	The differential transformation for A_j.

${}^{w}T_{E}$	The transformation relating the end effector and the world coordinate frame.
${}^{R_f}T_{e}$	The transformation relating the end effector and the reference coordinate frame.
K_{θ_j}	Correction factor for the TE in joint j.
K_{jc_j}	Correction factor for the joint compliance in joint j.
K_{lc_j}	Correction factor for the link compliance in joint j.
K_{b_j}	Correction factor for the backlash in joint j.
ΔR	Measurement accuracy of R.
Δr_1	Measurement accuracy of r_1.
Δr_2	Measurement accuracy of r_2.
$\Delta\alpha_i$	Azimuth angle resolution of the theodolite-A.
$\Delta\beta_i$	Azimuth angle resolution of the theodolite-B.
$\Delta\phi_i$	Elevation angle resolution of the theodolite-A.
α_{ij}	Azimuth angle for the theodolite A for the i^{th} location for the j^{th} joint.
β_{ij}	Azimuth angle for the theodolite B for the i^{th} location for the j^{th} joint.
ϕ_{ij}	Elevation angle for the theodolite A for the i^{th} location for the j^{th} joint.
ΔL	Estimation error for L.

$\Delta\gamma_1$	Estimation error for γ_1.
$\Delta\gamma_2$	Estimation error for γ_2.
Y_{opt}	Minimum optical focal distance for the theodolites.
ΔX_i, ΔY_i, ΔZ_i	Estimation error associated with the evaluated distances X_i, Y_i, and Z_i.
R_1 to R_6	Joints 1 to 6 radii of rotations of the reference point P_j.
$d\Delta\theta_{xj}$, $d\Delta\theta_{yj}$, $d\Delta\theta_{zj}$	Estimation error associated with the evaluated joint misalignments $\Delta\theta_{xj}$, $\Delta\theta_{yj}$, and $\Delta\theta_{zj}$.
Δa_j, Δd_j	Estimation errors for a_j and d_j.
ΔX_e, ΔY_e, ΔZ_e	Estimation errors for the parameters X_e, Y_e, Z_e.
${}^{t}{}_{fj}\theta_{mj}$	Estimation errors for the joint angles measured.
$K_{\theta 4}$	Correction factor for the transmission error for the joint 4.
$K_{\theta 6}$	Correction factor for the transmission error for the joint 6.
P_{61}, P_{62}	Pinion gears of the drive unit for the joint 6.
G_{61}, G_{62}	Mating gears.
σ_{56}	Cross coupling factor between joints 5 & 6.
σ_{46}	Cross coupling factor between joints 4 & 6.
σ_{45}	Cross coupling factor between joints 4 & 5.

CHAPTER 1

INTRODUCTION

1.1 Introduction

The performance specifications of robots, particularly repeatability and accuracy are important factors while considering robots for a specific application. An example for the effect of errors on accuracy for the Puma 600 robot presented by Mooring [13] shows that a joint misalignment of 1 deg in the XY plane of joint 2 produces a maximum tool position error of 1.28 inches. For applications using off-line programming, this amount of error in the tool position is unacceptable and therefore, accuracy is important in these cases in addition to repeatability. On the otherhand, if the robots are programmed on-line using the teach mode, repeatability may be more important than accuracy. This is because, the ability of the robot to reach the destination is independent of the errors in the robot.

1.2 Problem Definition

Since the joint encoders are normally mounted at the actuators end instead of at the joint end, the effect of transmission errors (gear transmission errors and cross coupling effects) will not be sensed by the controller. Hence any error in the transmission will show up as a location* error at the tool tip. The mathematical models used by some

*Position and Orientation

controllers assumes that there are no errors in the robot elements. Moreover, the mechanical elements of all robots undergo wear and tear as time goes on, and thus leading to changes in accuracy and repeatability. Manufacture of robots with mechanical elements that are wear resistant and precision machined to achieve higher accuracy in tool location increases the cost of robots and hence limits their use in industrial applications.

Considering all these factors, it is imperative to design a calibration technique that can measure the magnitude of all the errors and provide a compensation strategy to precisely position and orient the tool at the desired location at all times. Such techniques should be easy to use and the operating cost should be lower than the cost of high precision robots. In addition to these factors, it has been observed that important consideration has to be placed on the experimental technique itself. It has been observed that the geometrical factors of the experimental technique plays important role while considering a technique for implementation. These factors introduce additional error onto the measured robot errors. A calibration technique, should therefore include an analysis to estimate this error. A strategy should be included to minimize this error. This is the main contribution made by this thesis. The author has strong belief that most of the research work proposed by others have ignored this fact.

1.3 Classification of Robot Configurations

Some of the factors used to classify the robots are : the number of degrees of freedom, the type of joint configuration i.e., spherical,

revolute, prismatic, and the type of function it performs. For calibration, the first two factors are of utmost importance as the experimental setup needs modification depending upon the joint configuration and the number of link parameters to be estimated varies with the degrees of freedom the robot has. Robots in general have two major components namely, the arm and the wrist. The arm is normally provided with three degrees of freedom and the wrist is provided with anywhere from 1 to 3 degrees of freedom. The degrees of freedom of the arm is used to position the tool and that of the wrist is to orient the tool at the desired location. In the following discussions the various arm and wrist structures in use are presented :

Arm Structures

As mentioned above the joint configuration of the arm may be revolute, or prismatic, and or combinations of these. Spherical joints are not commonly used, exception being the Unimate 2000 robot. Since there are three joints, and two types of commonly used joint configurations, there can be 2^3 i.e., 8 combinations are possible with revolute or prismatic joints. Here the notation R refers to the Revolute joint whereas P refers to the Prismatic joint. The 8 possible arm structures are RRR or R^3, PRR or PR^2, RRP or R^2P, PRP, RPP or RP^2, PPP or P^3, RPR, PPR or P^2R. The various arm structures are shown in fig.1.1.

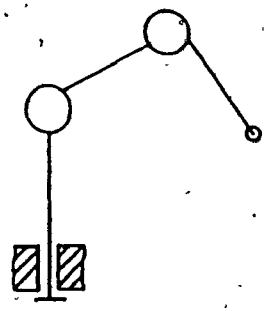

RRR or 3R – Class 1

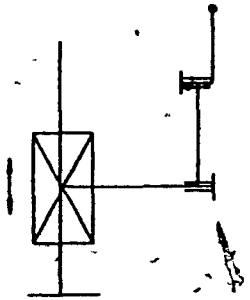

PRR or P2R – Class 2

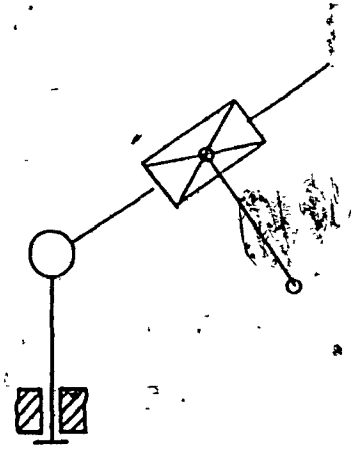

RRP or 2RP – Class 3

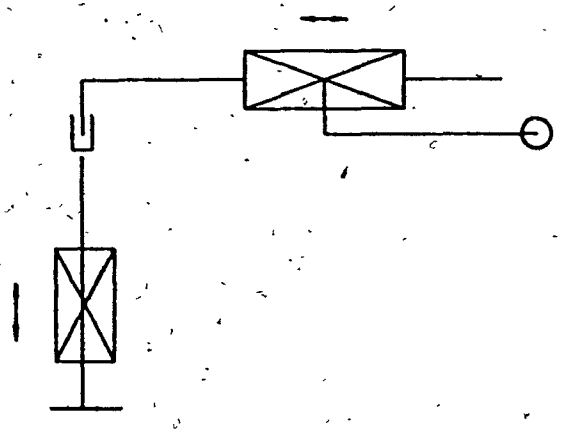

PRP or RPP or R2P – Class 4

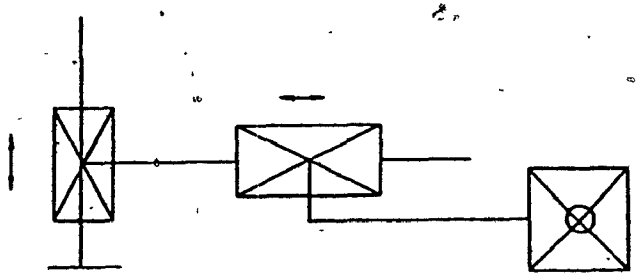

PPP or 3P – Class 5

Fig.1.1 Arm Structures

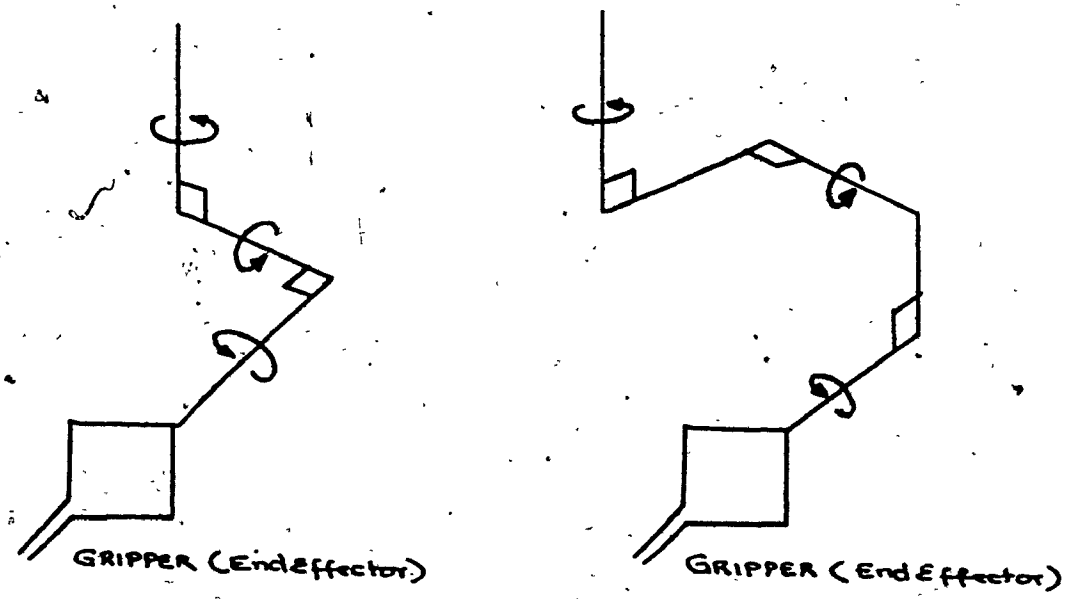

Fig.1.2 Wrist Structures

Wrist Structures

Mostly the wrist joints are rotary in nature. There are three possible rotations of the wrist about the three mutually perpendicular axes. In the case of Spherical Wrist, the three axes intersect at one point referred as the Wrist point. This wrist structure is preferable for the following reasons:

- it allows the tool to be oriented without any need for furthur translation.
- the robot becomes easily resolvable compared to other wrist structures.

In some designs of the wrist, the three axes of rotations are normal and intersect two by two and the three axes of rotations are normal and do not intersect at all as in fig.1.2.

1.4 Sources of Errors

The errors in tool position and orientation are due to manufacturing errors, assembling errors, servo positioning errors, and design errors. The overall tool position and orientation error is the machine error. Some of the sources of manufacturing and assembling errors are :

1. Deviations in the Denawit-Hartenberg parameters of the links from their design values.
2. Type of transmission system used.
3. Backlash due to gears.

4. Bearing Wobble.

the sources of design errors are :

1. Joint Compliance.
2. Link Compliance.
3. Cross coupling effects.
4. Thermal effects.
5. Controller design.
6. Resolution of the joint encoders.

the following discussions presents a brief description of these errors.

Denawit-Hartenberg Parameters

The Denawit-Hartenberg parameters of the robots are, joint j orientation with respect to joint (j-1) and link lengths and offset distances, where j =1,...N, and N be the number of degrees of freedom associated with the robot under consideration.

Joint Orientation and Misalignments

Joint orientation is defined as the orientation of the joint axis with respect to a reference coordinate frame. The reference coordinate frame may be the world coordinate frame of the robot, or the coordinate frame of the previous link or an external coordinate frame defined by the user. In this thesis, it refers to an external reference frame R_r. Joint misalignment is defined as the deviation of the actual joint orientation from the designed value. The conventional kinematic analysis of robots assumes that the axis of rotation of the joints or links to be either parallel or perpendicular to each other. The

kinematic analysis based on such assumptions will give erroneous results if there are misalignments in the joints.

Link Lengths and offset distances

The length a_j for the j^{th} joint is defined as the common normal distance between the axes of rotation of the j^{th} and the $(j+1)^{th}$ joints. The distance d_j for the j^{th} joint is defined as the distance between the common normals of the $(j-1)^{th}$ and the j^{th} joints. These relationships can be seen in fig.3.3. These lengths and the distances form a basis to establish a relationship between the location of an object in the world coordinate frame of the robot with respect to the tool coordinate frame. Due to manufacturing and assembling difficulties the actual magnitudes of a_j and d_j may deviate slightly from the design values.

Transmission Errors

Transmission error (TE) is an extension of position error in gears which is defined as the deviation of any portion of the gear's tooth profile from the true position it should have. The TE is the total error of meshed gears and the error resulting from the installations. The transmission error may be due to some or all of the following manufacturing and assembling difficulties: eccentricity (pitch line runout), side wobble (lateral runout), profile error, profile-spacing error, tooth thickness error, of some or all of the gears involved in the drive unit, installation errors attributed to compliance of the drive shaft coupling and so on.

Joint Compliance

Joint compliance is associated with the stiffness of the joint. The joint stiffness in turn is dictated by the stiffness of the components of the joint. A joint may consists of some or all of the following components : actuators, gears, transmission shafts, and couplings. Due to the self weight of the links themselves and external loads, the joint may rotate from its current position. This is due to a number of causes, some of which are listed below :

- Due to clearance between gear tooth in mesh.
- Play in the couplings.
- Holding torque of the actuator is less than the twisting moment due to gravity loading.

Link Compliance

Link compliance is attributed to stiffness of links. A link under an external load behaves like a cantilever beam. Hence the mathematical models to evaluate the link stiffness can be derived directly using the moment equation $E_j I_j \frac{d^2 Y_j}{dX_j^2} = M_j$, where E_j - modulus of elasticity of the link material, I_j - the link inertia, M_j is the twisting moment due to a load of F applied at a distance L_j from the joint center and $\frac{d^2 Y_j}{dX_j^2}$ is a measure of the curvature of the beam.

Cross Coupling Effects

The wrist joints of some of the manipulators with no direct drive systems are mechanically coupled and hence cross coupling effects are present in them. Due to this, when one of them moves, either the following joints or the actuators of those joints also moves. If the torque required to rotate the joint is greater than that for the actuator, the actuator moves; otherwise the joint moves. At higher joint speeds it is difficult to predict whether the joint or the actuator or both rotates. The joint actuators of these joints are not provided with locks to hold the joint in position. This is to avoid the coupling effect getting transferred to the joint instead of to the actuator. In the case of robots where the joint encoders are mounted at the actuator end, since the encoders rotates with the actuator the correction can be implemented in the software for the control loop of that joint directly. Hence it is necessary to determine the correction factor σ_{jk} for the k^{th} joint due to j^{th} joint and the correction to be added to the joint encoder reading of that joint is given by $\theta_j \sigma_{jk}$.

Backlash

Backlash can be observed in robots using geared drives. Backlash is the total lost motion for a geared pair or train caused by all contributions, such as thinned teeth, enlarged center distance, runouts of rotating parts, etc. Hence backlash can be defined as the amount by which tooth space exceeds the thickness of the engaging tooth, or for a gear train, the amount of motion a meshed gear has when its mate is held fixed. Lost motion includes deflection, bearing looseness, etc.

Manufacturing tolerances on gear dimensions, shaft center location, bearing dimensions etc., results in unavoidable backlash. The sources of backlash can be grouped under two main classes namely, the constant backlash sources and the variable backlash sources.

1.5 Layout of the Thesis

The method described in this thesis was developed at the Center for Industrial Control (CIC) of the Concordia University. This method can be used to calibrate robots of any type of joint configuration. The author has limited to identifying the Denavit-Hartenberg kinematic parameters and some of the five major sources of errors: transmission errors, joint compliance, link compliance, and cross coupling effects.

The method described here is similar to those described in references 11, 17, 18, and 19. In brief, the setup is as shown in fig.1.5. Figure 1.4 presents an outline of the methodology. Two theodolites are positioned at appropriate distance from the robot and between themselves. The robot carries a tool with target points for the optical measurements. Depending on the type of error that is being investigated, one need to use one or more targets points. Having realised the need to develop a calibration method that includes the above mentioned analysis, the author has proposed a calibration technique that adds new dimension to industrial robot calibration problem. This technique is at variance from the others in two aspects: there are two analysis called error analysis, and the computer runs for design of experiments are included here. The former estimates the confidence level whereas the latter is to identify the geometrical factors

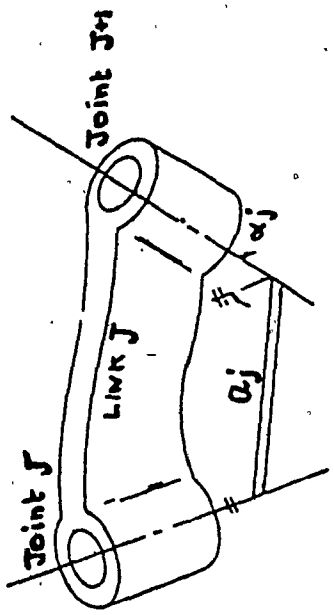

Fig.1.3. Link Parameters a_j and α_j definitions

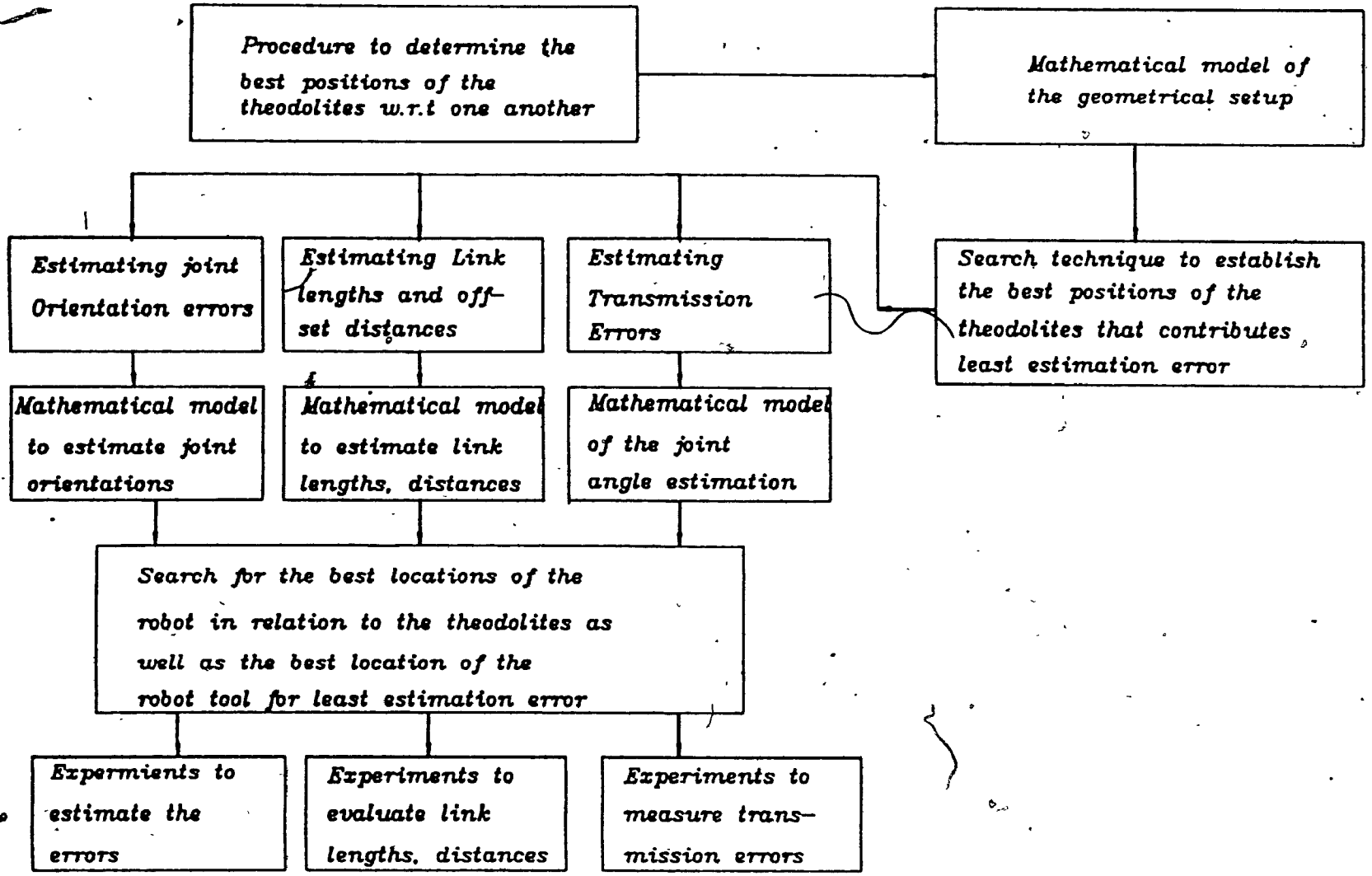

Fig.1.4 Layout of the Methodology

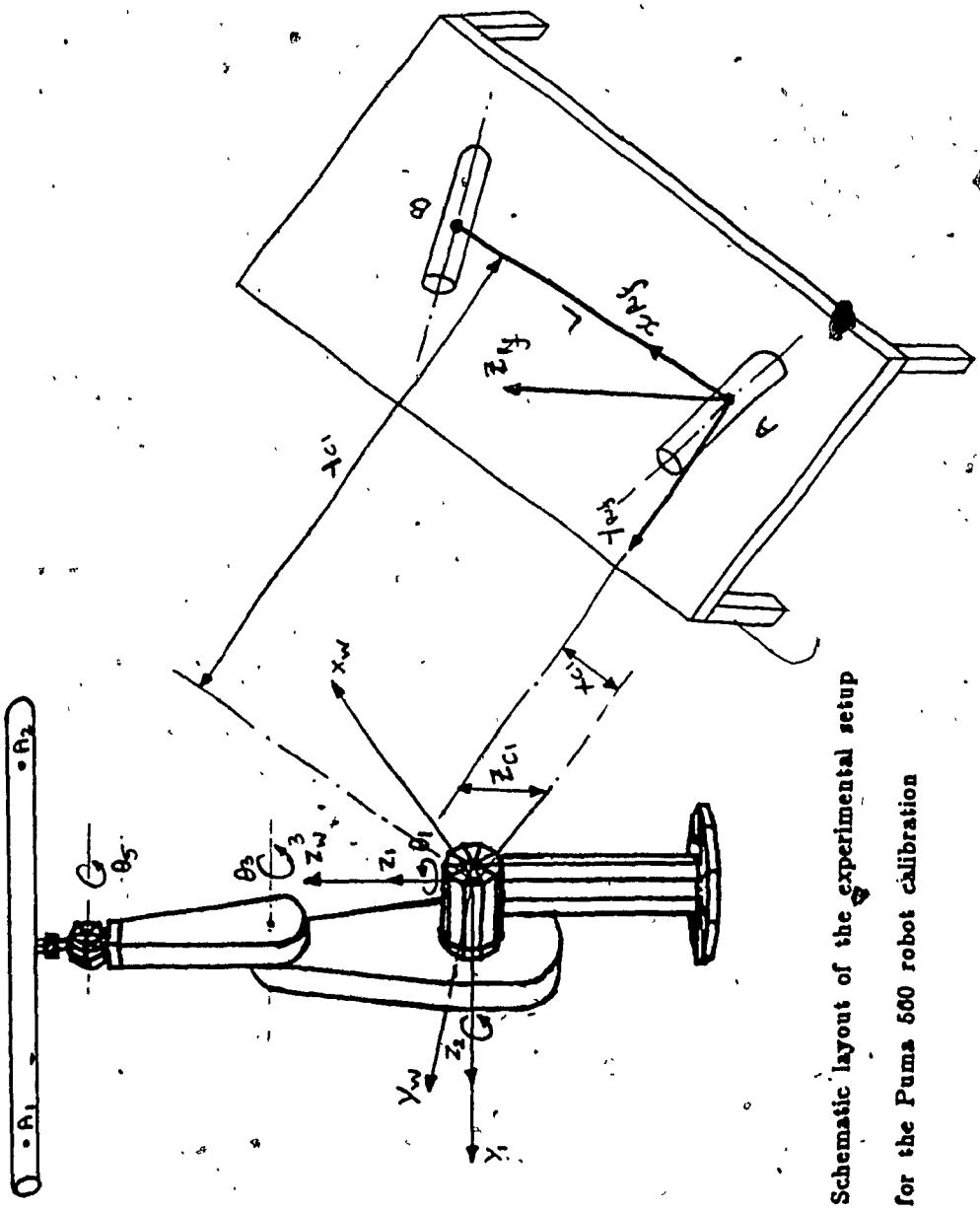

Fig.1.5. Schematic layout of the experimental setup for the Puma 560 robot calibration

that results in minimum error on the measured robot errors.

The mathematical models of the experimental setup required to evaluate the above mentioned errors and parameters are presented here. This calibration methodology measures the errors associated with the tool orienting axes in addition to those from the tool positioning axes. Two theodolites are used as the measuring instruments. Figure 1.5 shows the experimental setup consisting of the theodolites, the reference tool and the Puma 560 robot. The research presented here consists of the following analysis:

- The various possible sources of errors are identified.
- Mathematical model of the experimental setups required to evaluate some of these errors are developed.
- Error analysis is performed for the mathematical models to estimate the effect of additional errors introduced by the geometrical factors of the experimental setup on the measured value of the errors of the robot itself.
- By appropriately selecting the geometrical factors, it is possible to reduce the estimation errors introduced by them. Computer simulations are performed using the mathematical models and the error analysis to identify those factors.
- Experiments are conducted using the Puma 560 robot to test the suitability of this technique for industrial robots.

1.6 Summary

It can be realised from the discussions, that repeatability and accuracy are important factors, when the robots are considered for a specific application. For off-line programming applications, the calibration of robots is essential to improve accuracy of robots in positioning and orienting the tool at the desired location. On the other hand, for on-line programming applications, since repeatability is more important than accuracy, calibration plays little or no role at all. A calibration procedure is essential not only to improve the accuracy of less accurate robot but also to estimate and compensate for the loss of accuracy due to wear and tear of the mechanical components of the robot with time.

The errors in positioning the tool at the desired location are attributed to errors resulting from manufacturing, assembling, servo positioning, and designing errors. Some of the error sources common to most of the robots are; deviations in the link parameters from their design values, transmission errors, joint compliance, link compliance, gear backlash, and cross coupling effects. In the case of robots with non-direct drive systems, since the joint encoders are normally mounted at the actuator end rather than at the joint end, the joint errors will not be sensed by the robot controller. Due to this effect, there will be difference between the actual and the desired tool location.

A calibration technique should be reliable, easy to use and cheaper to operate. Hence, the selection of appropriate instruments and the procedure is very important. Also, the calibration experiments are

subjected to experimental errors. This is contributed by repeatability and the resolution of the instrument used, and human errors. Hence, an error analysis is necessary to evaluate these errors. This analysis gives us the confidence level that can be placed on the estimated robot errors. This experimental error results in another error referred to as estimation error in this thesis. It should be noted here that the resulting tool location error due to this error should be less than the repeatability of the robot itself. This error can be reduced in two ways. One is to select instruments with better resolution and/or repeatability, this leads to expensive experimental setup. Alternatively one can mathematically search for an appropriate set of experimental parameters that will result in minimum estimation error. This process is referred to as the design of experiments in this thesis. Some of the experimental parameters are ; the coordinates of the reference point on the tool with respect to a reference frame, the distance between the instruments which is used as the reference distance, and the location of the world coordinate frame of the robot. The author has strong belief that it is possible to reduce the estimation error by the appropriate choice of the experimental parameters. This is demonstrated in the following chapters.

CHAPTER 2

SURVEY AND SCOPE OF THE THESIS

2.1 Introduction

On-line and off-line calibration techniques can be used to calibrate robots. In an on-line technique, the tool location is measured in real time and the deviations in tool location from the desired value is calculated. Some of the equipment used in the off-line calibration techniques are: surveying instruments[8,19,20,23], laser equipment and camera vision equipment. Using laser equipment, very high measurement accuracy of the order of few fractions of a μm can be achieved. Automated calibration can be effected using laser and camera equipment. Surveying instrument theodolites are easy to use, can give measurement accuracy of 0.1mm over a distance of 3m depending upon the micrometer resolution, uses man power for focussing and reading the micrometer vernier and are relatively inexpensive too. In the case of on-line calibration systems, the real time computation of errors increases the controller computation time and the instrument themselves need frequent calibration to maintain accuracy, and are expensive too.

2.2 Present State of the Art

Anderson[7] presents on-line calibration technique which employs laser interferometry achieving a measurement accuracy of 0.03μm (RMS) over a distance of 10m. Scheffer[8] discusses the calibration problem from a philosophical point of view and does not provide a mathematical

model of the experimental technique for calibration. Fohanno[10] describes an experimental technique to assess the performance of industrial robots. A reference cube and six sensors are used to determine the position and orientation of the tool. Accuracy of this method largely relies on the sensor sensitivity. The geometrical factors of the experimental setup; size of the reference cube, and the robot arm configurations affect the validity of the results obtained by this method. The author did not include an analysis to estimate the error introduced by these factors on the measured tool location.

The parameter estimation algorithm presented by Mooring[13,21], evaluates the relative position and orientation of the axis of rotation of each joint with respect to a reference surface machined on the robot base. The measured positions of three non-collinear points marked on the tool are used for this purpose. This algorithm assumes the availability of an instrumented work space that can measure accurately the position of the points on the tool. The geometrical factors of the experimental setup: the relative location of the three points chosen on the tool, instrument accuracy and the choice of robot tool location with respect to the reference surface and the measuring instrument have an effect on the measured quantities. Mooring included neither a discussion nor analysis for the same.

Furuya and Makino[16] developed two techniques (three and four point) to determine the dimensions of two linked Scara type robots. Accuracy of the estimated link lengths depends on the resolution of the digitizer used and is within ± 0.1 mm. This is close to the repeatability of some of the robots available today. The above authors have

determined the effect of geometrical factors of the experimental setup on the measured link lengths from their experimental results. This could have been estimated off-line, using the mathematical model of the experimental setup, error analysis and computer simulations, without performing the experiments.

Lozinski[19] and Whitney et al.[20], described an optical calibration technique to estimate the link lengths, offset distances and to develop the error model for the tool positioning axes. They identified the various possible errors and proposed a methodology to measure some of them. Since this method uses a point tool, it can not be used to calibrate the tool orientation. Tool orientation is important for applications employing extended tools. As mentioned before, in this case also the geometrical factors of the experimental setup influences the validity of the results obtained from experiments. The error analysis provided by the authors is valid only for simple trigonometric relationship between the position of a point in space and the theodolite angles and does not take into account the contributions made by other geometrical factors.

Langmoen et al.[22] proposed a statistical method to determine tool position errors and repeatability of manipulators. The analysis are useful to design precise robots as it relates the joint error with the tool location error. The method described by the authors to estimate the tool orientation is exactly similar to the one described by Fohanno[10] and hence has the same limitations. Lau and Hocken[23] provided categorized information concerning the type of errors in robots and the various techniques used to measure them. This is basically a literature

survey to establish standards for robot metrology. Wu and Lee[26] described a modified kinematic model that accounts for errors in the kinematic parameters of robots, errors in the actual link lengths and offset distances and joint misalignments. A statistical approach is used to estimate the robot accuracy. A newly marketed robot check system consisting of LEDs, two TV cameras, a central processing unit and advanced software has been reported by Stauffer[27]. According to this report, this system can be used to measure repeatability, accuracy and trajectory under dynamic conditions.

Kirchner et al.[28] uses a perturbation approach. The position of a point on the tool at four different locations in space is used to estimate the link lengths, offset distances and the joint misalignments. The four locations of the calibration point will have an effect on the measured quantities. Although the authors were aware of it, they did not include an analysis to evaluate them. Benhabib et al.[30] proposes a methodology to relate the allowable joint errors to the given amount of errors in the tool location. This method will be useful to manufacture accurate robots. Dagalakis and Myers[31] describes a technique for gear adjustment using the joint velocity and position information to reduce transmission errors; gear backlash, binding in gears etc. This technique is simple to use and yields better results compared to conventional manual gear adjustment procedures, but does not provide any information on the sensitivity of backlash present with loose gear adjustment.

It can be realised from the literature survey that the various approaches for calibration recommended by the researchers can be

classified under 3 major groups :

1. Use of an instrumented work space consisting of high precision machined fixtures, tools, etc. This approach is recommended by Mooring[13,21], Lau. and Hocken[23], Warnecke and Schraft[11], and Grossman and Taylor[14]. These researchers discussed only the possibility of using this approach but did not include any experimental results. This method requires expensive high precision fixtures. This approach is slow, and expensive.

2. Use of a simple work space consisting of optical instruments such as the theodolites and target points. In this approach, the joints are calibrated individually and the joint errors such as the transmission errors, joint compliance, link compliance, backlash, and the cross coupling effects are evaluated. This approach is recommended by Lozinski[19] and Whitney et al.[20], Furuya and Makino[16], and Stauffer[27]. Using this approach, Lozinski[19] and Whitney et al.[20] evaluated some of the errors associated with the Puma 560 robot and Furuya and Makino[16] estimated link lengths of the two linked Scara robot. Stauffer[27] has reported the use of theodolites as the instrument for calibration at the National Bureau of Standards, U.S.A. Though this method is laborious and requires extensive man power, it is easy to operate, and less expensive.

3. The third approach also uses optical instruments. However instead of calibrating the joints individually it uses a mathematical search technique to evaluate the joint errors, and the link parameters from the measured tool positions. This approach is recommended by Wu and Lee[26], Kirchner et al.[28], Hsu and Everett[29], Chao and Yang[32]. This method involves a process of evaluating as many as 45 parameters using iterative techniques. The system of equation is non-linear and more than one solution is possible. This approach seems to be the simplest of all the approaches discussed above.

2.3 Scope of the Thesis

From the literature survey, it is clear that most of the researchers have neither discussed nor analysed the effect of geometrical factors of the experimental setup on the measured errors and parameters. They did not considered the importance of designing the experiments to justify the selection of various geometrical factors of the experimental setups. Since calibration experiments are subjected to instrumentation errors, it is imperative to include an analysis to estimate the confidence level that can be placed on the measured errors and parameters. This is the main objective of this thesis.

It should be noted that the following geometric dimensions contribute more or less to estimation errors ; namely, the distances L, X, Y, and Z and the offset angles γ_1 and γ_2. Hence the importance of determining the optimal set of values for these parameters before

proceding with experimentation. Furthurmore, it is proposed in this method to analytically evaluate the dimensions X, Y and Z from a predetermined values of L, γ_1 and γ_2. Consequently, it is necessary to have a pre-calibration setup (fig.4.1.a.) to accurately evaluate L, γ_1 and γ_2 by means of reference lengths R and r_1, which alone need to be accurately measured.

2.4 Summary

Robots can be calibrated using on-line and off-line calibration techniques. An on-line calibration technique normally uses laser equipment, and computer vision equipment as the instruments for calibration. An on-line technique is mostly automated and requires less manpower. The equipment used for calibration needs frequent calibration to maintain the level of accuracy that can be achieved. The calibration process is expensive and the time taken by the robot controller for on-line computations is increased due to on-line calculation of errors. On the other hand, the off-line technique is less expensive since the errors are computed off-line using a calibration station at the sight of robot manufacturing. It also does not affect the time taken by the controller for real time computations.

In this thesis, two major sections are included, namely: the error analysis, and the design of experiments to minimize the estimation errors. This thesis recommends that it is necessary to perform the error analysis and the design of experiments before the experiments are conducted. The search technique to evaluate the link parameters uses the joint errors evaluated individually. This removes non-linearity and

presence of singular solutions associated with the third approach, and the laborious nature of the second approach.

CHAPTER 3

KINEMATIC ANALYSIS FOR A ROBOT WITH REVOLUTE JOINT CONFIGURATION

3.1 Introduction

Kinematic analysis is a tool to study the spatial configurations of robots as a function of joint angles. This gives the relationship between the joint variable space and the cartesian space. The transformation that relates these two spaces are very important as the robot links are actuated at the joint space and the tasks are defined in the cartesian space. There are two phases in the kinematic problems : the first is the forward kinematic problem where the joint space information is used to find the cartesian location, the second problem is the inverse of it, where the cartesian space information is processed to yield the joint information.

The manipulators generally have features common to all of them. Mostly, the adjacent joint axes of the robots are either parallel or perpendicular. The other design feature is concerned with the wrist. The three joints nearest to the end effector have their axes intersecting at a point, known as Spherical wrist, which is kinematically equivalent to a spherical joint. The first three joints are normally dedicated for positional control of manipulators if the length of the link forming the last three joints is smaller than the first three links and the orientation point exists. The other three degrees of freedom associated with the

wrist are to orient the tool at the desired location. The approach described here for the forward kinematic solution of the Puma 560 robot is similar to the method described by Paul for the Stanford arm[6].

3.2 Description of the Puma 560 Robot Geometry

The Puma 560 robot shown in fig.3.1 has six degrees of freedom and has revolute joint configurations. The basic components of this robot are : Trunk, waist, shoulder (upper arm), elbow (forearm), wrist elements and a flange for the end effector. The joint 1 axis of rotation coincides with the center line of the trunk which is link 0. This axis also coincides with the world Z_0 axis(Z_w). When the robot is in its upright READY position (fig.3.2), the Z_w points upwards, world X axis(X_w) along the right side and the world Y axis(Y_w) passes through the shoulder axis. The joint angle θ_1 of the joint 1 is measured counter clockwise direction from the positive Y axis.

The joint 2 coordinate frame is perpendicular to and intersects the joint 1 coordinate frame. This coincides with the center line of the shoulder. The center of the coordinate frame of joint 1 and of joint 2 are at the same Z level with respect to the world frame. The joint angle θ_2 of the upper arm is measured counter clockwise with respect to the world Z_w axis.

The joint 3, the elbow has its coordinate frame parallel to joint 2. The axis of rotation of joint 3 is parallel to the axis of rotation of joint 2. The length of the link 3 is the center distance between this joint and the wrist twist joint. The joints 4, 5, and 6 has their axes

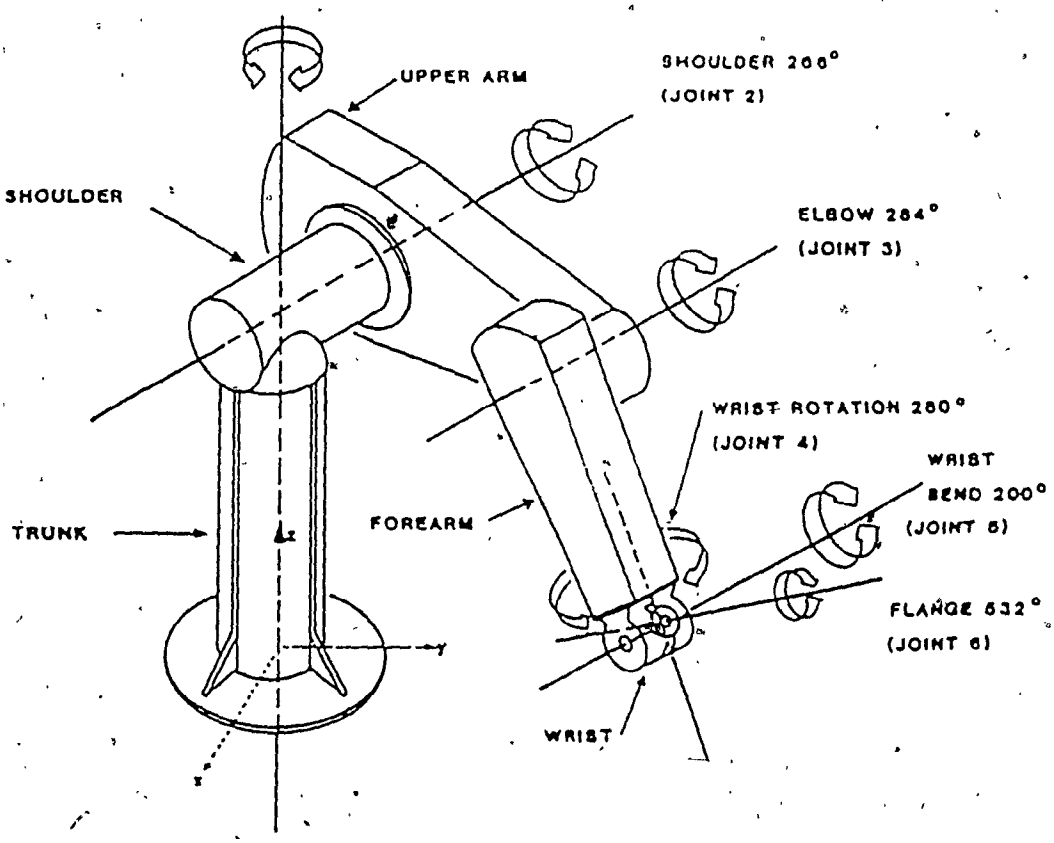

Fig.3.1. Puma 560 robot arm : Degrees of joint rotation and member identification

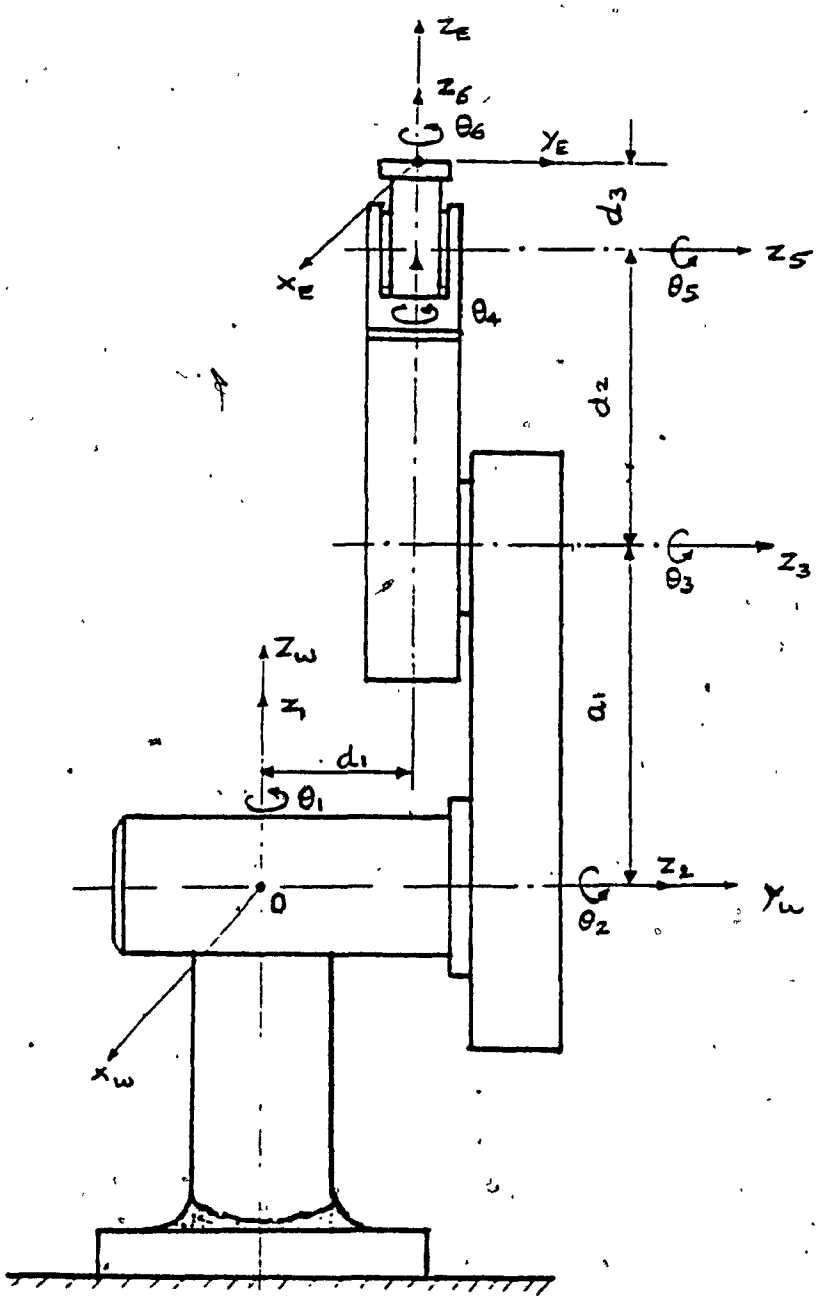

Fig.3.2. Puma 560 robot in Ready position

of rotation displaced by a_2 along the X_w axis with respect to the axis of rotation of joints 2 and 3. Also they are displaced by d_1 along the Y_w axis with respect to the joint 1 center.

Joint 4 is perpendicular to and intersects joint 2. Joint 5 has its axis of rotation parallel to joints 2 and 3. The angle θ_5 is the angle between the axis of rotation of the flange with respect to the Z axis of the link 4 (i.e., rotating the base coordinates through $\theta_1\underline{k}$, then through $-(\theta_2+\theta_3)\underline{i}$ and finally through $\theta_4\underline{k}$). The joint 6 axis is perpendicular to and intersects the joint 5 axis. It coincides with the center line of the gripper mounting flange.

The position of the flange expressed in joint coordinates is given by,

$$\overline{\Theta} = \left[\theta_1, \theta_2, \theta_3, \theta_4, \theta_5, \theta_6\right]$$

and in cartesian coordinates,

$$\overline{R} = \left[R_x, R_y, R_z, R_\phi, R_\theta, R_\psi \right]$$

where R_x, R_y, R_z is the position vector and R_ϕ, R_θ, R_ψ are the rotations about the new Z axis that aligns the base coordinates with the tool tip coordinates.

Arm Configurations

The Puma 560 robot can have right or left hand(K_1) configuration, i.e., the first three joints of the robot arm resemble a

human's right or left arm, respectively. The elbow can have two configurations: shoulder up and shoulder down(K_2). The wrist can also have two solutions; the flip wrist for which the joint 5 angle is positive and the flip wrist where the joint 5 angle is negative(K_3). From these, it is possible to have 8 sets of joint angles for each attainable position and orientation. Hence, parameters K_1, K_2, K_3 which will define the arm configurations can be used to select a particular solution out of the possible 8 solutions. This is to avoid singularity and degeneracy.

Singular Points

Singular points[3,6,12] are the dead zones or the degenerate points where the determinant value of the Jacobian matrix[6] is zero and as a result more than one solution exists. At these points, there is loss of accuracy and number of degrees of freedom of the robot decreases. This is due to the fact that the rank of the Jacobian matrix is less than the total number of degrees of freedom of the manipulator. Small displacements of the robot near the singular points in a certain direction can result in larger change in the joint angles.

The common practice to compute the joint informations at the singular points is to interpolate from the calculated values in the neighbourhood of the singular points. Uchiyamma[3] proposed a different approach to circumvent singularities. In this approach, the working envelop of the robot is kept at a distance from the singular points if the working areas are local. The trajectory generation algorithm should include additional constriants due to this approach.

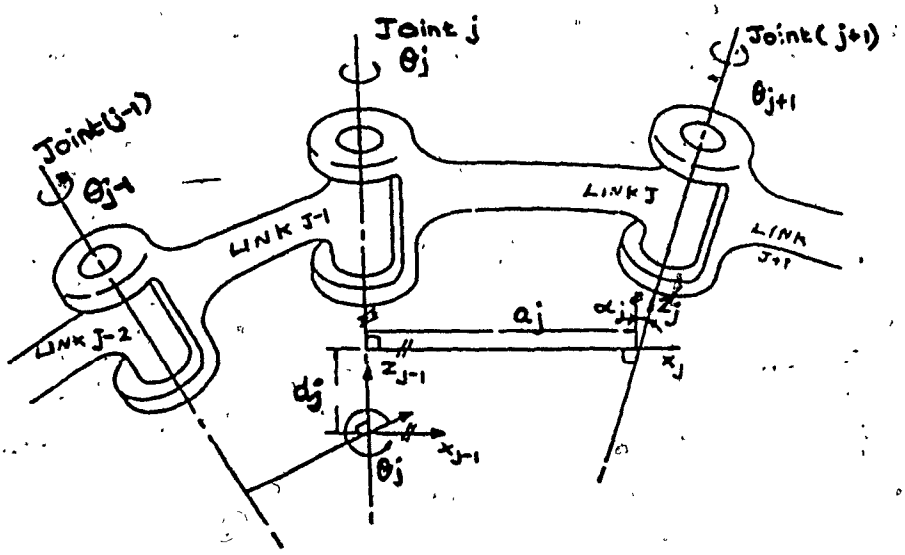

Fig.3.3. Link parameters d_j, a_j, θ_j, and α_j definitions

3.3 Coordinate Frame Assignment

A manipulator consists of links connected sequentially by actual joints. For a manipulator with N degree of freedom, there will be N links and N joints. The base of the manipulator is the Link 0 and is not considered as one of the N links. Link 1 is connected to the base link by the joint 1. There is no joint at the end of the final link. The only significance of links is that they maintain a fixed relationship between the manipulator joints at each end of the link. A link can be characterised by two dimensions: the common normal distance a_j, and the angle α_j, between the axes in a plane perpendicular to a_j. They are termed as a_j ' the length ' and α_j ' the twist ' of the j^{th} link (fig.1.3). Generally, two links are connected at each joint axis (fig.3.3). The axis will have two normals connected to it, one for each link. The relative position of two such connected links is given by d_j, the distance between the normals along the joint j axis, and θ_j the angle between the normals measured in a plane normal to the axis. d_j and θ_j are called ' the distance ' and ' the angle ' between the links respectively.

In order to describe the relationship between the links, a coordinate frame is assigned to each link. Let θ_j be the joint variable. The origin of the coordinate frame of link j is set to be at the intersection of the common normal between the joints j and j+1 and the axis of the joint j+1. In the case of intersecting axes, the origin is at the point of intersection of the joint axes. If the axes are parallel, the origin is chosen to make the joint distance zero for the next link where the coordinate origin is defined. The Z axis for link j shall be

aligned with the axis of joint j+1. The X axis will be aligned with any common normal which exists and is directed along the normal from joint j to joint j+1. In the case of intersecting axes, the direction of the X axis is parallel or antiparallel to the vector cross product $Z_{j-1} * Z_j$. This condition is also satisfied for the X axis directed along the normal between joints j and j+1. For the j^{th} revolute joint when X_{j-1} and X_j are parallel, and have the direction, θ_j is at its zero position.

The origin of the base link coincides with the origin of link 1. If it is desired to define a different reference coordinate system, then the relationship between the reference and the base coordinate systems can be described by a fixed homogeneous transformation. If a tool or end effector is used, whose origin and axes does not coincide with the coordinate system of link 6, the tool can be related by a fixed homogeneous transformation to link 6.

Having assigned the coordinate frames to all the links in this fashion, the relationship between the successive frames j-1 and j can be given by,

Rotate about Z_{j-1} axis through θ_j
Translate along the Z_{j-1} axis a distance d_j
Translate along the X_j axis a distance a_j
Rotate about the X_j axis through α_j

i.e., $A_j = Rot(Z_{j-1}, \theta_j)Trans(Z_{j-1}, d_j)Trans(X_j, a_j)Rot(X_n, \alpha_j)$

$$= \begin{bmatrix} C_{\theta j} & -S_{\theta j}C_{\alpha j} & S_{\theta j}S_{\alpha j} & a_jC_{\theta j} \\ S_{\theta j} & C_{\theta j}C_{\alpha j} & -C_{\theta j}S_{\alpha j} & a_jS_{\theta j} \\ 0 & S_{\alpha j} & C_{\alpha j} & d_j \\ 0 & 0 & 0 & 1 \end{bmatrix}$$

where S and C refers to the sine and the cosine of the angles respectively. Onee the link coordinate frames have been assigned to the manipulator, the various link parameters d, a and α for the links can be tabulated. Based on this, the six A matrices for a six degree of freedom robot can be derived.

3.4 Kinematic Equations

Having assigned the coordinate frames to the manipulator, the tool location is given by,

$$^{w}T_E = A_1 A_2 A_3 A_4 A_5 A_6 {}^{6}E$$

where ${}^{6}E$ is the fixed transformation between the link 6 and the end effector. The link coordinate frames assigned and the link parameter table for the Puma 560 robot are given in fig.3.4 and fig.3.5 respectively. These are arrived at, using the scheme outlined above. The A-matrices for the Puma 560 robot are given below :

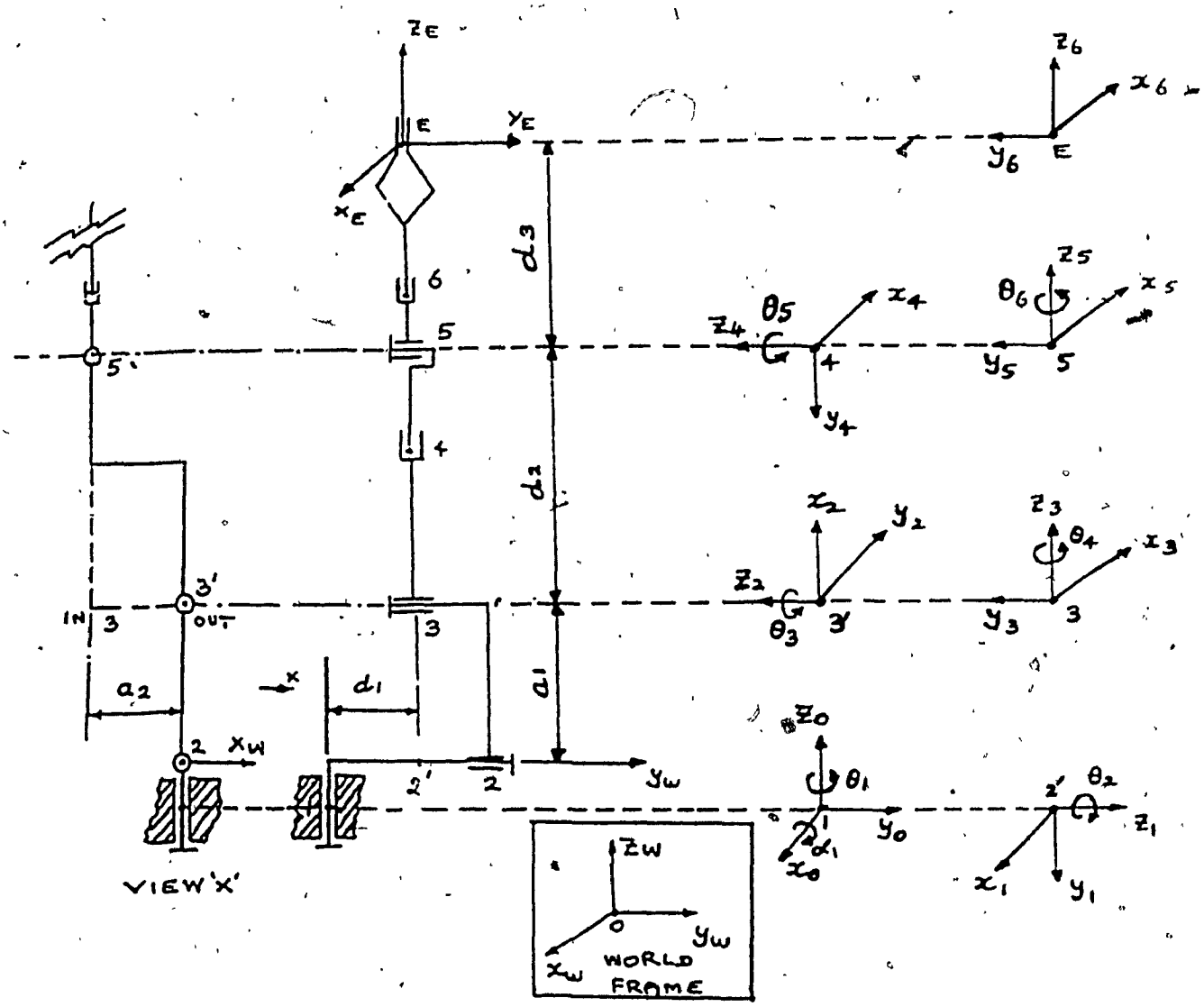

Fig.3.4. Joint coordinate frames assignment

LINK	VARIABLE	α_i Deg	a_i mm	d_i mm	$\sin\alpha_i$	$\cos\alpha_i$	θ_i Deg
1	θ_1	-90	0	0	-1	0	0
2	θ_2	+180	a_1	d_1	0	-1	-90
3	θ_3	+90	a_2	0	1	0	+90
4	θ_4	-90	0	d_2	-1	0	0
5	θ_5	+90	0	0	1	0	0
6	θ_6	0	0	d_3	0	1	0

Fig.3.5. Link parameter table

$$A_1 = \begin{bmatrix} C_1 & 0 & -S_1 & 0 \\ S_1 & 0 & C_1 & 0 \\ 0 & -1 & 0 & 0 \\ 0 & 0 & 0 & 1 \end{bmatrix}, \quad A_2 = \begin{bmatrix} C_2 & S_2 & 0 & a_1C_2 \\ S_2 & -C_2 & 0 & a_1S_2 \\ 0 & 0 & -1 & d_1 \\ 0 & 0 & 0 & 1 \end{bmatrix}$$

$$A_3 = \begin{bmatrix} C_3 & 0 & S_3 & a_2C_3 \\ S_3 & 0 & -C_3 & a_2S_3 \\ 0 & 1 & 0 & 0 \\ 0 & 0 & 0 & 1 \end{bmatrix} \quad A_2 = \begin{bmatrix} C_4 & 0 & -S_4 & 0 \\ S_4 & 0 & C_4 & 0 \\ 0 & -1 & 0 & d_2 \\ 0 & 0 & 0 & 1 \end{bmatrix}$$

$$A_5 = \begin{bmatrix} C_5 & 0 & S_5 & 0 \\ S_5 & 0 & -C_5 & 0 \\ 0 & 1 & 0 & 0 \\ 0 & 0 & 0 & 1 \end{bmatrix} \quad A_6 = \begin{bmatrix} C_6 & -S_6 & 0 & 0 \\ S_6 & C_6 & 0 & 0 \\ 0 & 0 & 1 & d_3 \\ 0 & 0 & 0 & 1 \end{bmatrix}$$

$$^6E = \begin{bmatrix} -1 & 0 & 0 & -X_t \\ 0 & -1 & 0 & -Y_t \\ 0 & 0 & -1 & -Z_t \\ 0 & 0 & 0 & 1 \end{bmatrix}$$

where S_1, S_2, ..., and C_1, C_2,... corresponds to $\text{Sin}\theta_1$, $\text{Sin}\theta_2$, ... and $\text{Cos}\theta_1$, $\text{Cos}\theta_2$, ... respectively.

3.5 Summary

Kinematic analysis is an efficient tool to study the spatial configurations of the robot as a function of joint angle. The

relationship between the joint space and cartesian work space of the robots can be derived easily with the help of kinematic analysis. Forward and inverse kinematic analysis of robots can be used to unravel the relationship between them if one of them is known.

A robot can reach a desired location in many different ways with the arm, shoulder, elbow and the wrist having different configurations. Some of them are ; arm left and arm right, shoulder up and shoulder down, elbow up and elbow down, wrist flip positive and flip negative. This condition is referred to as the singularity or degeneracy. During this condition, there is loss of degrees of freedom and accuracy.

Normally, the adjacent joint axes of the robots are either perpendicular or parallel to each other. In case of robots with short link length for the last three joints, the first three joints (waist, shoulder, elbow) are to position and the remaining joints (wrist) are to orient the tool at the desired location. A link can be characterized by two dimensions namely, the normal distance a_j and the angle α_j between the axes in a plane perpendicular to a_j. There are two dimensions associated with a joint namely, the distance d_j between the common normal along the joint j axis, and θ_j, the angle between the common normal measured in plane perpendicular to the axis. Using these characteristics of a joint, the coordinate frames of the joints are assigned. The relationship between successive frames is given by the A_j matrix which is given by,

$$A_j = \text{Rot}(Z_{j-1}, \theta_j)\ \text{Trans}(Z_{j-1}, d_j)\ \text{Trans}(X_j, a_j)\ \text{Rot}(X_j, \alpha_j)$$

the tool location with respect to the world coordinate frame of the robot is given by,

$$ {}^{w}T_{E} = \prod_{i=1}^{j} A_i \, {}^{j}E $$

where j is the number of degrees of freedom and ${}^{j}E$ is the fixed transformation between the tool and the j^{th} joint.

This thesis uses the kinematic parameters of the Puma 560 robot as the numerical example. This robot has 6 degrees of freedom and the joint configurations are of revolute in nature. The algorithm to analyse the kinematics of robots by Paul[6] is being applied here for the Puma 560 robot.

CHAPTER 4

DEVELOPMENT OF CALIBRATION MODEL

4.1 Introduction

The experimental setup and the mathematical models necessary to evaluate various errors associated with robots are explained in this chapter. The experimental setup uses optical instruments as the equipment for calibration. This thesis recommends the use of theodolites due to their relative ease of operation and reduced cost of operation. This equipment can give the position of a point chosen in space in terms of azimuth and elevation angles.

Use of two theodolites obviates the necessity for other optical accessories. The center distance between the theodolites A and B is used to as the reference distance to convert azimuth and elevation angles of the theodolites into coordinates of a point in space. In this thesis the coordinates of a point in space is expressed with respect to a reference coordinate frame R_f. The coordinate frame is chosen such that it is centered at the origin of the theodolite A, the X-axis directed along the line joining the centers of the theodolites A and B, and the Z-axis along the vertical axis of the theodolite A. The X-axes of the theodolites may be oriented at γ_1 and γ_2 with respect to the X-axis of R_f. Since the distance L and the angles γ_1 and γ_2 cannot be measured directly, it is necessary to have a pre-calibration setup to estimate these quantities. This is described in § 4.2.

Using these parameters and the computed coordinates of a reference point chosen on the tool at various locations, the Denawit-Hartenberg parameters can be evaluated. Section 4.3 explains the experimental setups and the mathematical analysis to evaluate the Denawit-Hartenberg parameters. With the help an extended tool with two reference points A_1 and A_2 marked on it and the distance L and the angles γ_1 and γ_2, the transmission errors can be evaluated. This is described in §4.4. A similar methodology can be used to analyse the joint and link compliances of a joint. These are discussed in §4.5 and §4.6 By tapping the joint encoders or resolvers the joint angles can be estimated to evaluate the cross coupling effects. Section 4.7 explains this process.

4.2 Calibration of Theodolite Parameters

The distance between the centers of the two theodolites and the offset angle between the axis of viewing and the line joining the two centers are the theodolite parameters estimated. The experimental setup consisting of the two theodolites and the reference unit is shown in fig.4.1.a. . This setup can be used to accurately evaluate L, γ_1, and γ_2. The angles γ_1 and γ_2 are the azimuth offset angles of the theodolites. The mathematical model is derived based on a good knowledge of the distances R and r_1. The distances R and r_1 depicts actually the distance of three points C, D and E precisely marked on a reference ruler made of a durable material.

Let α_1', α_2', α_3' and β_1', β_2', β_3' are the azimuth readings of the theodolites A and B for points C, D, and E respectively. Let r_1,

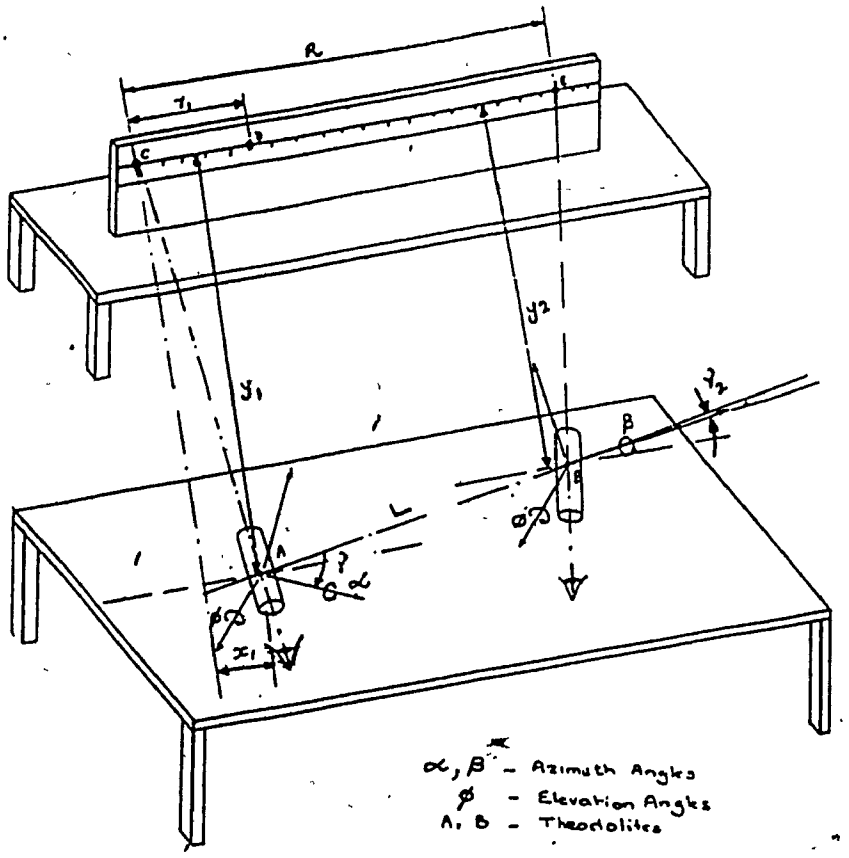

Fig.4.1.a. Schematic layout of the pre-calibration setup

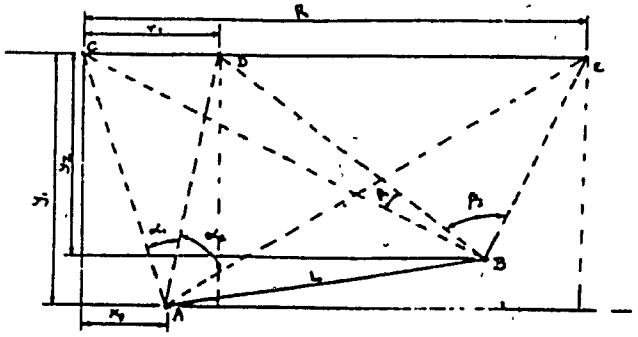

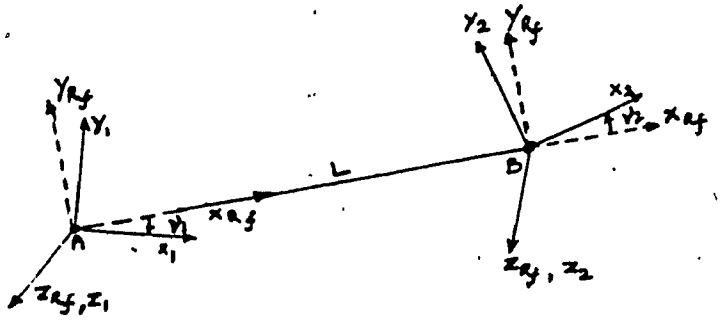

Fig.4.1.b. Geometrical layout of the pre-calibration setup

r_2, and R are the distances CD, DE, and CE respectively. The mathematical analysis to estimate the distance between the theodolites (L) and their offset angles (γ_1 and γ_2) is derived under the following assumptions :

1. The theodolites are levelled to the same degree of accuracy such that their vertical axes will be parallel to each other.

2. The reference ruler is levelled such that, the points C, D, and E lie in the plane of the optical centers of the theodolites.

The mathematical analysis to estimate the distance between the theodolites (L), and their offset angles γ_1 and γ_2 is presented below. A complete derivation of the expressions can be found in the Appendix A.

Referring to fig.4.1.b, from $\triangle ABC$,

$$BC\ Cos\theta_2\underline{i} + BC\ Sin\theta_2\underline{j} + \overline{V}_{BA} - AC\ Cos\theta_1\underline{i} - AC\ Sin\theta_2\underline{j} = 0$$

$$L = \sqrt{(AC\ Cos\theta_1 - BC\ Cos\theta_2)^2 + (AC\ Sin\theta_1 - BC\ Sin\theta_2)^2}. \qquad (4.2.1)$$

where ,

$$\theta_1 = \tan^{-1}\left[\frac{Sin\ (\alpha_1+\alpha_2)}{\frac{r_1\ Sin\alpha_1}{r_2 Sin\alpha_2} - Cos(\alpha_1+\alpha_2)}\right]$$

$$\theta_2 = \tan^{-1}\left[\frac{\mathrm{Sin}(\beta_1+\beta_2)}{\frac{r_1 \mathrm{Sin}\beta_1}{r_2\ \mathrm{Sin}\beta_2} - \mathrm{Cos}(\beta_1+\beta_2)}\right] \qquad (4.2.2)$$

$$AC = \frac{R\ \mathrm{Sin}\phi_1}{\mathrm{Sin}\ (\alpha_1+\alpha_2)}\ ; \qquad BC = \frac{R\ \mathrm{Sin}\phi_2}{\mathrm{Sin}\ (\beta_1+\beta_2)} \qquad (4.2.3)$$

$$\alpha_1 = \alpha_1' - \alpha_2'\ ; \quad \alpha_2 = \alpha_2' - \alpha_3'$$
$$\beta_1 = \beta_1' - \beta_2'\ ; \quad \beta_2 = \beta_2' - \beta_3' \qquad (4.2.4)$$

and offset angles γ_1 and γ_2 are given by,

$$\left.\begin{aligned}\gamma_1 &= -\alpha_3' + \mathrm{Sin}^{-1}\left[\frac{R\ \mathrm{Sin}\phi_2\ \mathrm{Sin}\ (\theta_1-\theta_2)}{L\ \mathrm{Sin}(\beta_1+\beta_2)}\right] \\ \gamma_2 &= -\beta_1' + \mathrm{Sin}^{-1}\left[\frac{R\ \mathrm{Sin}\theta_1\ \mathrm{Sin}\ (\phi_2-\phi_1)}{L\ \mathrm{Sin}(\alpha_1+\alpha_2)}\right]\end{aligned}\right\} \qquad (4.2.5)$$

Here the offset angles γ_1 and γ_2 are expressed in terms of L for simplicity only. L can be replaced by the equation 4.2.1 if necessary. Thus the distance L and the angles γ_1 and γ_2 are accurately determined based on 6 azimuth readings plus two reference distances R and r_1.

4.3 Denawit-Hartenberg Parameters Estimation

4.3.1 Joint Orientations and Misalignments

Figures 4.2.a and 4.2.b show the schematic layout of the experimental setup and the geometrical model of the analysis designed for robots with revolute type joint configuration. A reference point P_j is chosen on the link j of the joint j under consideration. When the link is rotated about its axis of rotation, the path traced by the reference point with respect to R_f depends on the orientation of the (link) joint coordinate frame j with respect to R_f. Let θ_{zj}, θ_{yj} and θ_{xj} are the orientations of the XY, XZ and YZ planes, of the joint (link) coordinate frame C_{fj} with respect to the corresponding planes of R_f respectively. The orientations are evaluated using the method described below :

To evaluate θ_{zj}, we require the positions of the reference point at the extremities P_2 and P_3. The projections of the coordinates of P_2 and P_3 on the reference frame are represented as (X_{p2}, Y_{p2}, Z_{p2}) and (X_{p3}, Y_{p3}, Z_{p3}) respectively. The coordinates of the reference point at these positions are derived from the expressions given below :

$$\left.\begin{aligned} X &= L \tan\beta \,/\, (\tan\alpha+\tan\beta) \\ Y &= L \tan\alpha \tan\beta \,/\, (\tan\alpha+\tan\beta) \\ Z &= L \tan\beta \tan\phi \,/\, \{(\tan\alpha+\tan\beta)\ \mathrm{Cos}(\alpha)\} \end{aligned}\right\} \quad (4.3.1)$$

the inclination θ_{zj}, θ_{yj}, θ_{xj} are given by,

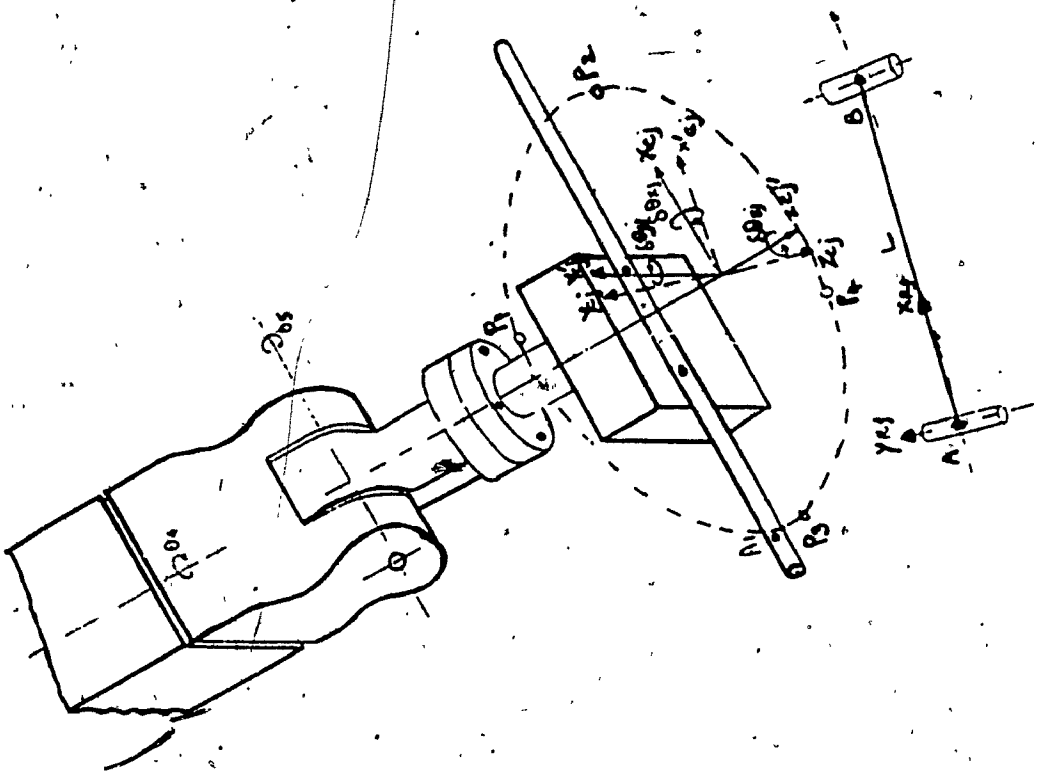

Fig.4.2.a. Schematic layout of the experimental setup to estimate joint orientation

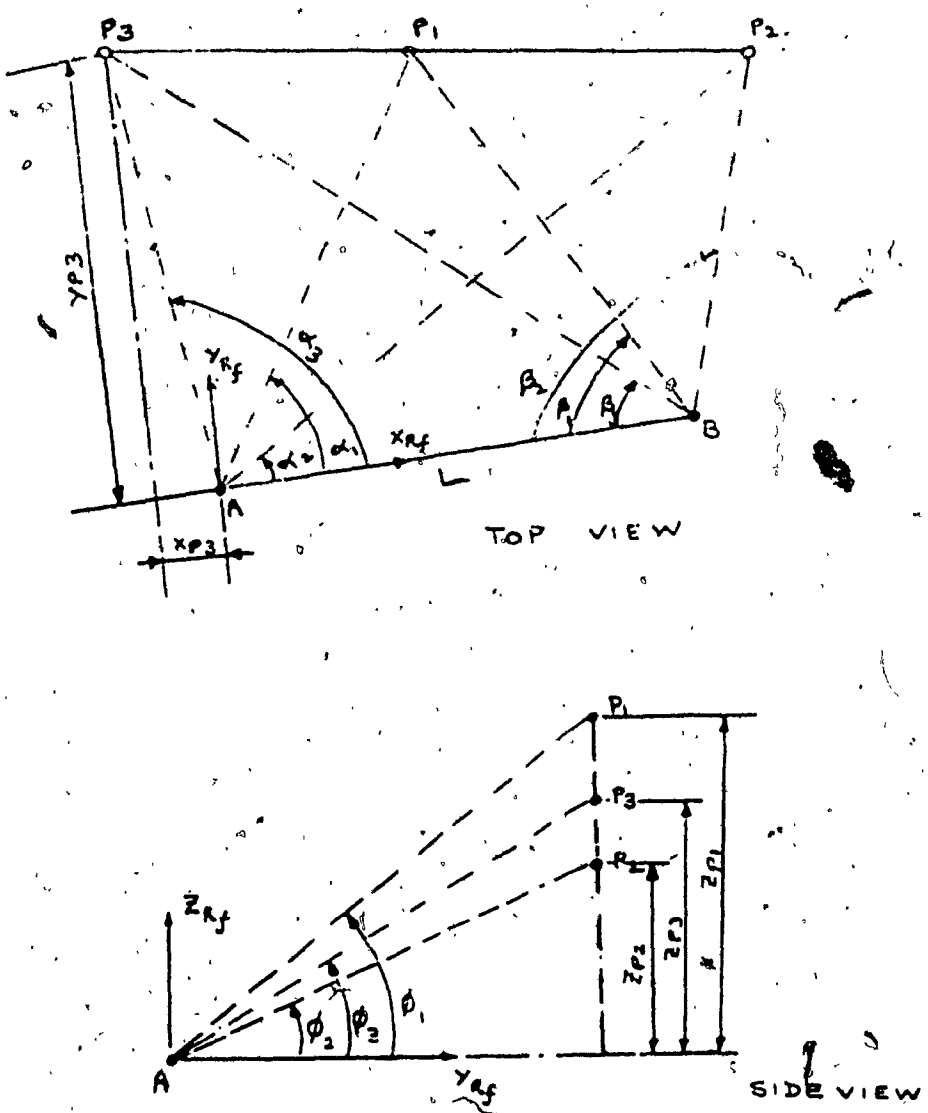

Fig.4.2.b. Geometrical model of the schematic layout

$$\left.\begin{aligned} \theta_{zj} &= \tan^{-1}\left[\frac{Y_{p2}-Y_{p3}}{X_{p2}-X_{p3}}\right] ; \quad \theta_{xj} = \mathrm{Sin}^{-1}\left[\frac{Y_{p4}-Y_{p1}}{X_{p2}-X_{p3}}\right] \\ \theta_{yj} &= \tan^{-1}\left[\frac{Z_{p2}-Z_{p3}}{X_{p2}-X_{p3}}\right] \end{aligned}\right\} \quad (4.3.2)$$

this procedure is repeated for all joints and their relative orientations with respect to the reference frame R_f are estimated. Using the results of this estimation the orientation of one joint with respect to the other ($\Lambda\theta_{xj}$, $\Lambda\theta_{yj}$, $\Lambda\theta_{zj}$) can be derived directly by taking the difference between θ_{xj} and θ_{xj-1}, θ_{yj} and θ_{yj-1}, and θ_{zj} and θ_{zj-1}. The joint misalignments ($\Delta\theta_{xj}$, $\Delta\theta_{yj}$, $\Delta\theta_{zj}$) are derived by taking the difference between the values of the design and the measured orientations of the joint under consideration.

Procedure to Compute the Differential Quantities

From Chapter 3, the A_j matrix for the j^{th} joint is given by,

$$A_j = \begin{bmatrix} \mathrm{Cos}\theta_j & -\mathrm{Sin}\theta_j\mathrm{Cos}\alpha_j & \mathrm{Sin}\theta_j\mathrm{Sin}\alpha_j & a_j\mathrm{Cos}\theta_j \\ \mathrm{Sin}\theta_j & \mathrm{Cos}\theta_j\mathrm{Cos}\alpha_j & -\mathrm{Cos}\theta_j\mathrm{Sin}\alpha_j & a_j\mathrm{Sin}\theta_j \\ 0 & \mathrm{Sin}\alpha_j & \mathrm{Cos}\alpha_j & d_j \\ 0 & 0 & 0 & 1 \end{bmatrix} \quad (4.3.3)$$

i.e., the A_j matrix is a function of the Denawit-Hartenberg parameters θ_j, α_j, a_j, and d_j. The differential transformation dA_j is given by,

$$dA_j = \frac{\partial A_j}{\partial \alpha_j} \Delta\alpha_j + \frac{\partial A_j}{\partial \theta_j} \Delta\theta_j + \frac{\partial A_j}{\partial a_j} \Delta a_j + \frac{\partial A_j}{\partial d_j} \Delta d_j \qquad (4.3.4)$$

partially differentiating (4.3.3) with respect to α_j, the term $\frac{\partial A_j}{\partial \alpha_j}$ is given by,

$$\frac{\partial A_j}{\partial \alpha_j} = \begin{bmatrix} 0 & -\mathrm{Sin}\theta_j \mathrm{Sin}\alpha_j & \mathrm{Sin}\theta_j \mathrm{Cos}\alpha_j & 0 \\ 0 & -\mathrm{Cos}\theta_j \mathrm{Sin}\alpha_j & -\mathrm{Cos}\theta_j \mathrm{Cos}\alpha_j & 0 \\ 0 & \mathrm{Cos}\alpha_j & \mathrm{Sin}\alpha_j & 0 \\ 0 & 0 & 0 & 0 \end{bmatrix} \qquad (4.3.5)$$

$$= A_j Q_\alpha$$

where Q_α is given by,

$$Q_\alpha = \begin{bmatrix} 0 & 0 & 0 & 0 \\ 0 & 0 & -1 & 0 \\ 0 & 1 & 0 & 0 \\ 0 & 0 & 0 & 0 \end{bmatrix}$$

differentiating (4.3.3) partially with respect to θ_j, the term $\frac{\partial A_j}{\partial \theta_j}$ is given as,

$$\frac{\partial A_j}{\partial \theta_j} = \begin{bmatrix} -\mathrm{Sin}\theta_j & -\mathrm{Cos}\theta_j\mathrm{Cos}\alpha_j & \mathrm{Cos}\theta_j\mathrm{Sin}\alpha_j & -a_j\mathrm{Sin}\theta_j \\ \mathrm{Cos}\theta_j & -\mathrm{Sin}\theta_j\mathrm{Cos}\alpha_j & -\mathrm{Sin}\theta_j\mathrm{Sin}\alpha_j & a_j\mathrm{Cos}\theta_j \\ 0 & 0 & 0 & 0 \\ 0 & 0 & 0 & 0 \end{bmatrix} \quad (4.3.6)$$

$$= A_j Q_\theta$$

where Q_θ is given by,

$$Q_\theta = \begin{bmatrix} 0 & -\mathrm{Cos}\alpha_j & \mathrm{Sin}\alpha_j & 0 \\ \mathrm{Cos}\alpha_j & 0 & 0 & a_j\mathrm{Cos}\alpha_j \\ \mathrm{Sin}\alpha_j & 0 & 0 & -a_j\mathrm{Sin}\alpha_j \\ 0 & 0 & 0 & 0 \end{bmatrix}$$

since we are interested in the deviations in the joint orientations only, the other error terms can be ignored. The net differential transformation dA_j is given by,

$$dA_j = A_j \left[Q_{\alpha_j} \Delta\alpha_j + Q_\theta \Delta\theta_j \right]$$

$$= A_j \, \delta A_j \quad (4.3.7)$$

where the differential transformation term δA_j is given by,

$$\delta A_j = \begin{bmatrix} 0 & -\Delta\theta_j \mathrm{Cos}\alpha_j & \Delta\theta_j \mathrm{Sin}\alpha_j & 0 \\ \mathrm{Cos}\alpha_j & 0 & -\Delta\alpha_j & \Delta\theta_j a_j \mathrm{Cos}\alpha_j \\ \mathrm{Sin}\alpha_j & 0 & 0 & -a_j \mathrm{Sin}\alpha_j \\ 0 & 0 & 0 & 0 \end{bmatrix}$$

The differential transformation Δ_j for differential rotations $\Delta\theta_{xj}$, $\Delta\theta_{yj}$, $\Delta\theta_{zj}$ about the three principle axes can be written as,

$$\Delta_j = \begin{bmatrix} 0 & -\Delta\theta_{zj} & \Delta\theta_{yj} & 0 \\ \Delta\theta_{zj} & 0 & -\Delta\theta_{xj} & 0 \\ -\Delta\theta_{yj} & \Delta\theta_{xj} & 0 & 0 \\ 0 & 0 & 0 & 0 \end{bmatrix} \qquad (4.3.9)$$

Since Δ_j and δA_j are one and the same, the elements of the two matrices can be compared to compute the errors $\Delta\alpha_j$ and $\Delta\theta_j$. The errors $\Delta\alpha_j$ and $\Delta\theta_j$ can be expressed in terms of $\Delta\theta_{xj}$, $\Delta\theta_{yj}$, and $\Delta\theta_{zj}$ as below :

$$\Delta\alpha_j = \Delta\theta_{xj} \qquad (4.3.10)$$

$$\Delta\theta_j = \pm \sqrt{\Delta\theta_{yj}^2 + \Delta\theta_{zj}^2} \qquad (4.3.11)$$

4.3.2 Link Lengths and Offset Distances

The link lengths and the offset distances can be evaluated from the joint coordinates of the links. The latter can be estimated as follows : A point P is chosen on the link associated with the joint under consideration. This point is moved to three different locations in space by rotating the joint. The coordinates of P at those locations are used to establish the joint coordinates. The coordinates of this point P can be computed from the measured theodolite angles, using equation 4.3.1. Let the orientations of the coordinate frame of the joint j with respect to R_f be θ_{xj}, θ_{yj}, and θ_{zj}. These angles can be evaluated using the method described in §4.3.1. and can be computed using equation 4.3.2.

Let the coordinates of the point P_j at one of those locations P_1 with respect to R_f be ${}^{R_f}(X_{p1}, Y_{p1}, Z_{p1})$. Let C_{fj} be the joint coordinate frame of the j^{th} joint. A third coordinate frame S_{fj} is chosen such that its origin is located at A and the coordinate axes parallel to those of the joint frame C_{fj}. S_{fj} can be derived from R_f by rotating R_f about its coordinate axes through small angles $-\delta\theta_{xj}$, $-\delta\theta_{yj}$, $-\delta\theta_{zj}$ respectively. The principle of differential rotations can be applied to compute the coordinates of P_1 with respect to S_{fj}. The process of transforming the known coordinates of a point with respect to R_f to another coordinate frame S_{fj} is referred to as the compensation scheme in this thesis. This scheme is necessary for the following reasons :

The length a_j for the j^{th} joint is defined as the common normal

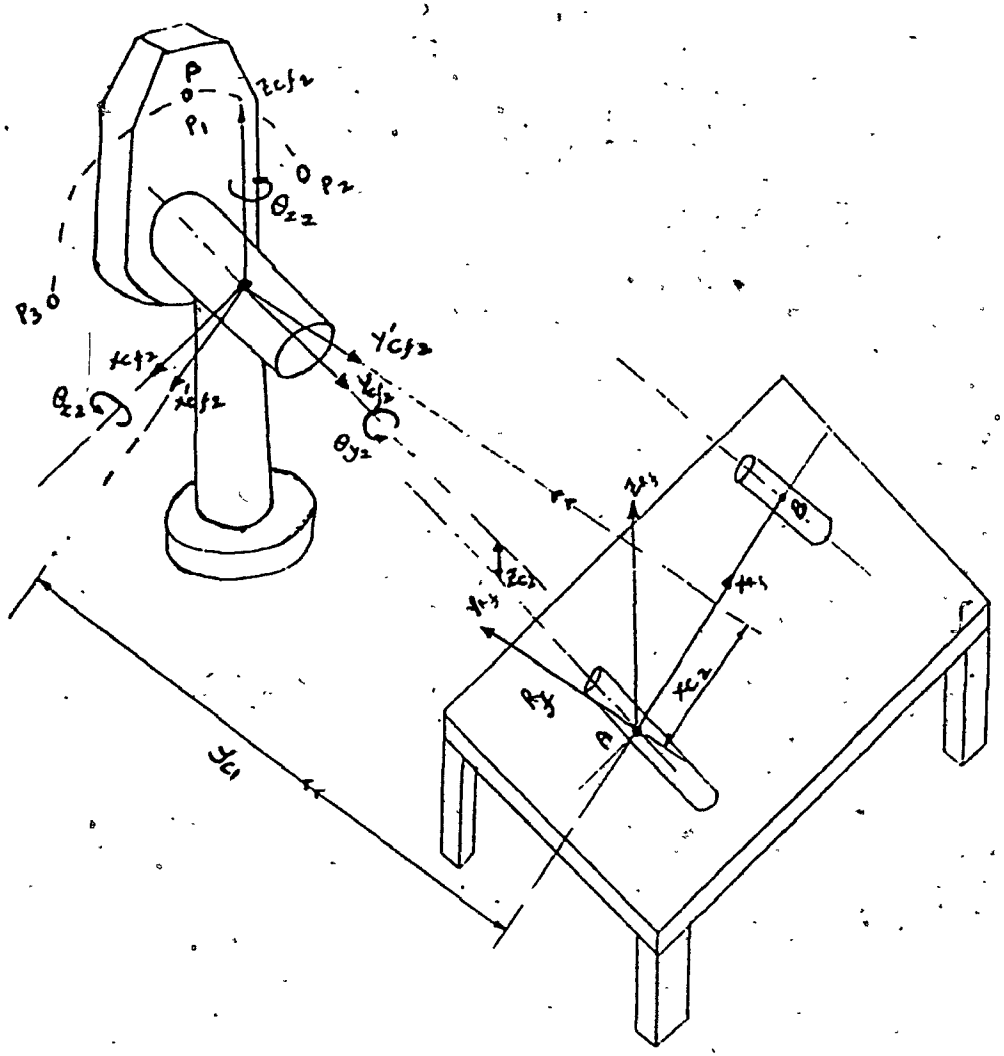

Fig 1.3. Schematic layout of the experimental setup to measure the link lengths and the offset distances

distance between the axis of rotation of the j^{th} and $(j+1)^{th}$ joints. The distance d_j for the joint j, is defined as the distance between the common normals of the $(j-1)^{th}$ and the j^{th} joints. This is shown in fig.3.3. To apply the principles mentioned above, the coordinate frames of the joints (j-1) and (j+1) should be realigned such that, the joints (j-1) and (j+1) are either parallel or perpendicular to the j^{th} joint. Also, the coordinates of the joints (j-1), j, (j+1) should be expressed with respect to the coordinate frame S_{fj}. These coordinates can be computed from the coordinates of the point P_j for those joints at the three locations with respect to S_{fj}. Hence the need to apply the compensation scheme. From the coordinates of the joints j-1, j, j+1 the distances d_j and the lengths a_j are estimated.

The differential rotations and the net transformation are given below :

$$\Delta_j = \text{Rot}(X, -\delta\theta_{xj})\ \text{Rot}(Y, -\delta\theta_{yj})\ \text{Rot}(Z, -\delta\theta_{zj})$$

$$\Delta_j = \begin{bmatrix} 0 & -\delta\theta_{zj} & \delta\theta_{yj} & 0 \\ \delta\theta_{zj} & 0 & -\delta\theta_{xj} & 0 \\ -\delta\theta_{yj} & \delta\theta_{xj} & 0 & 0 \\ 0 & 0 & 0 & 0 \end{bmatrix} \qquad (4.3.12)$$

where $\text{Rot}(X, -\theta_{xj})$ refers to rotation about the X-axis of the j^{th} joint through an angle $-\theta_{xj}$. Let the coordinates of P_1 with respect to R_f be

${}^{R_f}(X_{p1}, Y_{p1}, Z_{p1})^t$. The coordinates of this point with respect to S_{fj} is given by,

$$ {}^{S_{fj}}(X_{p1}, Y_{p1}, Z_{p1}, 1)^t = \Delta_j \; {}^{R_f}(X_{p1}, Y_{p1}, Z_{p1}, 1)^t \qquad (4.3.13) $$

where the superscript t refers to the transpose of the row vector. These relationships are valid, as long as θ_{xj}, θ_{yj} and θ_{zj} are sufficiently small such that $\mathrm{Sin}\theta_{xj} \approx \theta_{xj}$ and $\mathrm{Cos}\theta_{xj} \approx 1$.

This method assumes that the robot is in it's initial (READY) position during which the joint axes will be approximately parallel or perpendicular to the XY plane of R_f. Each joint is rotated with the other joints locked at their initial position. The joint coordinates can be estimated using one of the following equations :

$$ {}^{S_{fj}}(X_{cj}-X_{pi})^2 + {}^{S_{fj}}(Y_{cj}-Y_{ci})^2 = {}^{S_{fj}}R_{pj}^{\,2} $$

for axis of rotation perpendicular to the XY plane.

$$ {}^{S_{fj}}(X_{cj}-X_{pi})^2 + {}^{S_{fj}}(Z_{cj}-Z_{ci})^2 = {}^{S_{fj}}R_{pj}^{\,2} $$

for axis of rotation parallel to the XY plane.

(4.3.14)

where j refers to the joint and i =1,2,3 refers to the location of the point P_j, and R_{pj} is the distance between the joint center and the point P_j. This process is repeated for all joints and their joint center coordinates are established. Using the joint coordinates of each joint, the link lengths and the offset distances can be computed. For

illustration, the parameters a_1, a_2, d_1, d_2, d_3 of the Puma 560 robot are derived as below :

$$d_1 = Y_{c6} - Y_{c1} \; ; \qquad a_2 = X_{c6} - X_{c1}$$

$$d_2 = \sqrt{(X_{c3} - X_{c5})^2 + (Z_{c3} - Z_{c5})^2} \; ; \quad a_1 = \sqrt{(X_{c2} - X_{c3})^2 + (Z_{c2} - Z_{c3})^2}$$

$$d_3 = \sqrt{(Z_p - Z_{c6})^2 + (X_p - X_{c6})^2} - L_p$$

here X_{cj}, Y_{cj}, and Z_{cj} are the joint coordinates for the j^{th} joint, and j=1,....6. Hence, the three link lengths (a_1, d_2, d_3) and two offset distances (a_2, d_1) are accurately computed from the estimated center distances of the five joints.

4.4 Transmission Errors

The experimental setup shown in fig.4.4.a can be used to measure the joint angles in the joint 6 of the Puma 560 robot. The experimental setup may need to be modified depending upon the joint configuration of the robot. An extended tool with two reference points A_1 and A_2 is used to measure the joint angle. The angle between the axis of rotation of the joint, and the line joining A_1 and A_2 is the angle through which the joint j got rotated from the initial position. The axis of rotation may be oriented at θ_{xj}, θ_{yj}, and θ_{zj} with respect to R_f. These are computed using the method described in §4.4.1. and the compensation scheme can be performed using equations 4.4.1. and 4.4.2.

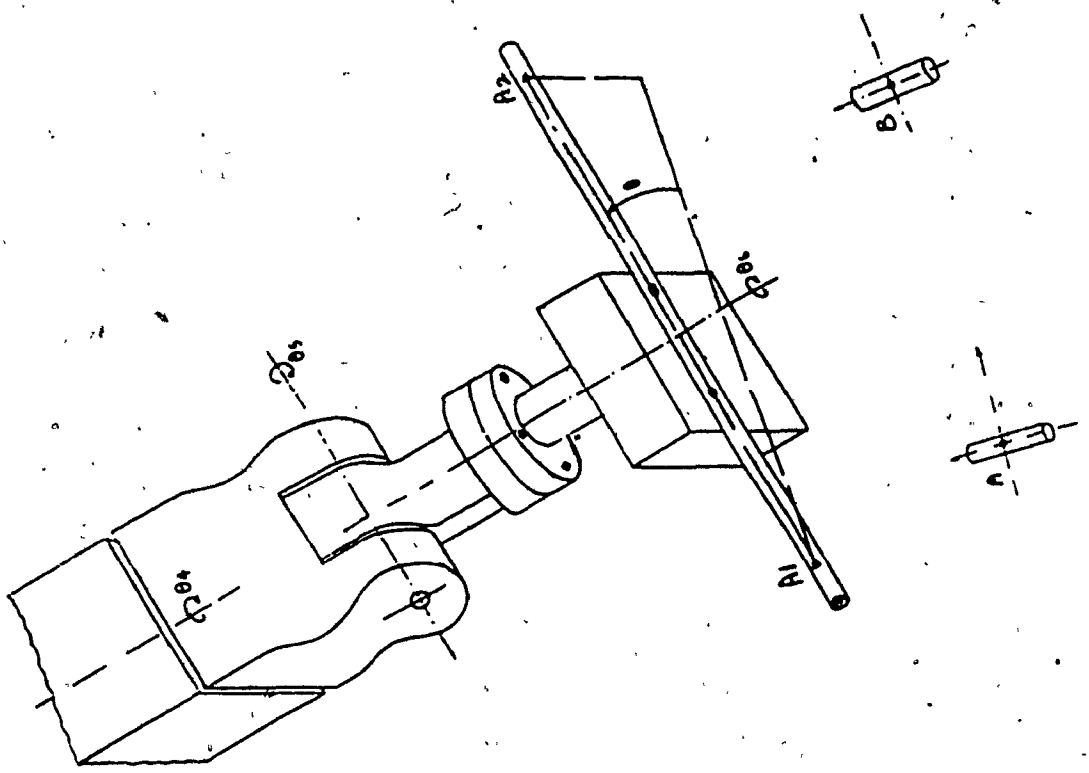

Fig.4.4.a. Schematic layout of the experimental setup to measure the joint angles

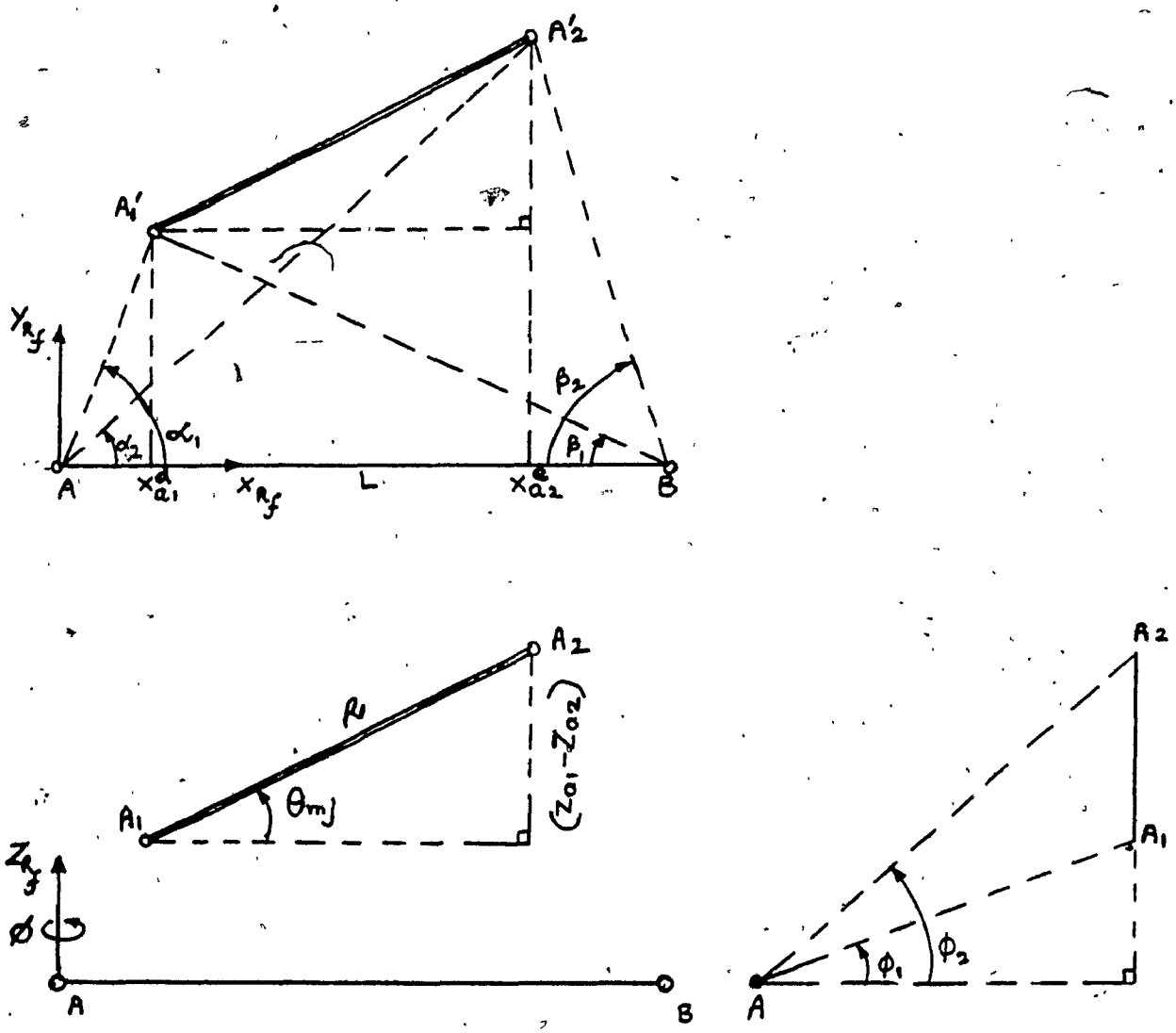

Fig.4.4.b. Geometrical model of the experimental setup to measure the joint angles

Let the coordinates of A_1 and A_2 being ${}^{R_f}(X_{a1}, Y_{a1}, Z_{a1})$ and ${}^{R_f}(X_{a2}, Y_{a2}, Z_{a2})$ with respect to R_f and ${}^{t_{fj}}(X_{a1}, Y_{a1}, Z_{a1})$ and ${}^{t_{fj}}(X_{a2}, Y_{a2}, Z_{a2})$ with respect to t_{fj} respectively. The joint angle can be computed as follows :

Let $A_1'A_2'$ be the projection of A_1A_2 on the XY plane of R_f. From $\Delta AA_1'd$ in fig.4.4.b,

$$A_1'e = (Y_{a1}-Y_{a2}) \text{ ; and } A_2'e = (X_{a1}-X_{a2})$$

$$\text{i.e., } A_1'A_2' = \sqrt{(X_{a1}-X_{a2}) + (Y_{a1}-Y_{a2})}$$

$$A_1A_2 = (Z_{a1}-Z_{a2})$$

From $\Delta A_2A_1'A_1$, the joint angle ${}^{t_{fj}}\theta_{mj}$ is given by,

$${}^{t_{fj}}\theta_{mi} = \tan^{-1}\left[\frac{{}^{t_{fj}}(Z_{a1}-Z_{a2})}{\sqrt{{}^{t_{fj}}(X_{a1}-X_{a2})^2 + {}^{t_{fj}}(Y_{a1}-Y_{a2})^2}}\right] \qquad (4.4.1)$$

Let ${}^{t_{fj}}\theta_{ij}$ be the initial angle between the points A_1 and A_2 for the j^{th} joint. Let ${}^{t_{fj}}\theta_{mj}$ be the measured angle after rotation, ${}^{t_{fj}}\theta_{dj}$ is the desired angle, θ_{cj} is the controller reading. The error between the desired and the actual joint angle E_{aj} and the error between the

controller reading and the actual value E_{cj} can be evaluated directly. Hence, the joint angle ${}^{t}{}_{fj}\theta_{rj}$ is accurately derived from the computed X, Y and Z distances of the two reference points A_1 and A_2 chosen on the tool.

4.5 Joint Compliance

The experimental setup shown in fig.4.5 can be used to evaluate the joint stiffness for the Puma 560 type robots. The joint under consideration may be oriented at θ_{xj}, θ_{yj}, and θ_{zj} with respect to the reference frame R_f. The procedure to evaluate the orientation angles and the compensation scheme to be used are described in §.4.3.1. Two reference points A_1 and A_2 are chosen on the reference tool attached to the end effector. Using equation 4.4.1, the angle between A_1 and A_2 can be computed from the theodolite readings.

The joint is loaded gradually from 0 to N_j units at a distance of L_j from the joint center. The angle between A_1 and A_2 is computed for increasing and decreasing loads. This is to identify the presence of dead zones which in turn leads to backlash. The magnitudes of N_j and L_j are selected based on the maximum static torque that the joint can take. Basically, the process of estimating the angle between A_1 and A_2 is the same as that described for the transmission errors but for one difference. In the former, the joint was commanded to rotate under no loads whereas here the joint rotates under gravity loading with no external command. The link can be considered as a cantilever beam with one end simply supported. Let θ_{ij} be the initial joint angle

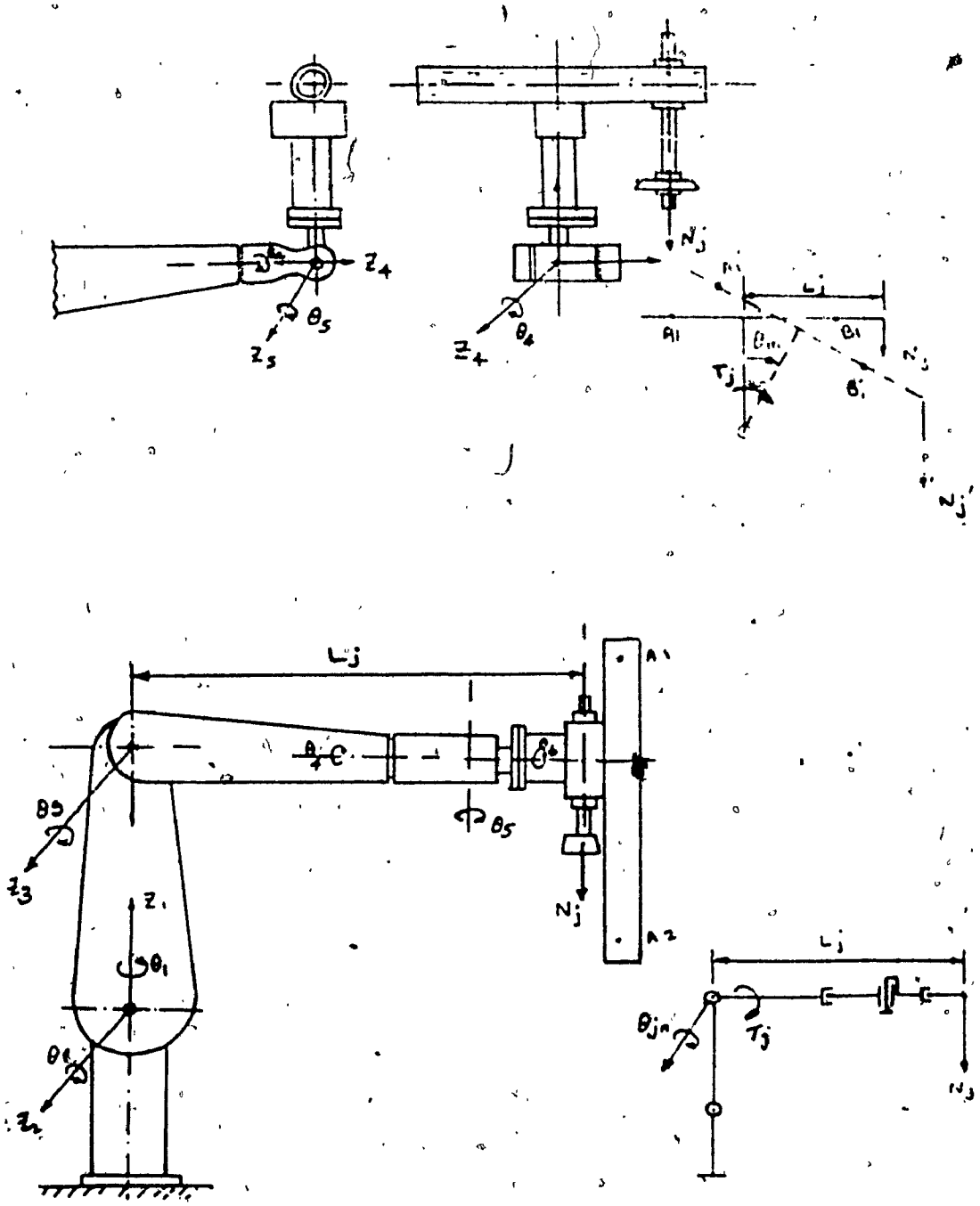

Fig.4.5. Schematic layout of the experimental setup to measure the joint compliance

between A_1 and A_2 with noload, θ_{jn} be the angle between A_1 and A_2 under a load of N_j units and hence the net change in the angle between A_1 and A_2 is given by,

$$\theta_{jn} = \theta_{ij} - \theta_{jn}$$

and the twisting moment is given by,

$$T_j = K_j \theta_{jn} = N_j L_j \cos\theta_{ij}$$

and hence the joint stiffness is given by,

$$K_j = N_j L_j \cos\theta_{ij} \text{ Kgf m/Deg (lb ft/Rad)} \qquad (4.5.1)$$

and $\frac{1}{K_j}$ is the angular deflection per unit torque (Deg/Kgf m).

4.6 Link Compliance

As mentioned in §1.4, the link compliance is associated with the stiffness of links. The setup shown in fig.4.6, with a number of reference points marked along the link can be used to evaluate the link stiffness. Dial gauges are positioned below or above the link at those locations to directly measure the linear deflection. If link bending exists the characteristics exhibited by the deflection curve resulting from this measurements will not be linear and will resemble that of a cantilever beam. The deflection Y_{x_j} at any §'XX' for the j^{th} link and it's stiffness E_j can be derived as below:

The bending moment at any §'XX' is given by,

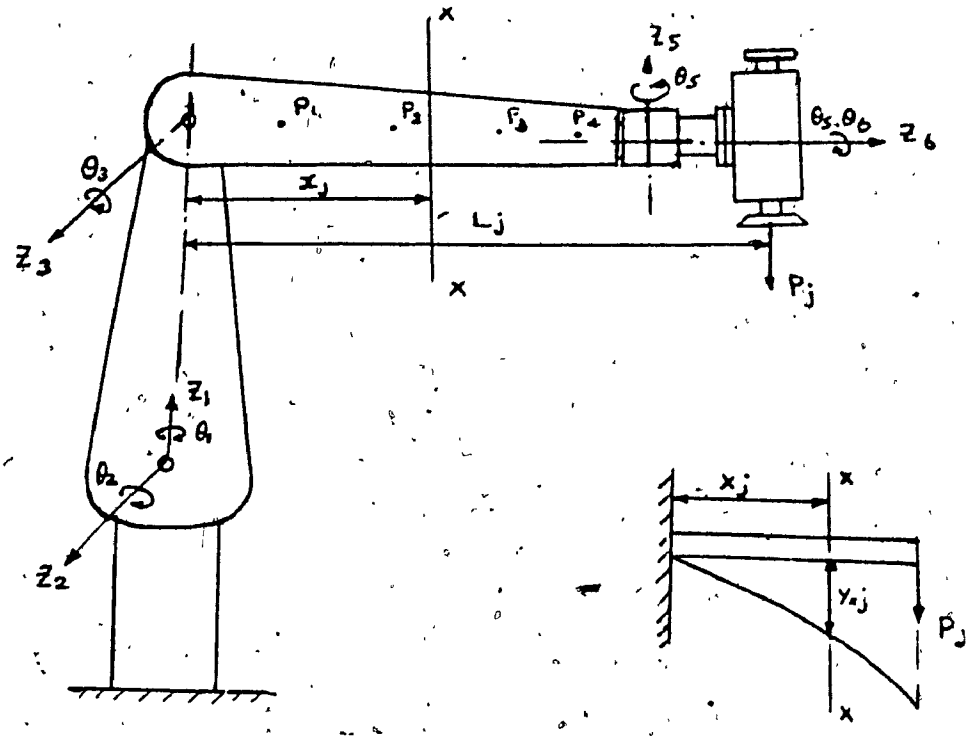

Fig.4.6. Schematic layout of the experimental setup to measure the link compliance

$$E_j I_j \frac{d^2 Y_{x_j}}{dX_j^2} = M_j = -P_{x_j}$$

integrating this twice and applying the initial conditions, the deflection Y_{x_j} at 'XX' is given by,

$$Y_{x_j} = \frac{1}{E_j I_j}\left[\frac{-P_j X_j}{6} + \frac{P_j L_j^2}{2} - \frac{P_j L_j^3}{3}\right]$$

and hence the link stiffness is given by,

$$E_j = \frac{1}{I_j Y_{x_j}}\left[\frac{-P_j X_j}{6} + \frac{P_j L_j^2}{2} - \frac{P_j L_j^3}{3}\right] \qquad (4.6.1)$$

where I_j is the moment of inertia of the j^{th} link and the values of Y_{x_j} obtained from the dial gauge measurements are used to evaluate the average value of E_j.

4.7 Cross Coupling Effects

The magnitude of cross coupling in joint k can be computed by tapping the respective joint encoders while j and k rotates. From the joint encoder counts and the resolution of the encoder, the angle through which the joint actuator of the k^{th} joint has been rotated can be calculated. Let ξ_k and S_k are the encoder counts and the resolution of the encoder (deg/encoder count) of the k^{th} joint respectively. The

joint actuator of the k^{th} joint rotates through an angle θ_{kr} given by,

$$\theta_k = S_k \ \xi_k$$

and the correction factor σ_{jk} is therefore given by,

$$\sigma_{jk} = 360 \ S_k \ \xi_k \ / \ \theta_j \qquad (4.7.1)$$

where θ_j is the angle through which the joint j was rotated. To verify the compensation provided for this effect by the manufacturer the following procedure can be adopted. The joints j and k are rotated at the same time through θ_j and θ_k respectively. Due to a cross coupling effect, the joint encoder reading for the k^{th} joint will be θ_k', and is represented as,

$$\theta_k' = \theta_k + \sigma_{jk} \ \theta_j \qquad (4.7.2)$$

the joint angle calculated by tapping the k^{th} joint encoder is compared with that calculated using equation (4.7.2). The difference between the two gives the furthur correction to be provided by the calibration model.

4.8 Summary

In the Calibration technique discussed here, two theodolites are used as the instruments for calibration. The distance between the centers of the theodolites L is used as the reference distance for calibration. A reference coordinate frame R_f centered at the origin of the theodolite A is chosen. The axis of viewing of the theodolites

makes γ_1 and γ_2 with respect to the Y axis of the reference frame. Since the distance L and the angles γ_1 and γ_2 can not be measured directly, a calibration procedure is mandatory to estimate them. Section 4.2 described the experimental setup and the mathematical analysis to estimate L, γ_1, and γ_2.

The Denawit-Hartenberg parameters of the robot namely, the angles α_j, and θ_j, the link lengths and the offset distances can be evaluated using the method described in §4.3. The joint orientations θ_{xj}, θ_{yj}, and θ_{zj} with respect to R_f can be evaluated by rotating the joints through 360 degrees and then evaluating the positions of a point P_{dj} at the extremities. The orientation of the joint j with respect to (j-1) can be obtained by finding the difference between their orientations with respect to R_f. The error terms $\Delta\alpha_j$, and $\Delta\theta_j$ can be evaluated using the principle of differential rotations. The A_j matrix is differentiated partially with respect to α_j, and θ_j. Equating the coefficients of the net dA_j matrix with that of the differential rotations matrix Δ_j, the error terms $\Delta\alpha_j$, and $\Delta\theta_j$ can be estimated.

There are two methods presented in this thesis to evaluate the link lengths and the offset distances. The first method determines the coordinates of the center of rotation from the measured coordinates of a point at three different locations. This scheme uses the method of solving a system of simultaneous equations to determine the center and radius of a circle. The second method that uses the A matrices and T - transformations is described in Chapter 6.

The transmission errors are evaluated using an extended tool and

rotating the joints incrementally one by one. The measured joint angle is compared with that of the controller reading and the error is estimated. The joint compliance is estimated using a similar method as the transmission errors, but with external loading and no joint rotations. The link stiffness is estimated from the measured positions of a number of reference points chosen along the link for different loads. The joint cross coupling effects are computed by tapping the joint encoders of the joints j and k while the joint j is rotated. A system consisting of hardware and software is used for this purpose.

CHAPTER 5

DESIGN FOR OPTIMUM CONFIGURATIONS OF THE EXPERIMENTAL SETUP AND RESULTS

5.1. Introduction

The accuracy of the estimated theodolite parameters (L, γ_1, γ_2) using the pre-calibration setup are functions of the measuring accuracies associated with the distances R, r_1, and r_2 marked on the reference ruler, and in the readability of the theodolites. The latter refers to the azimuth and elevation angle resolutions of the theodolites ($\Delta\alpha_i$, $\Delta\beta_i$, $\Delta\phi_i$). The accuracy associated with the process of estimating the Denawit-Hartenberg parameters, the transmission errors, joint and link compliances of the robot in turn are limited by the accuracy of estimating the theodolite parameters and as well as the readability of the theodolites. Hence an error analysis is required to evaluate these errors known as estimation errors in this thesis. This analysis provides the confidence level that can be placed on the estimated parameters. This also provides informations concerning the readability of the theodolites, and the measurement accuracy needed to achieve the desired calibration accuracy. The expressions for the estimation errors are derived by partially differentiating the mathematical expressions of these parameters with respect to the variables R, r_1, r_2, L, γ_1, γ_2, α_i, β_i, ϕ_i.

It can be seen from the mathematical expressions that the theodolite and the robot parameters are functions of distances X, Y, Z,

R_{dj}, R, L, R_{pj} etc., These distances in turn can be expressed in terms of theodolite angles. Hence for a given set of $\Delta\alpha_i$, $\Delta\beta_i$, $\Delta\phi_i$, ΔR, Δr_1, Δr_2, the estimation errors can be altered by varying these distances. The estimation errors can be minimized in two ways. One is to select instruments with better resolution and/or repeatability. The alternative is to use a computerized search technique to identify an optimum set for the parameters of the experimental setup that will result in minimum estimation errors. This search technique is referred to as Design of Experiments in this thesis. This scheme determines the magnitudes for the parameters of the experimental setup that results in minimum estimation errors. This scheme uses the mathematical models of the experimental setup, the error analysis, and an inverse trigonometric analysis to compute the theodolite angles for the assumed values of L, R, r_1, r_2, X, Y, and Z.

This chapter also presents discussions on the results of these computerized estimation error minimization. Experimental results are included for the Puma 560 robot employing the technique described in this thesis.

5.2 Calibration of Theodolite Parameters

This section provides the expressions to compute the estimation errors associated with the process of evaluating the theodolite parameters L, γ_1, and γ_2. Discussions on the effect of varying X_1, Y, L, and R on the estimation errors ΔL, $\Delta\gamma_1$, and $\Delta\gamma_2$ and, experiments results are also included.

5.2.1 Error Analysis, Design of Experiments and Discussions

Referring to equation 4.2.1, L can be expressed as a function of independent variables represented as,

$$L = F_1 (\theta_1, \theta_2 \phi_1, \phi_2, \alpha_1, \alpha_2, \beta_1, \beta_2, R, r_1, r_2) \qquad (5.2.1)$$

by differentiating L with respect to these variables, the effect of small variations in those variables on L can be obtained. This is given by,

$$\Delta L = \frac{\partial L}{\partial \theta_1}\Delta\theta_1 + \frac{\partial L}{\partial \theta_2}\Delta\theta_2 + \frac{\partial L}{\partial \phi_1}\Delta\phi_1 + \frac{\partial L}{\partial \phi_2}\Delta\phi_2 + \frac{\partial L}{\partial \alpha_1}\Delta\alpha_1 + \frac{\partial L}{\partial \alpha_2}\Delta\alpha_2 + \frac{\partial L}{\partial \beta_1}\Delta\beta_1 + \frac{\partial L}{\partial \beta_2}\Delta\beta_2 + \frac{\partial L}{\partial R}\Delta R + \frac{\partial L}{\partial r_1}\Delta r_1 + \frac{\partial L}{\partial r_2}\Delta r_2 \qquad (5.2.2)$$

referring to equation 4.2.2, θ_1, θ_2, ϕ_1, ϕ_2 are functions of α_1, α_2, β_1, and β_2 are written as,

$$\left.\begin{aligned} &\theta_1 = F_2 (\alpha_1, \alpha_2, r_1, r_2) ; \quad \theta_2 = F_3 (\beta_1, \beta_2, r_1, r_2) \\ &\phi_1 = F_4 (\alpha_1, \alpha_2, \theta_1) ; \quad \phi_2 = F_5 (\beta_1, \beta_2, \theta_2) \end{aligned}\right\} \qquad (5.2.3)$$

and from equation 4.2.4, α_1, α_2, β_1, β_2 are functions of theodolite angles given by,

$$\left.\begin{aligned} &\alpha_1 = F_6 (\alpha_1', \alpha_2') ; \quad \alpha_2 = F_7 (\alpha_2', \alpha_3') \\ &\beta_1 = F_8 (\beta_1', \beta_2') ; \quad \beta_2 = F_9 (\beta_2', \beta_3') \end{aligned}\right\} \qquad (5.2.4)$$

and hence the differential quantities of $\Delta\phi_1$, $\Delta\phi_2$, $\Delta\theta_1$, $\Delta\theta_2$, $\Delta\alpha_1$, $\Delta\alpha_2$, $\Delta\beta_1$, and $\Delta\beta_2$ are obtained by differentiating 5.2.3, and 5.2.4,

$$\left.\begin{aligned}
\Delta\theta_1 &= \frac{\partial\theta_1}{\partial\alpha_1}\Delta\alpha_1 + \frac{\partial\theta_1}{\partial\alpha_2}\Delta\alpha_2 + \frac{\partial\theta_1}{\partial r_1}\Delta r_1 + \frac{\partial\theta_1}{\partial r_2}\Delta r_2 \\
\Delta\theta_2 &= \frac{\partial\theta_2}{\partial\alpha_1}\Delta\alpha_1 + \frac{\partial\theta_2}{\partial\alpha_2}\Delta\alpha_2 + \frac{\partial\theta_2}{\partial r_1}\Delta r_1 + \frac{\partial\theta_2}{\partial r_2}\Delta r_2 \\
\Delta\phi_1 &= \frac{\partial\phi_1}{\partial\theta_1}\Delta\theta_1 + \frac{\partial\phi_1}{\partial\alpha_1}\Delta\alpha_1 + \frac{\partial\phi_1}{\partial\alpha_2}\Delta\alpha_2 \\
\Delta\phi_2 &= \frac{\partial\phi_2}{\partial\theta_1}\Delta\theta_1 + \frac{\partial\phi_2}{\partial\beta_1}\Delta\beta_1 + \frac{\partial\phi_2}{\partial\beta_2}\Delta\beta_2
\end{aligned}\right\} \quad (5.2.5)$$

The partial derivatives and the final expression for L can be found in the Appendix B. From these analysis, it can be inferred that the estimation error L can be controlled by selecting suitable values for the resolutions of the theodolites and the measuring accuracy of the reference ruler. Referring to equation 4.2.5, γ_1 and γ_2 can be expressed in terms of variables θ_1, θ_2, ϕ_1, ϕ_2, α_1, α_2, β_1, and β_2 given by,

$$\left.\begin{aligned}
\gamma_1 &= G_1\,(\beta_1, \beta_2, \theta_1, \theta_2, \phi_1, R, L, \alpha_3') \\
\gamma_2 &= G_2\,(\alpha_1, \alpha_2, \phi_1, \phi_2, \theta_1, R, L, \beta_3')
\end{aligned}\right\} \quad (5.2.6)$$

differentiating γ_1 and γ_2 with respect to these variables, the deviations in γ_1 and γ_2 from their actual value due to a variation in those variables is given by,

$$\Delta\gamma_1 = \frac{\partial\gamma_1}{\partial\beta_1}\Delta\beta_1 + \frac{\partial\gamma_1}{\partial\beta_2}\Delta\beta_2 + \frac{\partial\gamma_1}{\partial\theta_1}\Delta\theta_1 + \frac{\partial\gamma_1}{\partial\theta_2}\Delta\theta_2 + \frac{\partial\gamma_1}{\partial\phi_2}\Delta\phi_2 + \frac{\partial\gamma_1}{\partial R}\Delta R + \frac{\partial\gamma_1}{\partial L}\Delta L + \frac{\partial\gamma_1}{\partial\alpha_3'}\Delta\alpha_3'$$

$$\Delta\gamma_2 = \frac{\partial\gamma_2}{\partial\alpha_1}\Delta\alpha_1 + \frac{\partial\gamma_2}{\partial\alpha_2}\Delta\alpha_2 + \frac{\partial\gamma_2}{\partial\theta_1}\Delta\theta_1 + \frac{\partial\gamma_2}{\partial\phi_1}\Delta\phi_1 + \frac{\partial\gamma_2}{\partial\phi_2}\Delta\phi_2 + \frac{\partial\gamma_2}{\partial R}\Delta R + \frac{\partial\gamma_2}{\partial L}\Delta L + \frac{\partial\gamma_2}{\partial\beta_1}\Delta\beta_1 \qquad (5.2.7)$$

the final expressions for $\Delta\gamma_1$ and $\Delta\gamma_2$ are given in Appendix B.

In the computerized search technique used here, the inverse trigonometric analysis is used to evaluate the theodolite angles from the assigned values for the distances r_1, r_2, R, L, X_1, Y_1, and Y_2. Using fig.4.1.b, the theodolite angles α_i, β_i can be derived as below :

$$\alpha_1 = 180.0 - \tan^{-1}\left[\frac{Y_1}{X_1}\right] - \tan^{-1}\left[\frac{Y_1}{r_1 - X_1}\right]$$

$$\alpha_2 = \tan^{-1}\left[\frac{Y_1}{r_1 - X_1}\right] - \tan^{-1}\left[\frac{Y_1}{R - X_1}\right]$$

similarly β_1, and β_2 can also be obtained. This part of the analysis provides the theodolite angles which is used to evaluate the estimation errors for a particular set of distances selected. In these experiments, the quantities ΔR and Δr_1 are interpreted as the measurement errors associated with the variables R and r_1. Analytically, the exercise involved here may be summarized as follows :

$$\underset{(L,R,r_1,r_2,X_1,Y_1,Y_2)}{\text{Minimize}} \quad F(\Delta L, \Delta\gamma_1, \Delta\gamma_2)$$

subject to the physical constraints such as, the accuracy that can be achieved for R, r_1, and r_2, loss of reading accuracy with distance,

resolution of the theodolite available, the size of the room, etc. It is to be noted here that besides R, r_1 and L, it is necessary to manipulate the dimensions X_1, Y_1 and Y_2 also to achieve this objective. A different objective function has been used by the author. The author adopted the root square sum error as the total error and found it quite adequate. The minimization function can be defined as,

$$\underset{(L,R,r_1,r_2,X_1,Y_1Y_2)}{\text{Minimize}} \quad \sqrt{A\,\Delta L^2 + B\,\Delta\gamma_1^{\,2} + C\Delta\gamma_2^{\,2}} \qquad (5.2.9)$$

Subject to : Physical constraints given by,

$$500 \text{ mm} < R,\ L < 3000 \text{ mm}$$

$$4000 \text{ mm} < Y_1,\ Y_2 < Y_{opt} \text{ mm}$$

where Y_{opt} is the minimum optical focal distance for the theodolites. The values of the constants are appropriately chosen to achieve minimum error in all three parameters. The results of the computerised search technique that uses the above described analysis are discussed below :

Computer runs have been conducted in order to demonstrate the importance of the exercise in selecting (deciding) the appropriate values of R, r_1 and L before proceeding to the calibration of the robot itself.

a. Effect of R and L

Figures 5.1.a to 5.1.c summarizes the results of the computer runs for the effect of R and L on L, γ_1, and γ_2. When the magnitude

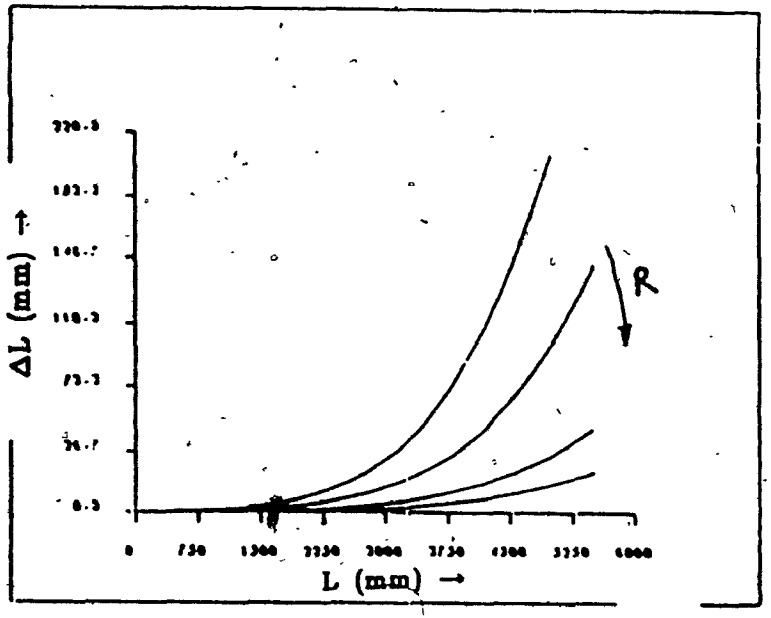

Fig.5.1.a. Effect of R and L on L

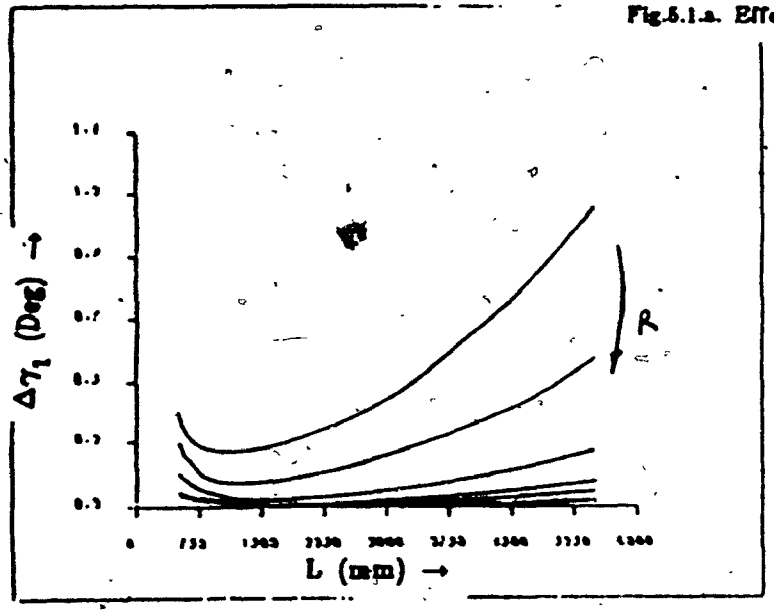

Fig.5.1.b. Effect of R and L on γ_1

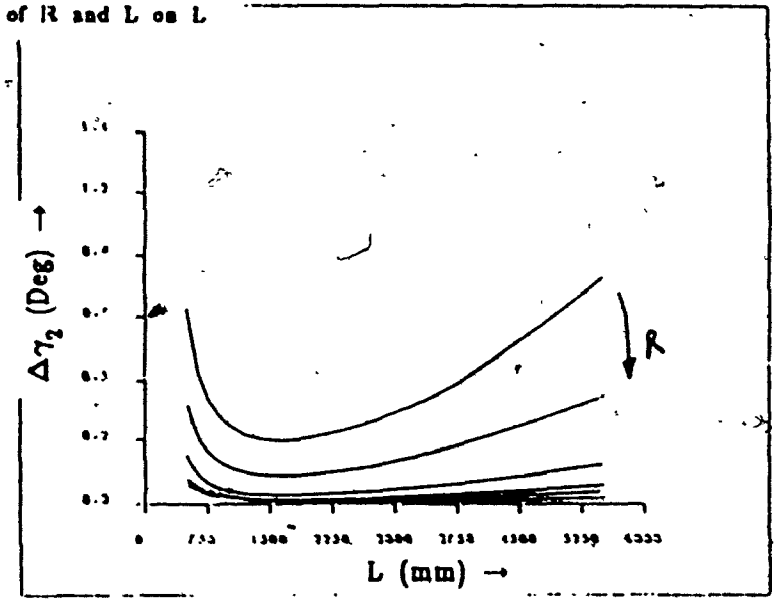

Fig.5.1.c. Effect of R and L on γ_2

of L is approximately 800 mm, as the value of R is increased from 500 mm to 1800 mm, the estimation errors $\Delta\gamma_1$, and $\Delta\gamma_2$ both decrease approximately by 85% and 89%, respectively, with no change in the value of ΔL. The absolute values of the errors ΔL, $\Delta\gamma_1$, and $\Delta\gamma_2$ are 0.1 mm, 0.05 deg, and 0.04 deg respectively. When L is around 1600 mm, for a similar change in R, the errors $\Delta\gamma_1$ and $\Delta\gamma_2$ decrease by 97%, and 96% respectively and again no effect on ΔL. The absolute values of the errors ΔL, $\Delta\gamma_1$, and $\Delta\gamma_2$ are 0.1 mm, 0.02 deg, and 0.02 deg respectively. When the L chosen is within the vicinity of 4800 mm, for a similar change in R the estimation errors decreases rapidly. The absolute values of the errors ΔL, $\Delta\gamma_1$, and $\Delta\gamma_2$ are 10.0 mm, 0.04 deg, and 0.06 deg respectively. In all these cases, for all values of R the errors $\Delta\gamma_1$ and $\Delta\gamma_2$ decreases as L is increased upto a certain value and thereafter the errors increases again. For large values of R, as L is increased the response is monotonically decreasing function. It can be seen that there is a distinct unmistakable minimal characteristics for $\Delta\gamma_1$ and $\Delta\gamma_2$. The only exception seems to be 5.1.a. In this case, the function increases monotonically.

b. Effect of R and Y

The effects of varying Y distance and R on ΔL, $\Delta\gamma_1$, $\Delta\gamma_2$ are shown in fig.5.2.a to 5.2.c. When the value of R chosen is around 800 mm, a reduction in the Y distance from 4000 mm to 1400 mm, the estimation errors ΔL, $\Delta\gamma_1$, and $\Delta\gamma_2$ decreases by 70%, 60% and 40% respectively. The absoulte value of the errors at Y equal to 1400 mm are 0.6 mm, 0.04 deg and 0.05 deg respectively. At R equal to 1800 mm, a similar variation in Y produces absolute errors 0.4 mm, 0.02 deg,

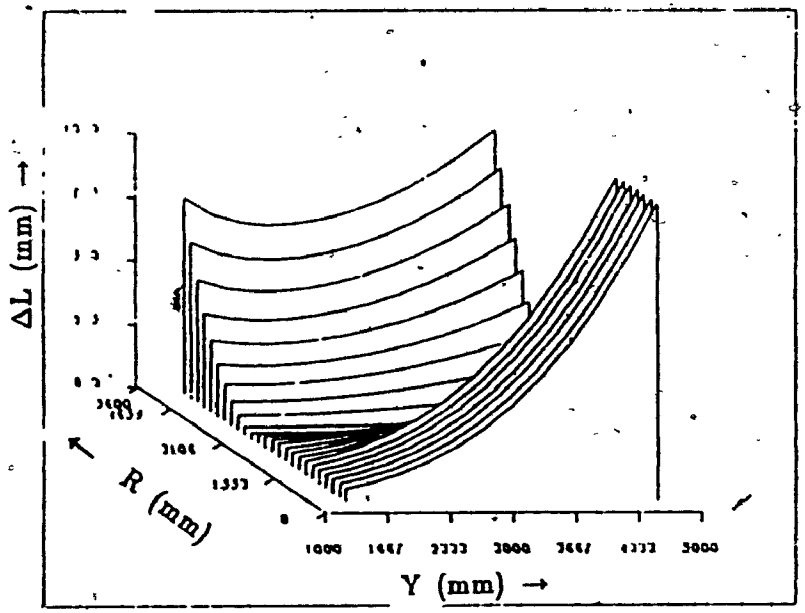

Fig.5.2.a. Effect of R and Y on L

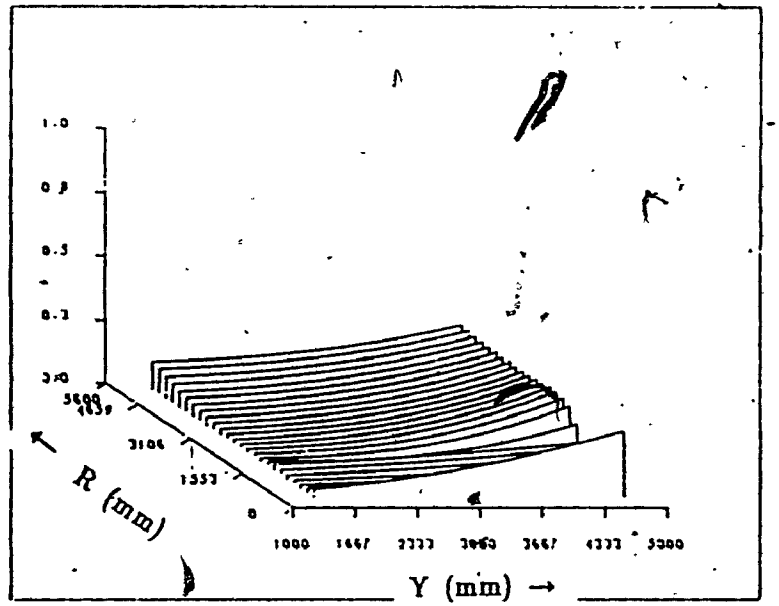

Fig.5.2.b. Effect of R and Y on γ_1

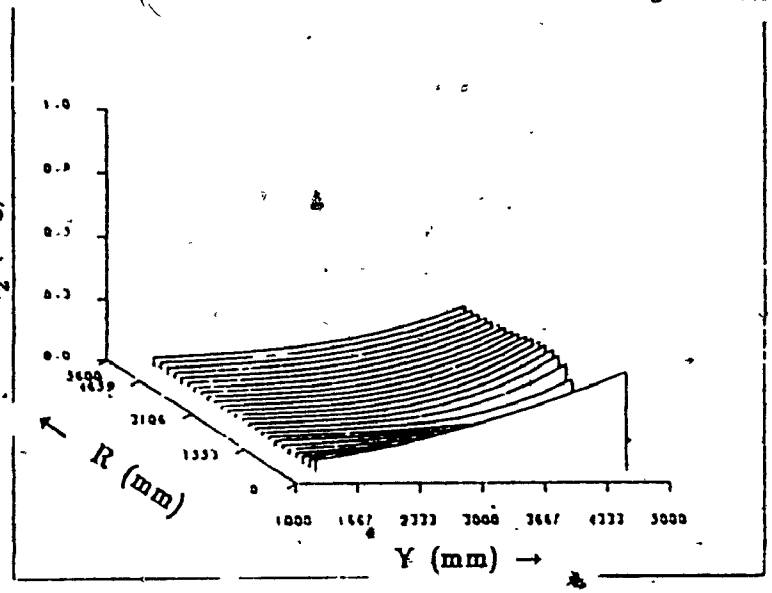

Fig.5.2.c. Effect of R and Y on γ_2

and 0.01 deg respectively. The estimation error ΔL is observed to be approximately constant for R from 1600 to 1800 mm and is equal to 0.4 mm and for R equal to 700 to 1400 mm, the estimation errors $\Delta\gamma_1$, and $\Delta\gamma_2$ are nearly constant and equal to 0.03 deg. At higher values of R, the estimation error ΔL is observed to be approximately constant and the magnitude is very high, whereas the errors $\Delta\gamma_1$, and $\Delta\gamma_2$ exhibits monotonic decrease.

c. Effect of R and X_1

Figures 5.3.a to 5.3.c shows the effect of X_1 and R on ΔL, $\Delta\gamma_1$ and $\Delta\gamma_2$ respectively. When the R chosen is around 800 mm, for a change in the X_1 distance from -1800 mm to +1800 mm, initially the error ΔL decreases and thereafter the effect is less significant. On the otherhand, the errors $\Delta\gamma_1$ and $\Delta\gamma_2$ exhibits monotonically decreasing and then increasing function. The error is minimum when the value of X_1 is around 100 mm. The absolute value of the errors at X_1 100 mm are 0.6 mm, 0.04 deg, and 0.06 deg respectively. When R is around 1600 mm, the characteristics remains the same and the absolute errors are 0.2 mm, 0.01 deg and 0.01 deg respectively. When R is around 2500 mm, the effects on $\Delta\gamma_1$ and $\Delta\gamma_2$ are the same as before but the error ΔL shows monotonic increase as X_1 is increased beyond 600 mm. Consequently, based on these computer runs, one gets a clear indication as to the choice of an appropriate set of experimental parameters(R, r_1, L, X_1, Y_1 and Y_2).

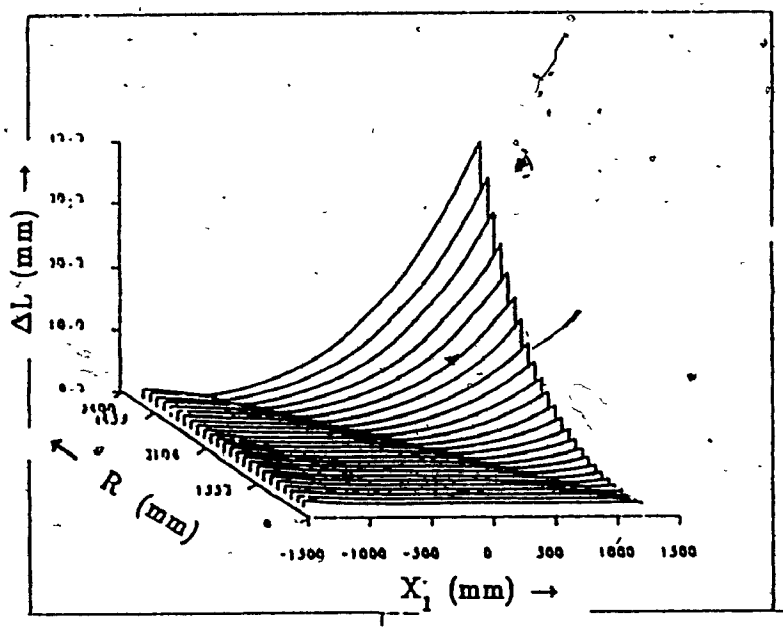

Fig.5.3.a. Effect of R and X_1 on L

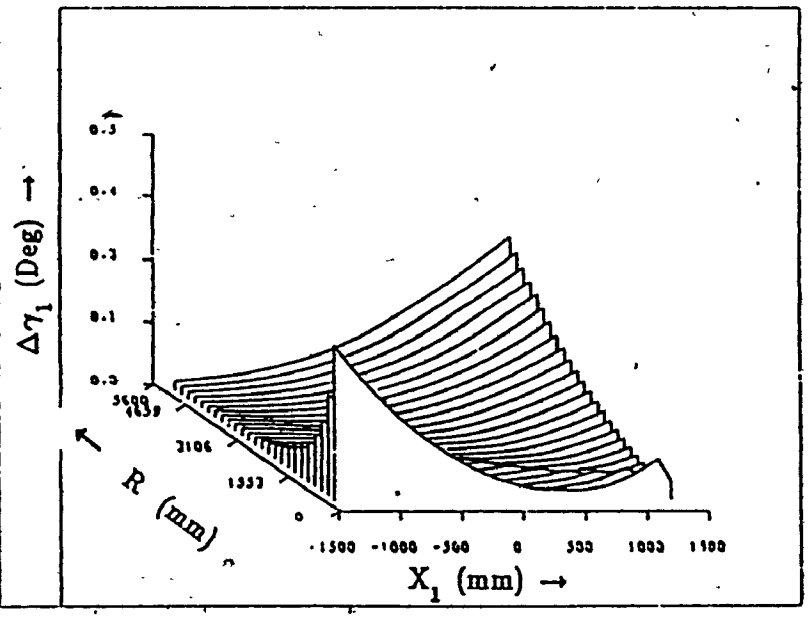

Fig.5.3.b. Effect of R and X_1 on γ_1

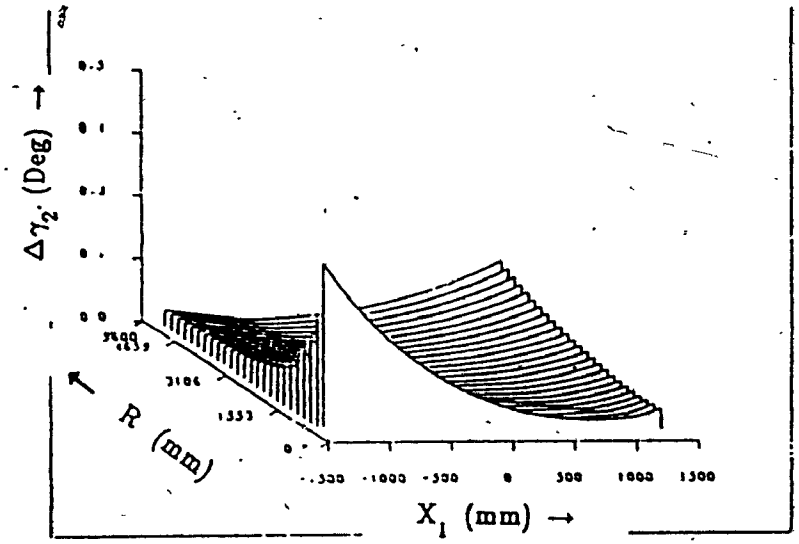

Fig.5.3.c. Effect of R and X_1 on γ_2

5.2.2 Experimental Results

Two TM-20C theodolites made by the Sokkisha, Instruments are selected as the optical instruments for measurements. These instruments have 30X magnification resolving down to 3 seconds of an arc. The sum of the circle reading and the micrometer reading is displayed to 20 seconds and by estimation to 3 seconds. The experimental setup uses a ruler of two meters long as the reference length. Three points C, D, and E are marked on it such that the distances R, r_1, and r_2 corresponds to that recommended by the design of experiments analysis. The distances X_1, Y_1, Y_2, and L are also approximately set to be equal to the optimum distance values evaluated in the §5.2.1. The distances r_1, R, and r_2 are slightly varied from this value and the theodolite parameters evaluated. The results are presented in fig.5.4. The estimated mean square values of L, γ_1, and γ_2 are 1609.9 mm, -1.489 and 1.356 degrees respectively.

5.3 Denawit-Hartenberg Parameters Estimation

5.3.1 Joint Orientations and Misalignments

5.3.1.1 Error Analysis, Design of Experiments and Discussions

The accuracy of the derived misalignments relies on the accuracy of estimating the distances X, Y and Z of the point P_j at the four locations. This in turn depends on the accuracy associated with the estimated values of L, γ_1 and γ_2 in the pre-calibration setup and also on the azimuth and elevation angle resolutions of the theodolites. Hence as before an error analysis can be designed to calculate the deviations in

R(mm)	L(mm)	γ_1(deg)	γ_2(deg)	ΔL(mm)	$\Delta\gamma_1$(deg)	$\Delta\gamma_2$(deg)
1860.0	1609.9	-1.489	1.356	0.3	0.013	0.010
1856.0	1609.9	-1.487	1.353	0.3	0.013	0.010
1852.0	1609.8	-1.489	1.357	0.3	0.013	0.010
1848.0	1609.8	-1.487	1.359	0.3	0.013	0.010
1844.0	1610.1	-1.499	1.357	0.3	0.013	0.011
1840.0	1609.9	-1.492	1.358	0.3	0.013	0.011
1836.0	1609.9	-1.493	1.360	0.3	0.014	0.011
1832.0	1610.0	-1.497	1.361	0.3	0.014	0.011
1828.0	1609.9	-1.494	1.362	0.4	0.014	0.011
1824.0	1610.0	-1.494	1.356	0.4	0.014	0.011
1820.0	1610.0	-1.498	1.360	0.4	0.014	0.011
1816.0	1609.7	-1.491	1.362	0.4	0.014	0.011
1812.0	1610.0	-1.503	1.362	0.4	0.014	0.011
1808.0	1609.8	-1.494	1.365	0.4	0.014	0.011
1804.0	1609.7	-1.489	1.362	0.4	0.014	0.011
1800.0	1609.7	-1.490	1.362	0.4	0.014	0.011
1796.0	1609.7	-1.497	1.367	0.4	0.014	0.011
1792.0	1609.9	-1.498	1.364	0.4	0.015	0.011

Fig.5.4 Experimental results - Theodolite parameters estimation.

the estimated joint orientations from their actual value for the given values of ΔL, $\Delta\gamma_1$, $\Delta\gamma_2$, α_i, β_i, and ϕ_i. Referring to equation 4.3.2, the inclinations θ_{xj}, θ_{yj}, and θ_{zj} can be expressed as a function of distances given by,

$$(\theta_{xj},\ \theta_{yj},\ \theta_{zj}) = f_1\ (X_{pi},\ Y_{pi},\ Z_{pi}) \qquad (5.3.1)$$

where i=1,2,3,4 are the number of locations used to estimate the orientations. But from equation 4.3.1, the distances X_{pi}, Y_{pi}, and Z_{pi} are function of theodolite angles and the distance L given by,

$$(X_{pi},\ Y_{pi},\ Z_{pi}) = f_1\ (L,\ \alpha_i,\ \beta_i,\ \phi_i) \qquad (5.3.2)$$

by partially differentiating θ_{xj}, θ_{yj} and θ_{zj} with respect to X_{pi}, Y_{pi}, and Z_{pi}, the estimation errors can be evaluated as,

$$\Delta\theta_{xj} = \frac{\partial\theta_{xj}}{\partial Y_{p2}}\Delta Y_{p2} + \frac{\partial\theta_{xj}}{\partial X_{p2}}\Delta X_{p2} + \frac{\partial\theta_{xj}}{\partial Y_{p3}}\Delta Y_{p3} + \frac{\partial\theta_{xj}}{\partial X_{p3}}\Delta X_{p3}$$

$$\Delta\theta_{yj} = \frac{\partial\theta_{yj}}{\partial Z_{p2}}\Delta Z_{p2} + \frac{\partial\theta_{yj}}{\partial X_{p2}}\Delta X_{p2} + \frac{\partial\theta_{yj}}{\partial Z_{p3}}\Delta Z_{p3} + \frac{\partial\theta_{yj}}{\partial X_{p3}}\Delta X_{p3}$$

$$\Delta\theta_{zj} = \frac{\partial\theta_{zj}}{\partial X_{p2}}\Delta X_{p2} + \frac{\partial\theta_{zj}}{\partial Y_{p4}}\Delta Y_{p4} + \frac{\partial\theta_{zj}}{\partial X_{p3}}\Delta X_{p3} + \frac{\partial\theta_{zj}}{\partial Y_{p1}}\Delta Y_{p1}$$

to evaluate the errors ΔX_{pi}, ΔY_{pi}, ΔZ_{pi} the expressions for X_{pi}, Y_{pi}, and Z_{pi} are partially differentiated with respect to α_i, β_i, ϕ_i, and L and is given by,

$$\Delta X_{pi} = \frac{\partial X_{pi}}{\partial L}\Delta L + \frac{\partial X_{pi}}{\partial\alpha_i}\Delta\alpha_i + \frac{\partial X_{pi}}{\partial\beta_i}\Delta\beta_i + \frac{\partial X_{pi}}{\partial\phi_i}\Delta\phi_i$$

$$\Delta Y_{pi} = \frac{\partial Y_{pi}}{\partial L}\Delta L + \frac{\partial Y_{pi}}{\partial \alpha_i}\Delta\alpha_i + \frac{\partial Y_{pi}}{\partial \beta_i}\Delta\beta_i + \frac{\partial Y_{pi}}{\partial \phi_i}\Delta\phi_i$$

$$\Delta Z_{pi} = \frac{\partial Z_{pi}}{\partial L}\Delta L + \frac{\partial Z_{pi}}{\partial \alpha_i}\Delta\alpha_i + \frac{\partial Z_{pi}}{\partial \beta_i}\Delta\beta_i + \frac{\partial Z_{pi}}{\partial \phi_i}\Delta\phi_i$$

the expressions for $\frac{\partial X_{pi}}{\partial L}$, $\frac{\partial X_{pi}}{\partial \alpha_i}$, and so on are provided in the Appendix-B.

As mentioned in §5.2, a computerized scheme to minimize the estimation errors has to be designed before proceeding with the experiments. Referring to fig.13.b, the theodolite angles are given by,

$$\alpha_{ij} = \tan^{-1}\left[\frac{Y_{pij}}{X_{pij}}\right]; \qquad \beta_{ij} = \tan^{-1}\left[\frac{Y_{pij}}{L\text{-}X_{pij}}\right]$$

$$\phi_{ij} = \tan^{-1}\left[\frac{Z_{pij}}{\sqrt{X_{pij}^2 + Y_{pij}^2}}\right]$$

using the mathematical model, the error analysis, and the inverse trigonometric analysis, the estimation errors $d\Delta\theta_{xj}$, $d\Delta\theta_{yj}$, $d\Delta\theta_{zj}$ are computed for various values of the distances X_{cj}, Y_{cj}, and Z_{cj} of the joint j, and the radius of rotation R_{pj}. The objective function may be defined as,

$$\underset{(R_{pj}, X_{cj}, Y_{cj}, Z_{cj})}{\text{Minimize}} \quad f(d\Delta\theta_{xj}, d\Delta\theta_{yj}, d\Delta\theta_{zj})$$

subject to the physical constraints namely, the maximum radius of rotation R_{pj} is restricted by the working envelope of the robots, the maximum X_{cj} distance is limited by the experimental room size, the minimum Y_{cj} distance is constrained by the minimum optical distance of the theodolites and so on.

a. Effect of X_{c1} and R_{pj}

Figures 5.5.a and 5.5.b presents the effect of X_{c1} and R_{pj} on $\Delta\theta_{yj}$, and $\Delta\theta_{zj}$ for one set of Y_{c1} and Z_{c1}. The orientations θ_{yj} and θ_{zj} are assumed to be each one degree. For θ_{zj}, as R_{pj} is increased, initially the estimation error decreases rapidly and thereafter exhibits less effect. As X_{c1} increases the estimation error decreases monotonically. For θ_{yj}, when X_{c1} is negative, the effect of R_{pj} is observed to resemble that for θ_{zj} but of smaller magnitude. On the other hand, when X_{c1} is positive, there is a zone where the error is minimum. The error increases monotonically as we move away from this zone. This indicates that the presence of optimum value for R_{pj} and X_{c1} where the error is in the vicinity of its minimum value. The minimum value of the errors attainable with this arrangement for $\Delta\theta_{yj}$, and $\Delta\theta_{zj}$ are 0.05 deg and 0.10 deg respectively at R_{pj} and X_{c1} 700 mm and -500 mm (approximately) respectively. The maximum error observed for the testing environment considered is nearly equal to the joint orientation value chosen for analysis.

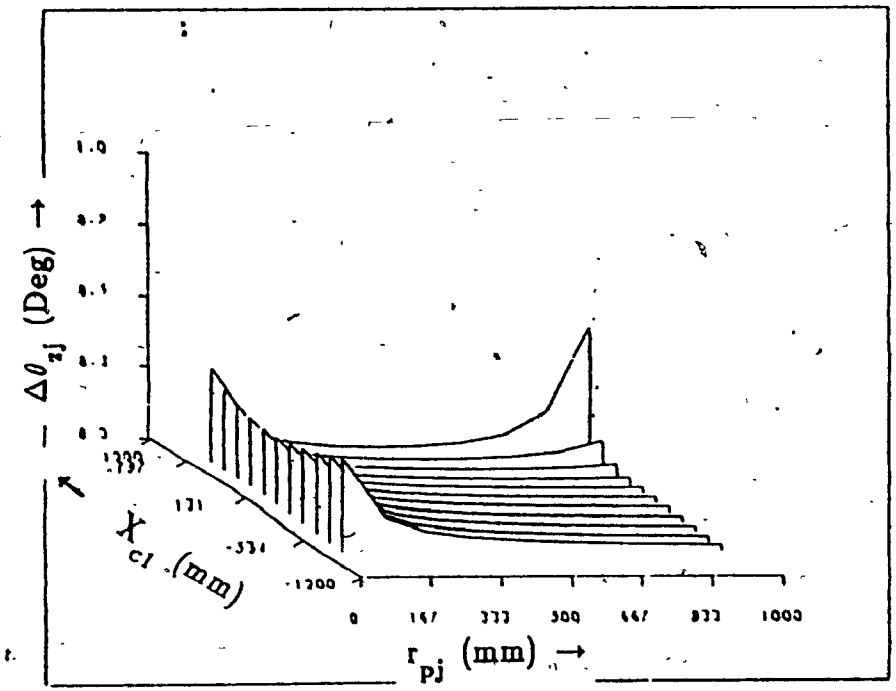

Fig.5.5.a. Effect of X_{cj} and R_{pj} on θ_{yj}

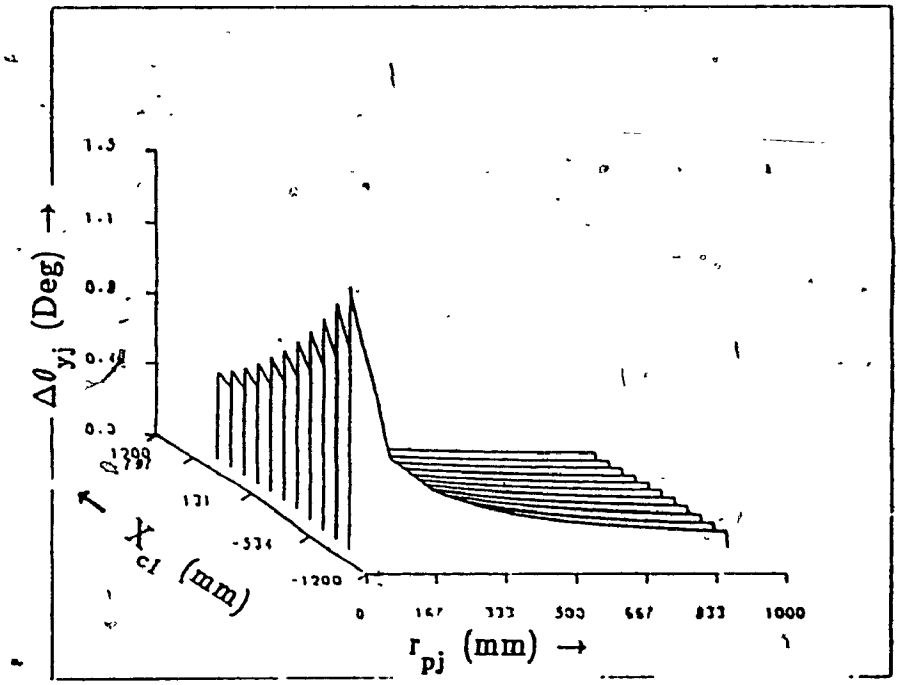

Fig.5.5.b. Effect of X_{cj} and R_{pj} on θ_{zj}

b. Effect of Y_{c1} and R_{pj}

The effect of Y_{c1} and R_{pj} on $\Delta\theta_{yj}$ and $\Delta\theta_{zj}$ for one set of θ_{yj} and θ_{zj} is shown in fig.5.6.a and 5.6.b. As before, the orientations θ_{yj}, and θ_{zj} both are assumed to be 1 degrees. For θ_{zj}, as R_{pj} is increased the estimation error decreases rapidly and thereafter shows less influence. At higher values of Y_{c1}, the effect is observed to be the same as before but the estimation error increases again as the value of R_{pj} is increased beyond 700 mm. It can be seen from plots that the estimation error remains the same for all Y_{c1} values when the R_{pj} lies between 300 and 700 mm. In the case of θ_{zj}, initially the error decreases rapidly and thereafter exhibits less influence for all Y_{c1} values. The estimation errors $\Delta\theta_{yj}$ and $\Delta\theta_{zj}$ both increases monotonically as Y_{c1} is increased. The minimum error value that can be achieved for $\Delta\theta_{yj}$ and $\Delta\theta_{zj}$ is 0.1 deg. The maximum error for the testing area considered here is same as that of the previous section.

c. Effect of Z_{c1} and R_{pj}

Figures 5.7.a and 5.7.c shows the effect of Z_{c1} and R_{pj} on $\Delta\theta_{yj}$, and $\Delta\theta_{zj}$ for one set of θ_{yj}, and θ_{zj}. Here also the orientations are assumed to be one degree each. For θ_{zj}, the estimation error initially decreases rapidly as R_{pj} is increased and thereafter the effect is less significant for all values of Z_{c1} distances. For θ_{yj}, the estimation error initially drops faster and thereafter remains constant upto R_{pj} equal to 800 mm. After this value of R_{pj} the error increases again. As Z_{c1} is varied from -1000 mm to 1000 mm, the error decreases and then increases again. This shows that there is an operating zone where the

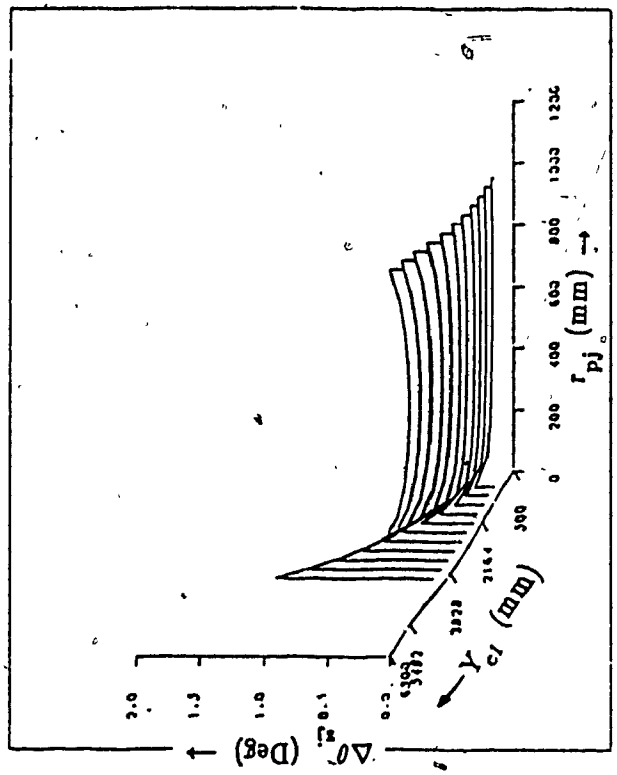

Fig.5.6.b. Effect of Y_{cj} and R_{pj} on θ_{xj}

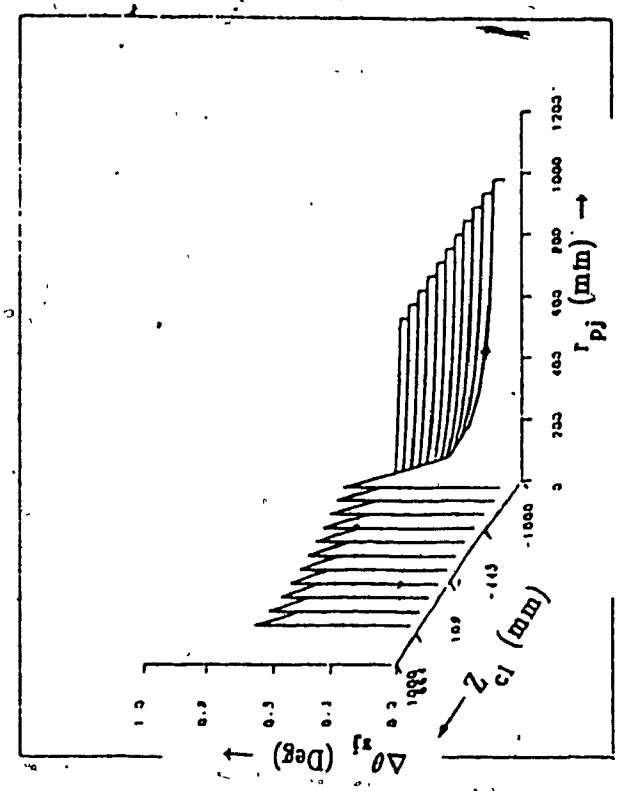

Fig.5.7.b. Effect of Z_{cj} and R_{pj} on θ_{xj}

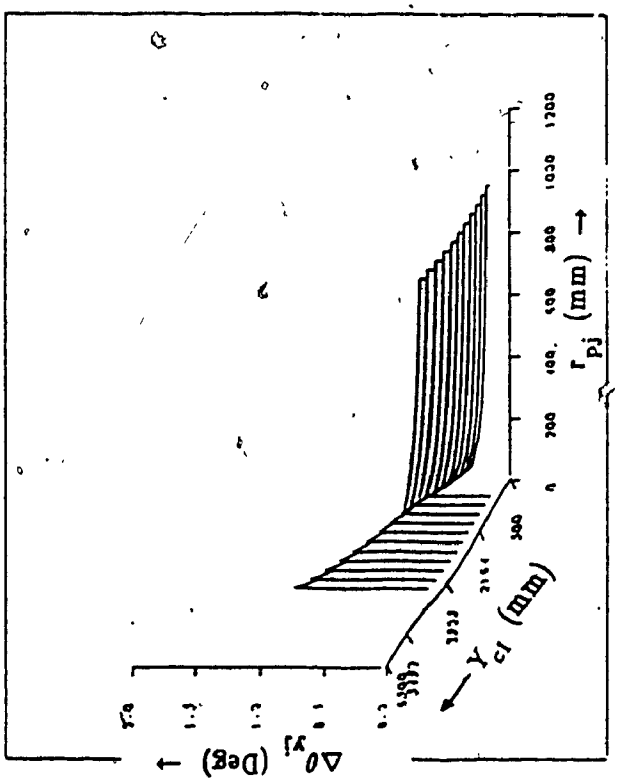

Fig.5.6.a. Effect of Y_{cj} and R_{pj} on θ_{yj}

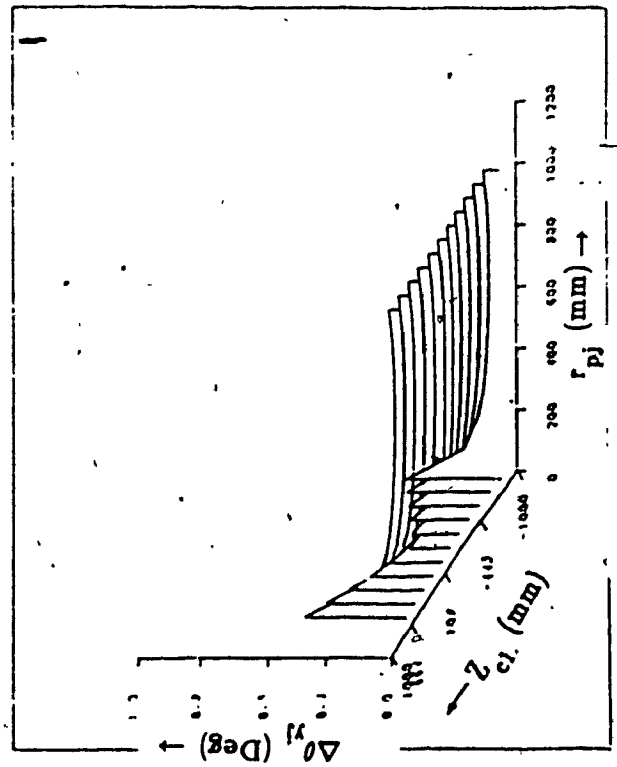

Fig.5.7.a. Effect of Z_{cj} and R_{pj} on θ_{yj}

error is minimum. In this case the error value at the operating zone of R_{pj} and Z_{c1} be 700 mm, and -200 mm is 0.08 deg each. The maximum error value attained for the experimental zone considered here is approximately 50% and 75% of the actual value for $\Delta\theta_{zj}$ and $\Delta\theta_{yj}$ respectively.

5.3.2. Link Lengths and Offset Distances

5.3.2.1 Error Analysis, Design of Experiments, and Discussions

The accuracy of the computations are dictated by the accuracy with which the the center distances are estimated. This in turn, depends on a number of factors namely, accuracy of the evaluated L, γ_1, and γ_2, and the azimuth and the elevation angle resolutions ($\Delta\alpha_i$, $\Delta\beta_i$, $\Delta\phi_i$) of the theodolites. By partially differentiating the expressions for the link lenghts and the offset distances with respect to the joint center distances X_{cj}, Y_{cj}, and Z_{cj}, the effect of small variations in the latter on the former can be evaluated. By partially differentiating the expressions of the latter with respect to the parameters L, γ_1 γ_2, α_i, β_i, and ϕ_i the effect of these parameters on the computed center distances can be obtained. The estimation errors Δa_i, Δd_i can be evaluated from,

$$\Delta a_i = \frac{\partial a_i}{\partial X_i}\Delta X_i + \frac{\partial a_i}{\partial Y_i}\Delta Y_i + \frac{\partial a_i}{\partial Z_i}\Delta Z_i + \frac{\partial a_i}{\partial X_{i+1}}\Delta X_{i+1} + \frac{\partial a_i}{\partial Y_{i+1}}\Delta Y_{i+1} + \frac{\partial a_i}{\partial Z_{i+1}}\Delta Z_{i+1} \qquad (5.3.7)$$

for Δd_i, replace a_i by d_i in the expression given above, and the

expressions for X_i, Y_i, and Z_i are given by the equations 4.3.1, in §5.3.1.

As mentioned in §5.3.1.2, here also a computerized scheme to minimize the estimation error has to be used before proceeding with the experiments. The inverse kinematic model to evaluate the theodolite angles described in the §5.3.1 is used here. In this particular section, the objective is to search for the magnitudes of the parameters X_{cj}, Y_{cj}, Z_{cj} and R_{pj} for the j^{th} joint, such that the estimation error will be close to the minimum value attainable. The objective function of this scheme can be defined as,

$$\begin{aligned} &\underset{(X_{cj},Y_{cj},Z_{cj},R_{pj},L)}{\text{Minimize}} && f_1(\Delta a_j) \\ &\underset{(X_{cj},Y_{cj},Z_{cj},R_{pj},L)}{\text{Minimize}} && f_2(\Delta d_j) \end{aligned} \qquad (5.3.8)$$

where $j = 1,2,3$ and subject to the following constraints :

$$4000 \text{ mm} > Y_{ij} > Y_{opt}$$

$$100 \text{ mm} < R_j < 1200 \text{ mm}$$

where Y_{opt} is the minimum optical distance for the theodolites specified by the manufacturer.

a. Effect of R_1 to R_6

The effect of radii of rotations of the joints on the estimated values of d_j and a_j is presented in fig.5.8, for one set of X_{c1}, Y_{c1}, and Z_{c1} distances. The estimation error is very high for low values of the radii of rotations and it decreases rapidly as the radii of rotation is increased. As the radii of rotation increases beyond 500 mm, the error

is observed to be constant and the effect becomes less significant. The suggested value for the radius rotation is around 600 mm.

b. Effect of X_{c1} and R_j

The effect of R_j and X_{c1} of the world coordinate frame with respect to R_f and R_j is shown in fig.5.9, for one set of Y_{c1} and Z_{c1}. For the parameters d_1 and d_2, the estimation error is minimum when the X_{c1} value is in the vicinity of zero. On either side of this value, the error increases monotonically. For positive values of X_{c1}, the increase in the error is less stepper than that for the negative values of X_{c1}. For a_1 also there is a minima. The estimation error is minimum when X_{c1} is close to -100 mm, and on either side of this value, the error exhibits monotonic increase. The effect of X_{c1} on a_2 is different from those discussed above. The error is minimum when X_{c1} is more negative, and it increases as the value becomes more positive.

5.3.2.2 Experimental Results

The Puma 560 robot has six degrees of freedom. When the robot is in it's Ready position, the axes of rotation of the joints 1, 4, and 6 are perpendicular to and that of the joints 2, 3, and 5 are parallel to the world XY plane of the robot. Hence, there should be two sets of experimental setups required to analyse these joints. The robot itself is positioned with respect to the reference frame R_f such that the axis of rotation of the joint 2 in the READY position will make a small angle $^{R_f}\delta\theta_x$ with respect to R_f The distances X_{c1} and Z_{c1} of the joint 1 and the Y_{c2} of the joint 2 are set to be the values

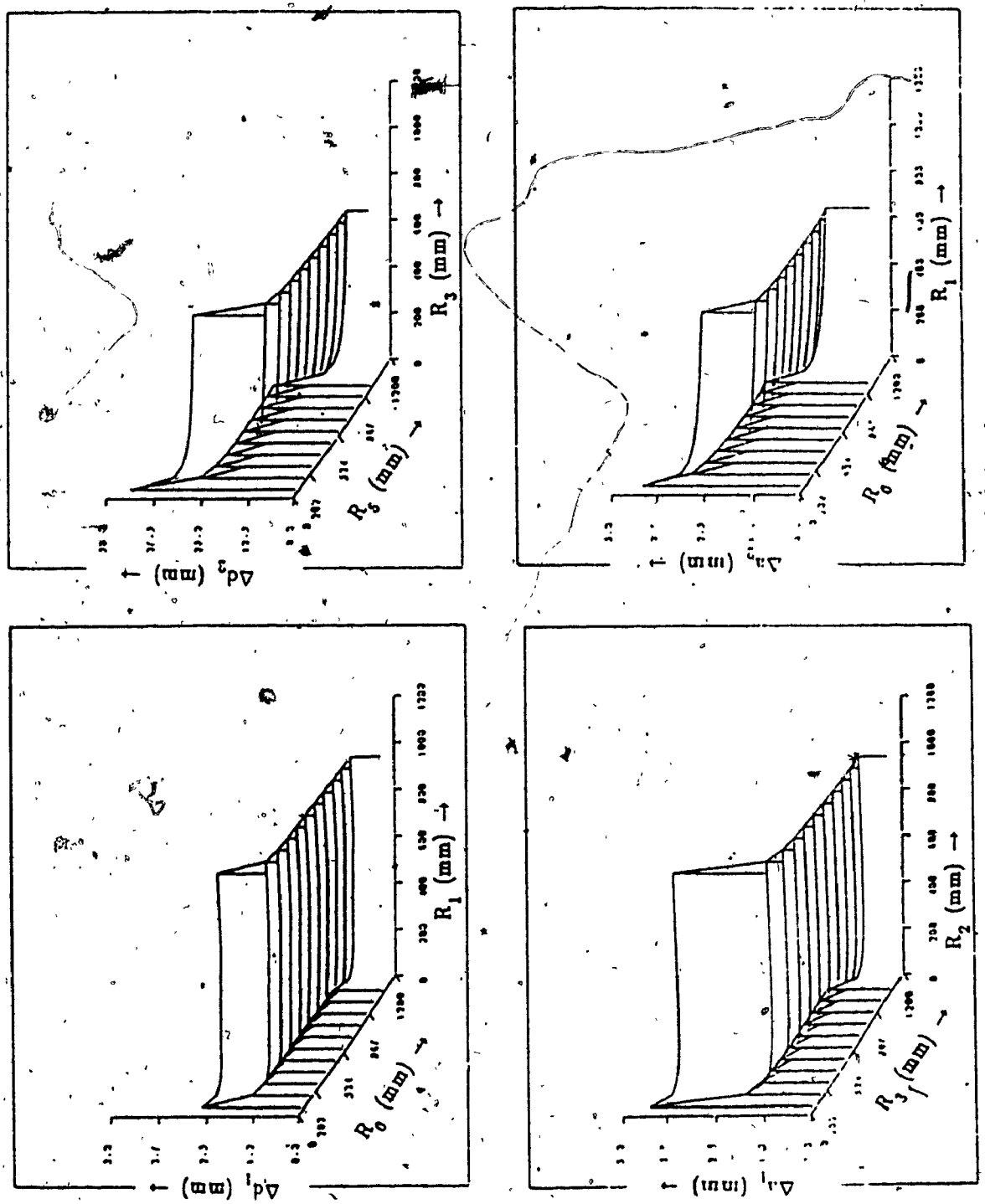

Fig.5.8. Effect of R_1 to R_3 on the link lengths and the offset distances

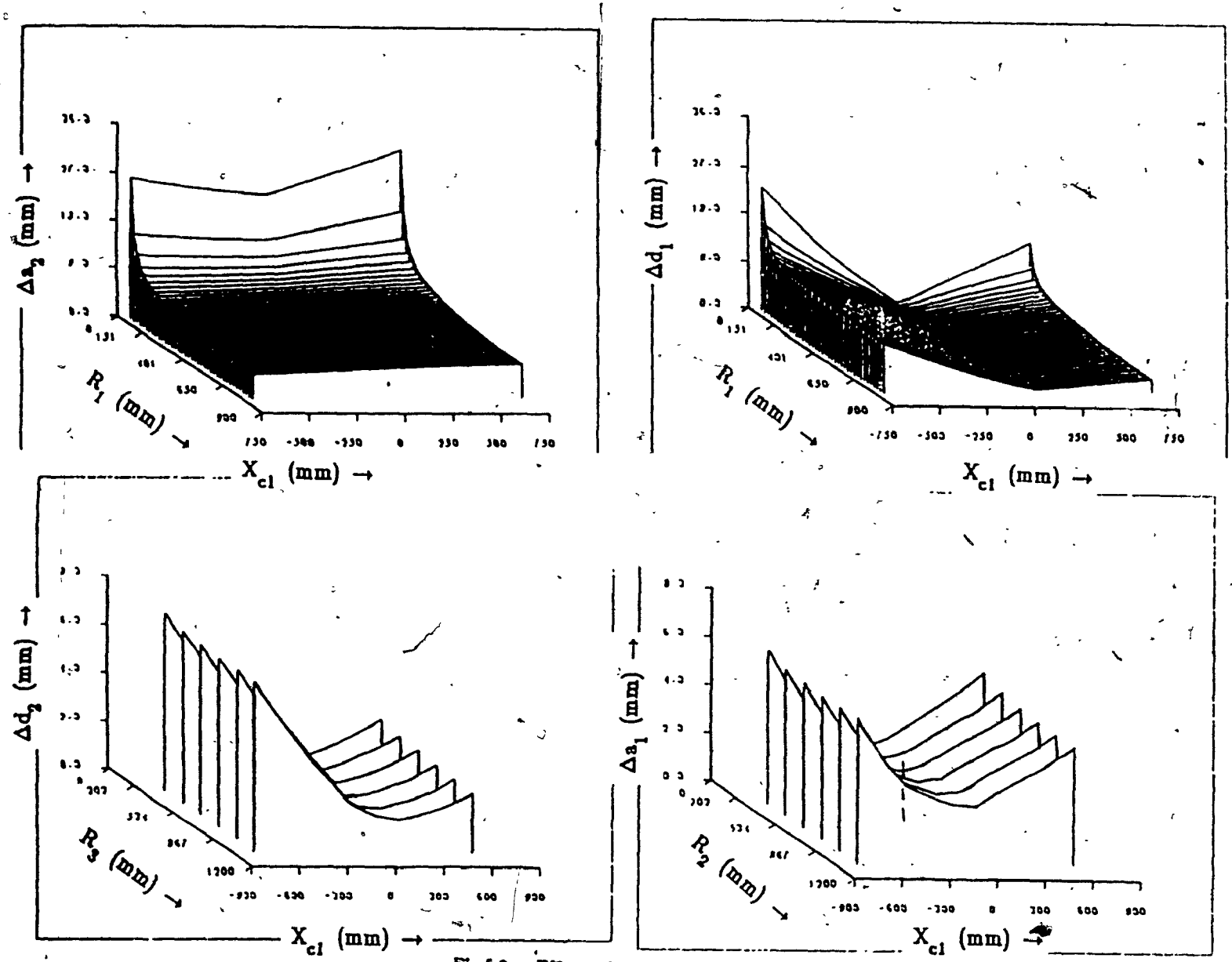

Fig.5.9. Effect of X_{c1} and R_j on the link lengths and the offset distances

Computed Center distances (mm) of the Puma 560 robot joints with respect to R_f

Joint 1 : X_{c1} = 474.9 mm; Y_{c1} = 2853.0 mm; Z_{c1} = **** **; R_1 = 112.4 mm

Joint 2 : X_{c2} = 474.7 mm; Y_{c2} = ****** ; Z_{c2} = 184.9 mm; R_2 = 733.3 mm

Joint 3 : X_{c3} = 474.6 mm; Y_{c3} = ****** ; Z_{c3} = -247.1 mm; R_3 = 301.8 mm

Joint 5 : X_{c5} = 444.9 mm; Y_{c5} = ****** ; Z_{c5} = -679.4 mm; R_5 = 152.4 mm

Joint 6 : X_{c6} = 444.4 mm; Y_{c6} = 3007.4 mm; Z_{c6} = ****** ; R_6 = 360.5 mm

Where ****** - Undefined

Link Parameter	Specified(deg/mm)	Estimated (deg/mm)
θ_{x23}	0.0	0.143
θ_{y23}	0.0	-0.107
θ_{z23}	0.0	-0.152
θ_{x25}	0.0	0.166
θ_{y25}	0.0	-0.010
θ_{z25}	0.0	-0.322
θ_{x46}	0.0	1.202
θ_{y46}	0.0	-0.738
θ_{z46}	0.0	-0.032
a_1	432.0	431.9
a_2	- 20.3	- 29.7
d_1	149.1	154.5
d_2	432.0	432.2
d_3	57.1	56.4

Fig.5.10 Experimental results for the Denawit-Hartenberg parameters

recommended by the design of experiments.

Figure 5.10 present the results from the experiments to estimate the joint coordinates with respect to the reference frame R_f, the joint orientations, the link lengths, and the offset distances.

5.4 Transmission Errors

5.4.1 Error Analysis, Design of Experiments, and Discussions

The accuracy of the estimated joint angle depends on the accuracy of computing the 6 distances from the theodolite angles. As explained in §5.3, this accuracy is controlled by ΔL, $\Delta\gamma_1$, $\Delta\gamma_2$, $\Delta\alpha_i$, $\Delta\beta_i$, and $\Delta\phi_i$. From equation 4.4.1, it can be inferred that the joint angle ${}^{t_{fj}}\theta_{mj}$ can be expressed as,

$$ {}^{t_{fj}}\theta_{mj} = F\ (X_{a1},\ Y_{a1},\ Z_{a1},\ X_{a2},\ Y_{a2},\ Z_{a2}) \qquad (5.4.1) $$

by partially differentiating ${}^{t_{fj}}\theta_{mj}$ with respect to these variables, the effect of small variations in those on ${}^{t_{fj}}\theta_{mj}$ can be evaluated. The relations for the distances X, Y, Z are given by the equations 4.3.1, in §4.3.1, can be used here also. Partially differentiating ${}^{t_{fj}}\theta_{mj}$ with respect to those variables, the estimation error ${}^{t_{fj}}\theta_{mj}$ is given by,

$$
{}^{t_{fj}}\Delta\theta_{mj} = \frac{\partial F}{\partial X_{a1}}\Delta X_{a1} + \frac{\partial F}{\partial X_{a2}}\Delta X_{a2} + \frac{\partial F}{\partial Y_{a1}}\Delta Y_{a1} + \frac{\partial F}{\partial Y_{a2}}\Delta Y_{a2} + \frac{\partial F}{\partial Z_{a1}}\Delta Z_{a1} + \frac{\partial F}{\partial Z_{a2}}\Delta Z_{a2} \qquad (5.4.2)
$$

the error quantities ΔX_{a1}, ΔX_{a2}, ΔY_{a1}, and ΔY_{a2}, and the complete expression for ${}^{t_{fj}}\theta_{mj}$ are given in the Appendix-B.

As in the other sections, here also a computerized estimation error minimization scheme is designed to search for the best combination of the distances X_{a1}, X_{a2}, Y_{a1}, Y_{a2}, Z_{a1}, and Z_{a2} of the reference points A_1 and A_2 respectively that results in minimum estimation error. The inverse trigonometric analysis described in §5.3.1 is used to evaluate the theodolite angles for the distances chosen for analysis. The objective of this scheme can be defined as,

$$
\underset{(X_{cj}, Y_{cj}, Z_{cj}, R_{dj})}{\text{Minimize}} \quad F(\Delta\, {}^{t_{fj}}\theta_{mj}) \qquad (5.4.3)
$$

subject to the physical constraints of the experimental setup.

The importance of the minimization scheme discussed above is supported by the results obtained from the computer runs performed. Figure 5.11 shows the effect of varying R_{dj} and Y on the estimated joint angle for one set of X and Z distances. It can be seen from the plots, initially an increase in the distance R_{dj} decreases the estimation error rapidly and thereafter the effect is less significant. Whereas an increase in the Y distance increases the error monotonically. The minimum error attainable for the given set of ΔL, $\Delta\gamma_1$, $\Delta\gamma_2$, $\Delta\alpha_1$, $\Delta\beta_1$,

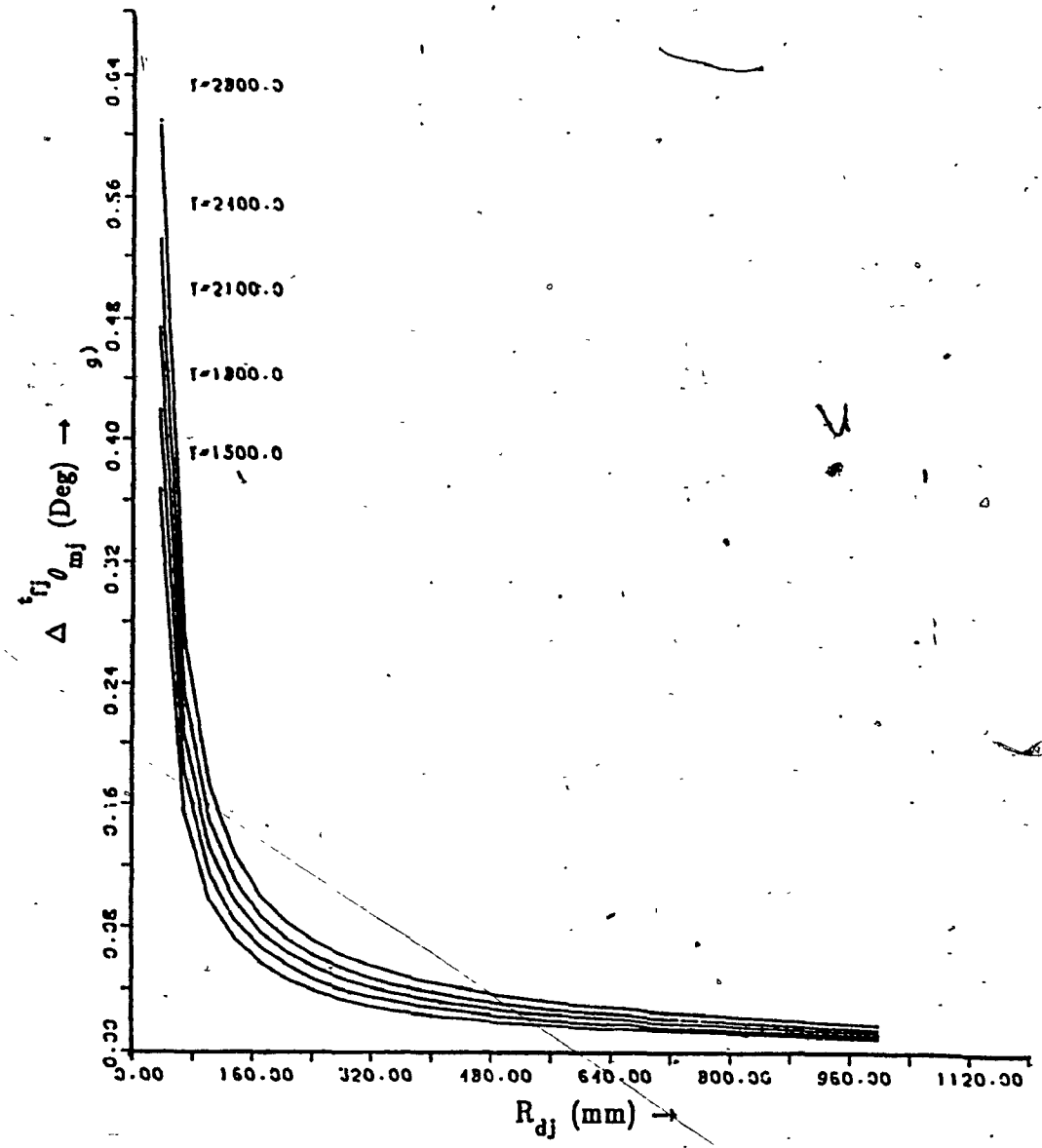

Fig.5.11. Effect of R_{dj} and Y on the estimated joint angle

and $\Delta\phi_i$ is 0.015 deg and is within the joint encoder resolution of the Puma 560 robot.

5.4.2 Experimental Results

The experimental setups shown in fig.5.12 can be used to estimate the transmission errors in the joints 2, 3, 4, and 6 of the Puma 560 robot. The results for the joints 4 and 6 are presented in fig.5.13 and fig.5.14 shows the joint resolutions for those joints. To avoid the effect of backlash, the joints are rotated at slow speeds in one direction only. The estimated joint angle errors has an upper and a lower limit. This is the estimation error. The actual joint angle may lie any where in between the two limits. Hence, curve fitting technique is used to approximate the relationship between the joint angle and the error. One such fitting performed for the joint 4 and 6 have the following relations :

$$K_{\theta_4} = 0.050 \text{ Sin } \frac{9}{10}\,\theta_4$$

$$K_{\theta_6} = 0.047 \text{ Sin } \frac{9}{5}\,\theta_6$$

5.5 Joint Compliance

5.5.1 Error Analysis and Design of Experiments

From equation 4.5.1 it can be seen that the joint stiffness K_j is a function of joint angle θ_{ij}, the external load applied N_j, and the distance between the joint center and the point of application of the load L_j. This is given by,

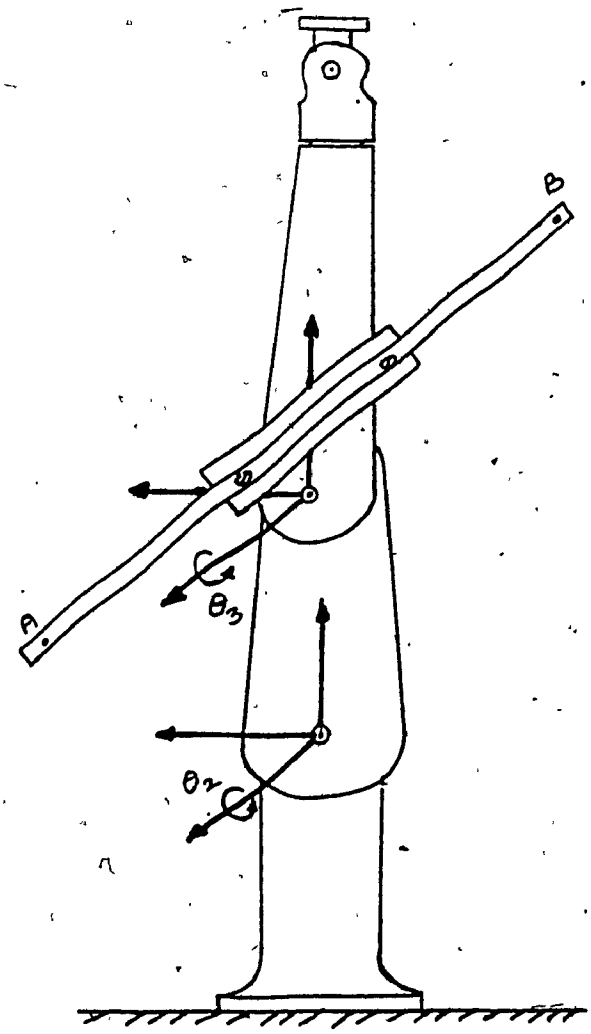

Fig.5.12. Experimental setup for the transmission errors in joints 2,3, 4 & 6 of the Puma 560 robot

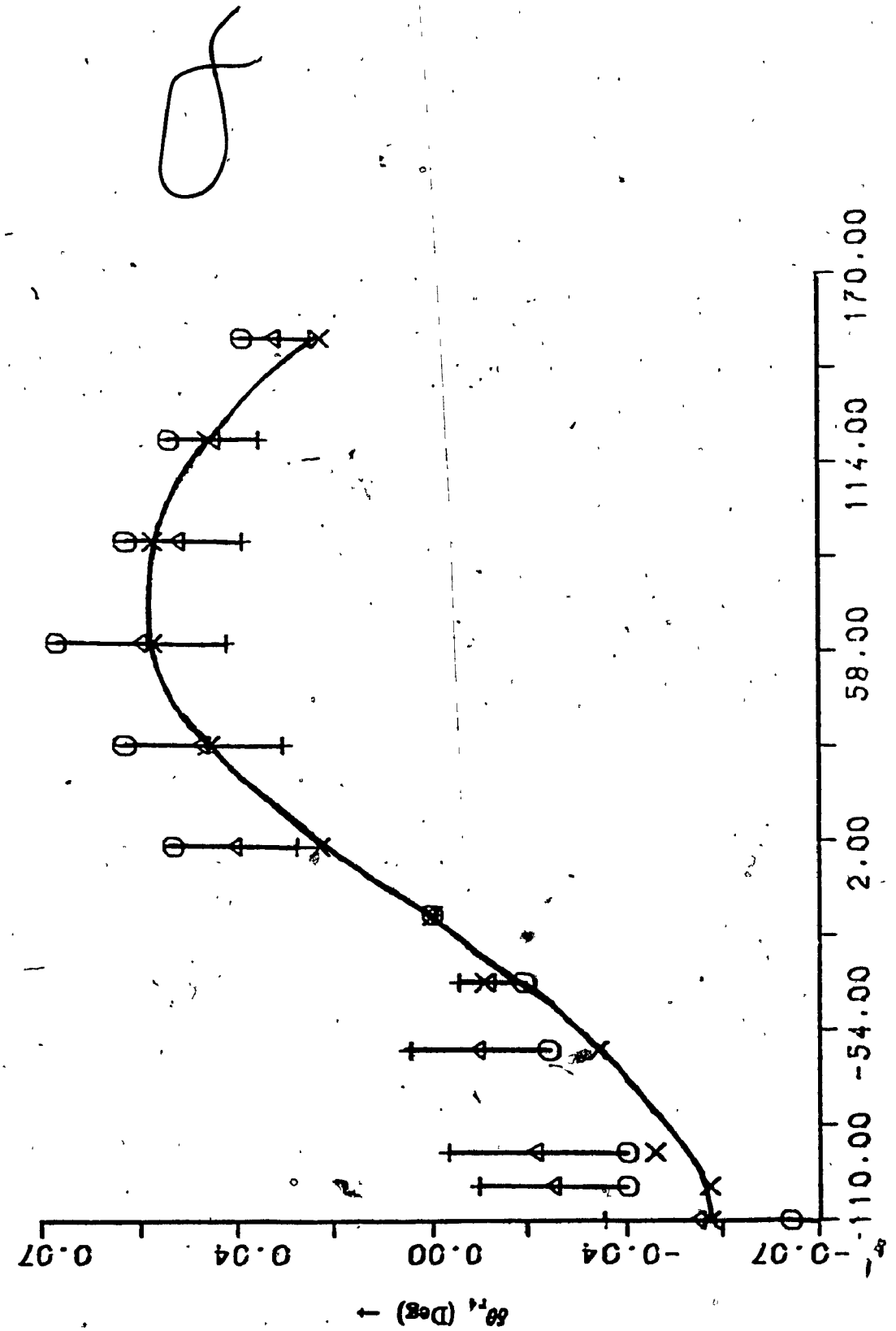

Fig.5.13. Experimental results for the transmission errors in joints 4 & 6 of the Puma 560 robot

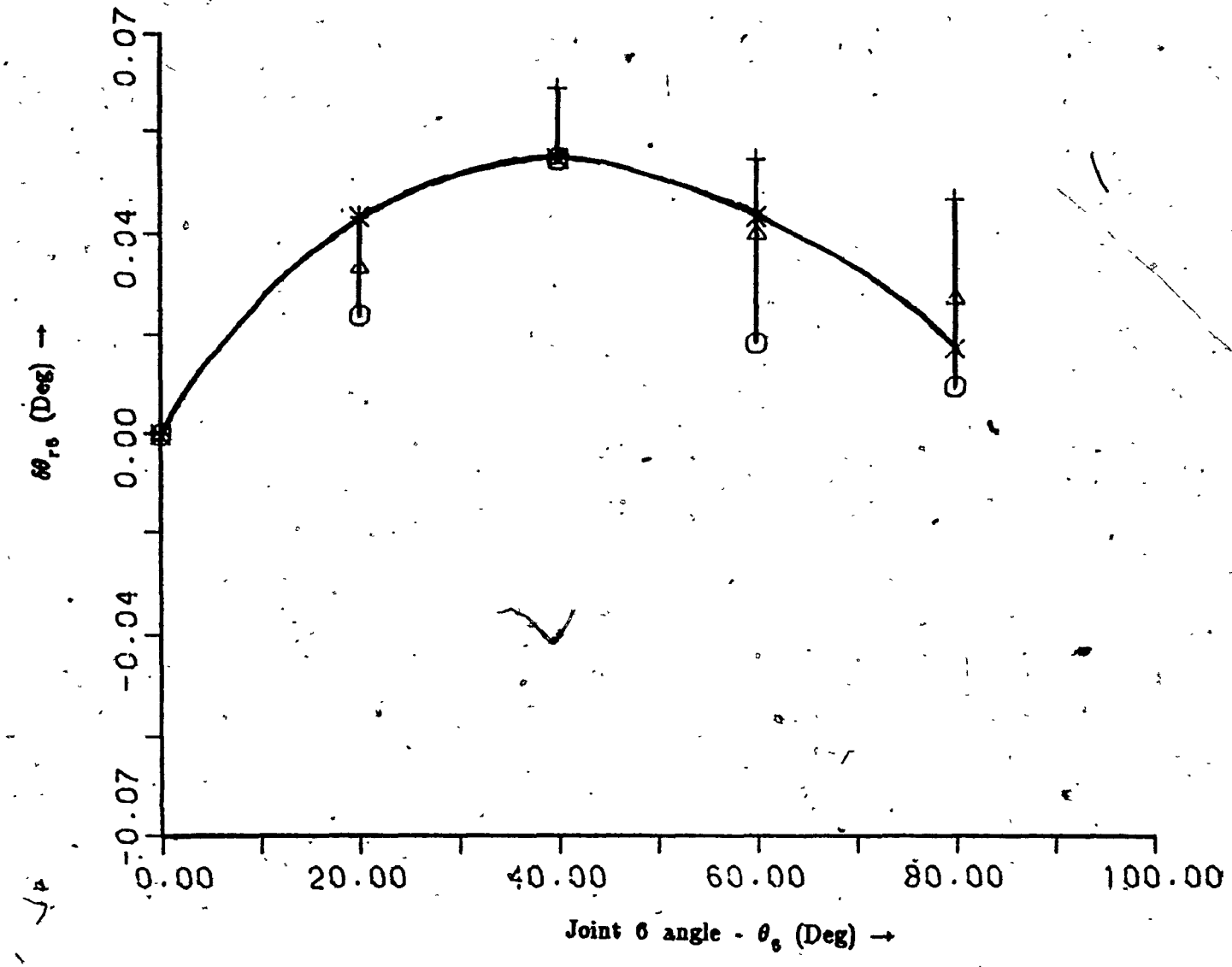

Fig.5.13. Experimental results for the transmission errors in joints 4 & 6 of the Puma 560 robot

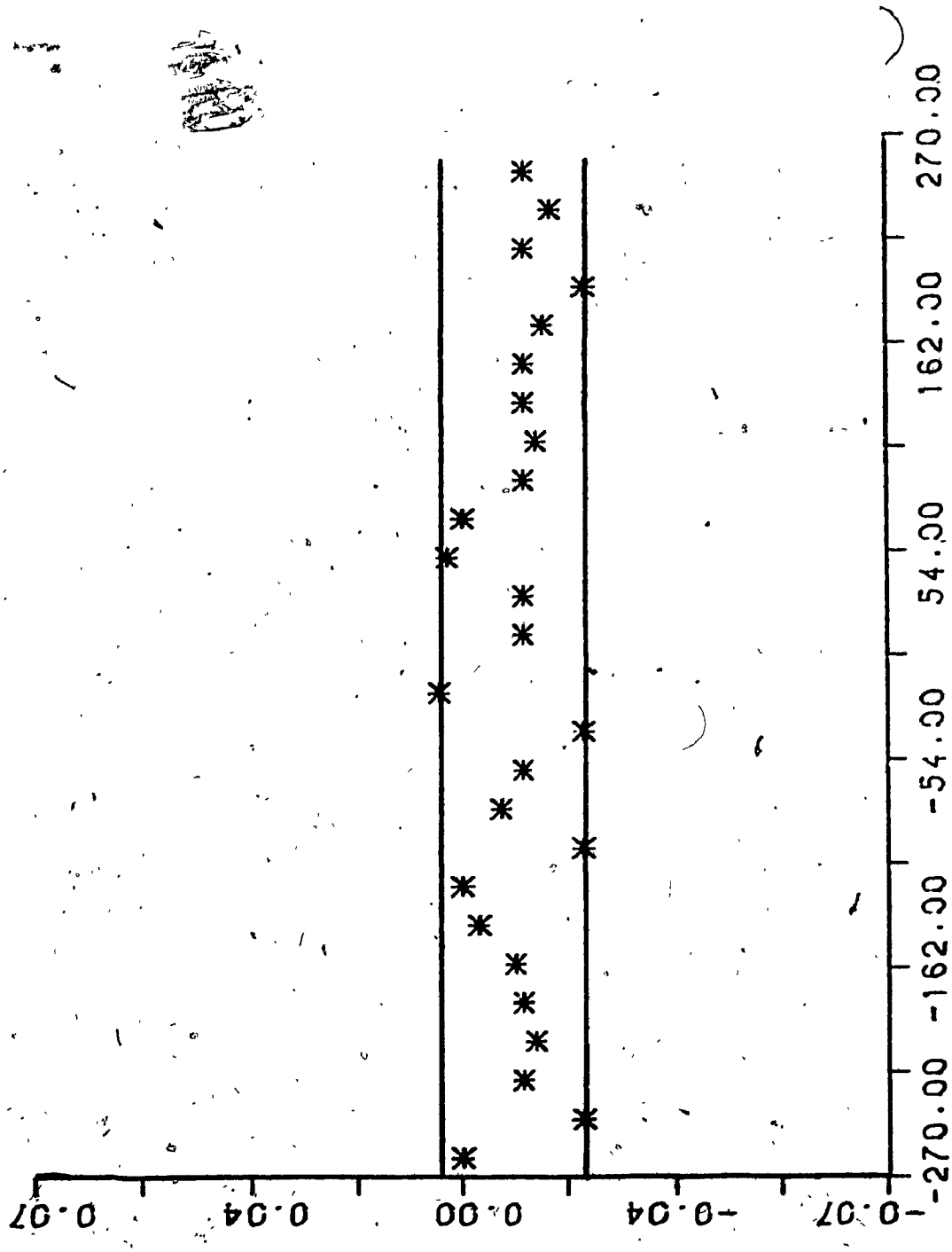

Fig.5.14. Joint encoder resolution for joint 6

$$K_j = f\ (\ \theta_{ij},\ N_j,\ L_j\ ) \qquad (5.5.1)$$

by partially differentiating K_j with respect to its independent parameters, the estimation error ΔK_j can be computed. This is given by,

$$\Delta K_j = \frac{\partial K_j}{\partial \theta_{ij}}\ \Delta\theta_{ij} + \frac{\partial K_j}{\partial N_j}\ \Delta N_j + \frac{\partial K_j}{\partial L_j}\ \Delta L_j \qquad (5.5.2)$$

the expression to compute the error $\Delta\theta_{ij}$ is provided in the previous section. The error ΔL_j can be calculated from the estimation error for the joint center calculations. The error ΔN_j is associated with the accuracy with which the weights were calibrated by the manufacturer.

The objective here is to minimize the estimation errors by minimizing the error terms $\Delta\theta_{ij}$, ΔL_j. It has been shown in the previous sections that these errors in turn can be reduced by the appropriate choice of the joint center location and the radius of rotation. The objective function is given by,

$$\underset{(L, X_{cj}, Y_{cj}, Z_{cj}, R_{pj})}{\text{Minimize}} \qquad f(\Delta K_j)$$

It can be inferred from the discussions presented above that the estimation error ΔK_j can be minimized by reducing the errors $\Delta\theta_{ij}$, and ΔL_j. Sections 5.3.2.1 and 5.4.1 present the discussions for the computerized minimization schemes. Hence it is not necessary here to include a separate analysis on minimizations.

5.5.2 Experimental Results

The experimental setup shown in fig.4.5 is used to compute the joint stiffness of the joints 3 and 4 of the Puma 560 robot. Figures 5.15 and 5.16 presents the results for the same joints. The loads were applied at a distance approximately 500 mm from the joint centers. It can be seen that there is a monotonic increase in the joint angle as the twisting torque is increased. The slope of the joint deflection versus torque remains the same upto a certain value of the twisting torque. After this value, there is a change in the slope with a definite offset. The joint angles were calculated for the decreasing loads also. In this case also after the same joint torque, a change in the torque-deflection curve was observed. This slope is the same as that for the increasing load but with an offset. The stiffness of the joints 3 and 4 computed experimentally are given below :

For Joint 3 :

$K_{jc3} = 1.156 \times 10^5$ lb in/rad. for torque less than 100 lbin.

$K_{jc3} = 1.223 \times 10^5$ lb in/rad. for torque greater than 100 lbin.

For Joint 4 :

$K_{jc4} = 2.275 \times 10^5$ lb in/rad. for torque less than 45 lbin.

$K_{jc4} = 1.698 \times 10^5$ lb in/rad. for torque greater than 45 lbin.

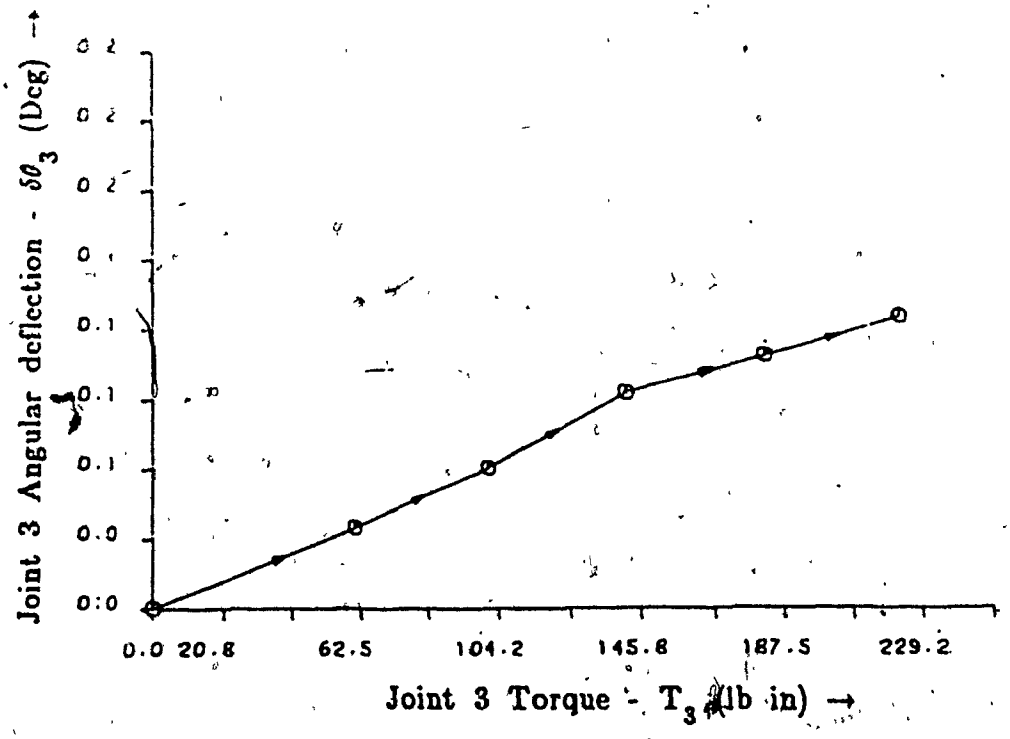

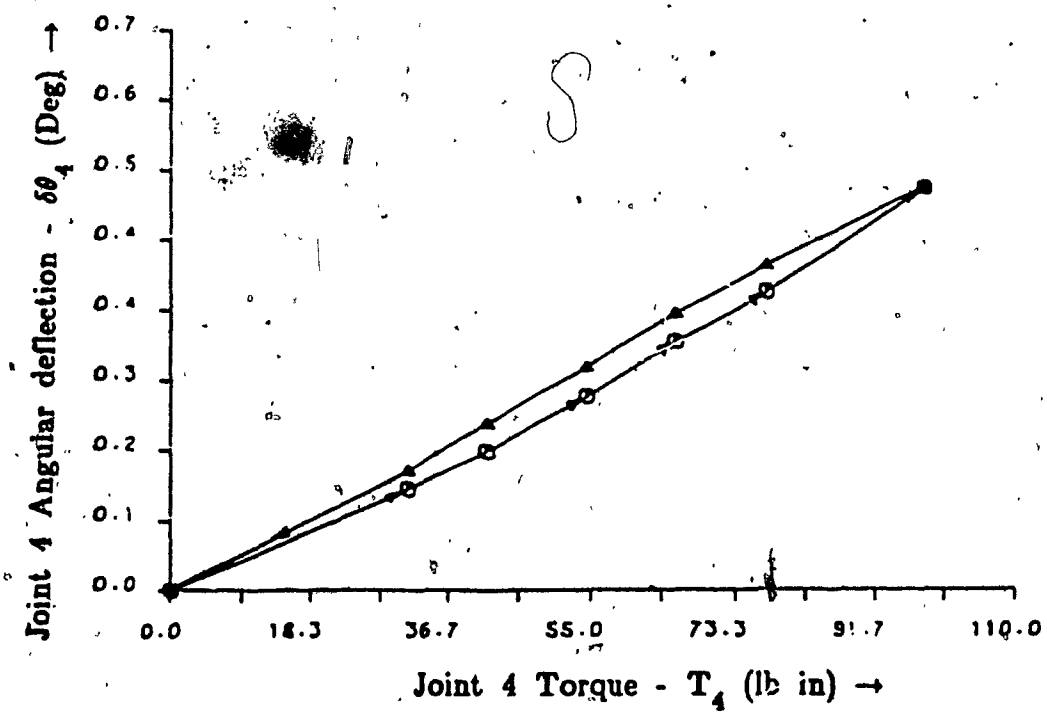

Fig.5.15. Experimental results for joint 3 stiffness

Fig.5.16. Experimental results for joint 4 stiffness

5.6 Cross Coupling Effects

5.6.1 Error Analysis and Design of Experiments

The method proposed in this thesis to evaluate the Cross Coupling effects doesn't involve any mathematical expressions in terms of distances and theodolite angles. The accuracy of the computed joint encoder readings depends on the resolution of the Analog to Digital converter used. Hence an error analysis, design of experiments and discussions on computerized minimization are not neceesary for this particular section.

5.6.2 Discussions on Cross Coupling Effects between the Wrist joints of the Puma 560 robot

The Puma 560 robot uses D.C. servo motors as the actuators. The joint encoders are mounted at the motor end. The wrist joints 4, 5, and 6 of the Puma 560 robot are mechanically coupled and hence exhibits cross coupling effects. Due to this, when the joint 5 motor rotates the joint 6 and/or the motor of the joint 6 also rotates. Similarly when the joint 4 rotates, the joints 5 and 6 and/or the motors of those joints also rotates. Figure 5.17 shows the mechanical arrangement of the wrist joints.

The following discussions explains how cross coupling takes place between the joints 5 and 6. The joint 6 motor and the joint (link) are connected through a drive shaft S6, a bevel gear drive arrangement consisting of the gears G_{61}, and G_{62}, and the pinions P_{61} and P_{62}, where P and G refers to the pinions and the mating gears respectively.

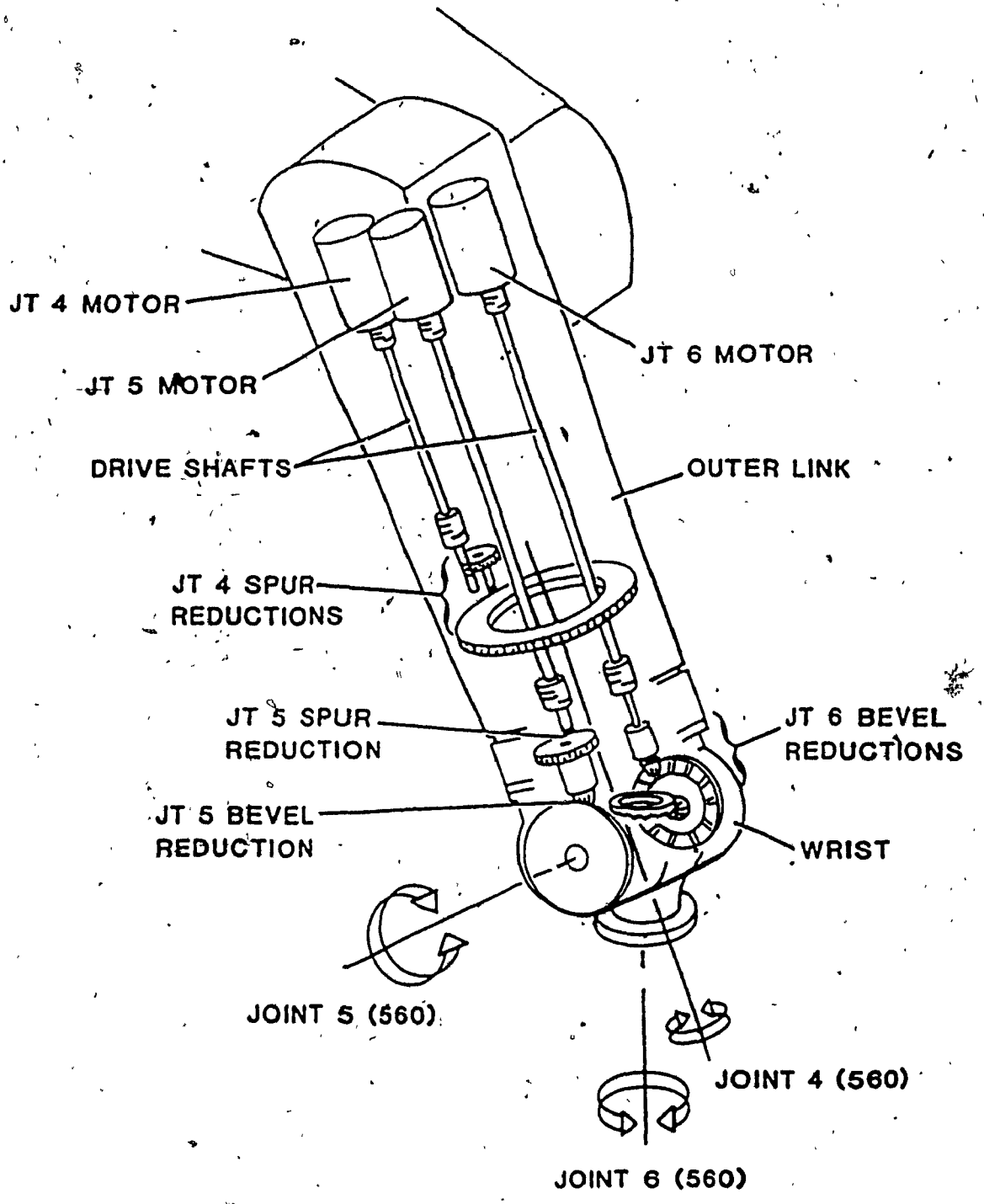

Fig.5.17. Mechanical arrangement of the Puma 560 robot wrist joints

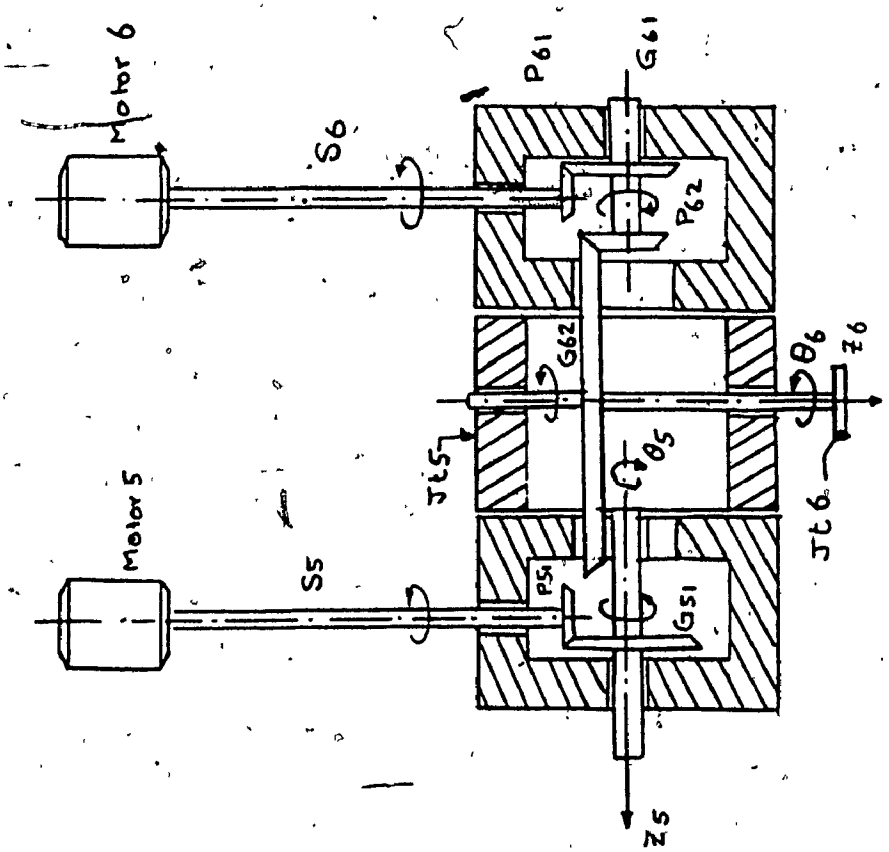

Fig.5.18. Schematic layout of the drive unit for the joints 5 & 6 of the Puma 560 robot

The link 6 is connected to the gear G_{62}. A split section on the wrist is the joint 5 (link 5) of the robot. This houses the gear G_{62}. Hence, when the joint 5 rotates, the split section rotates and therefore the gear G_{62} also moves with it. During this process two things can happen; one is the gear G_{62} may rotate about its axis inside the split section and hence the joint 6 rotates; the other is, it can drive the mating pinion P_{62}, and hence the joint 6 encoder rotates. It is also possible for both actions to take place simultaneously. This arrangement is analogous to the sun-planet arrangement used in differential drive systems and is shown in fig.5.18.

5.6.3 Experimental Results

From these discussions it can be inferred that the magnitude of cross coupling can be estimated by tapping the joint encoders of the joints 5 and 6 while 4 is rotated, and tapping 6 when 5 is rotated. To achieve this, an interface consisting of hardware and software was designed to tap the joint encoders and convert the number of pulses received into joint angles. To evaluate the correction factor σ_{56}, first joint 6 is rotated alone through an angle θ and then joints 5 and 6 are rotated through the same angle together. In both cases the joint encoder of joint 6 is tapped and the joint angles were plotted aginst time. Figure 5.19, shows such plots for θ equal to 10 degrees. σ_{56} is computed as follows :

The joint 6 encoder reading with joint 5 rotation θ_{56} = 11.711 deg
The joint 6 encoder reading without joint 5 rotation θ_6 = 9.909 deg
The error Δ = 1.802 deg for 10 degrees of joint 5 rotation.

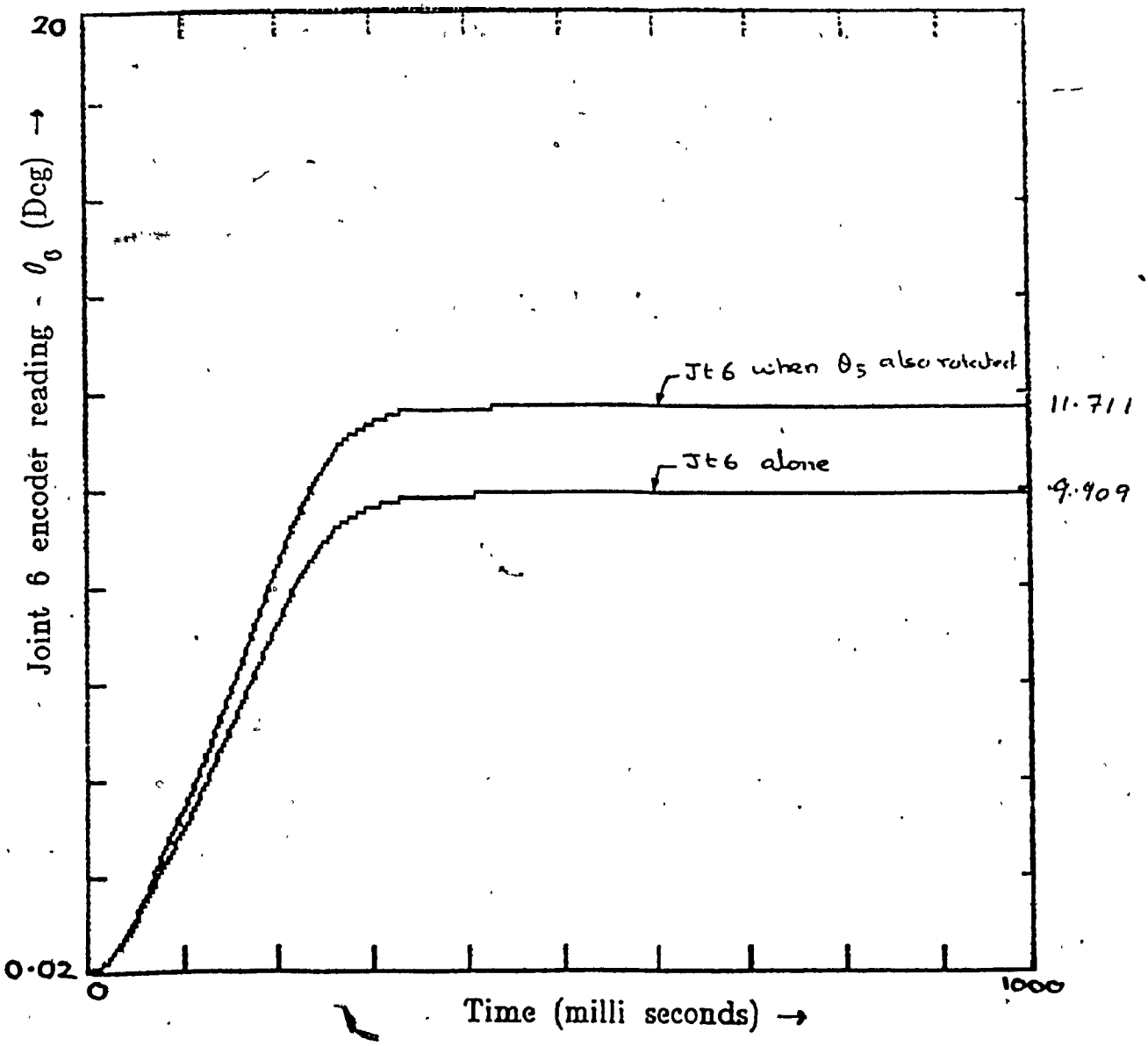

Fig.5.19. Experimental results for the cross coupling between joints 5 & 6

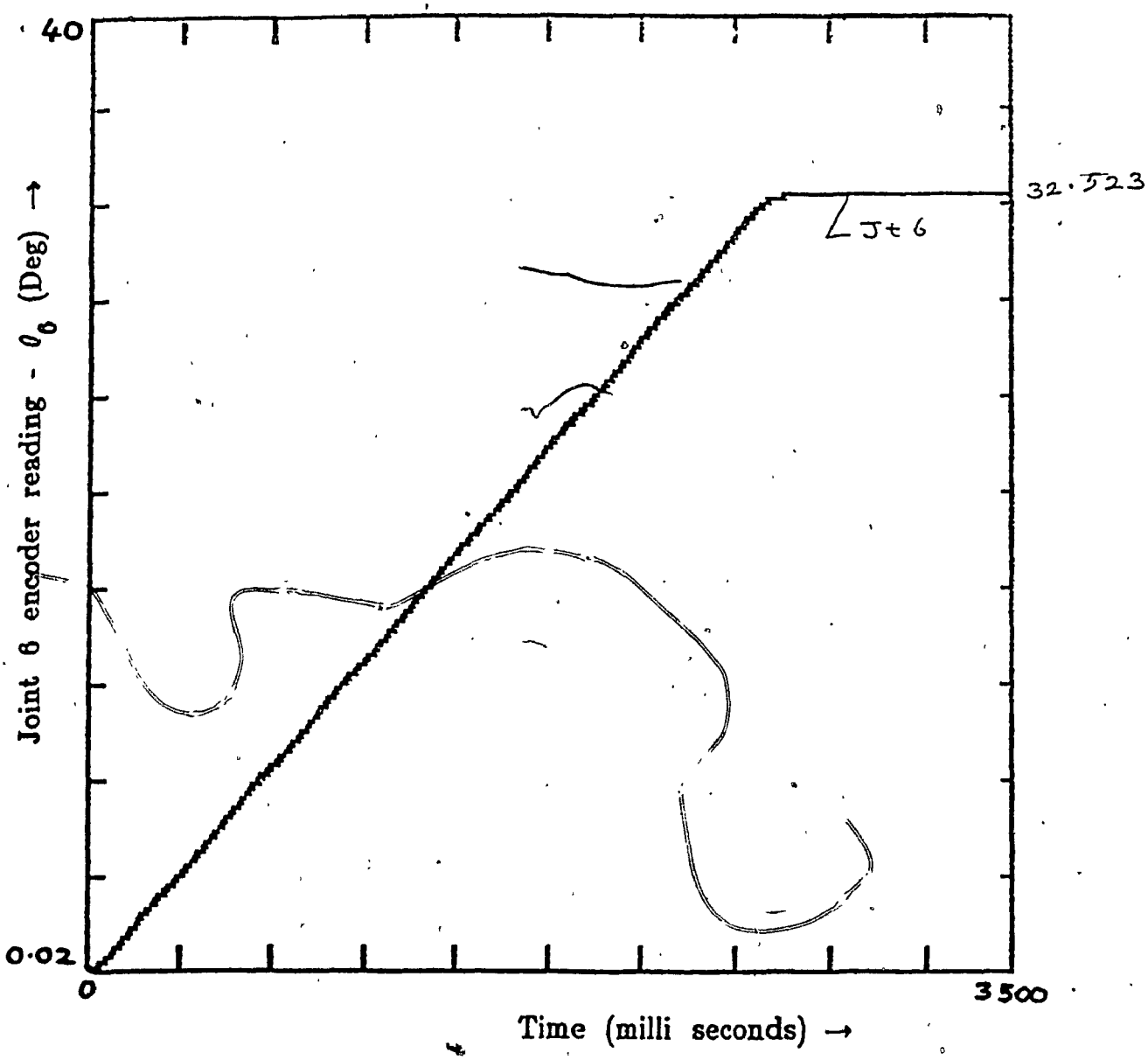

Fig.5.19. Experimental results for the cross coupling between joints 5 & 6

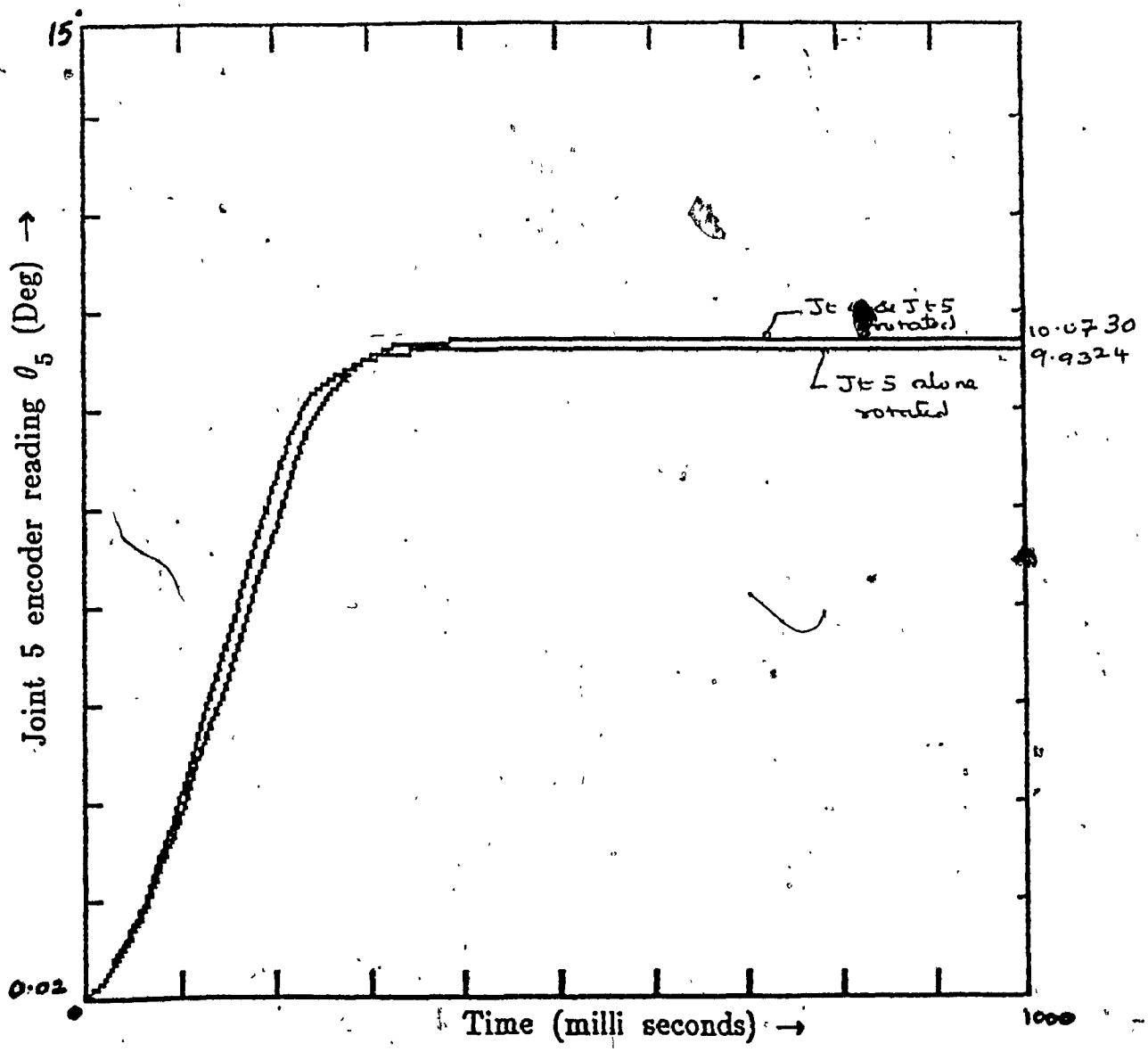

Fig.5.20. Experimental results for the cross coupling between joints 4 and 5 & 6

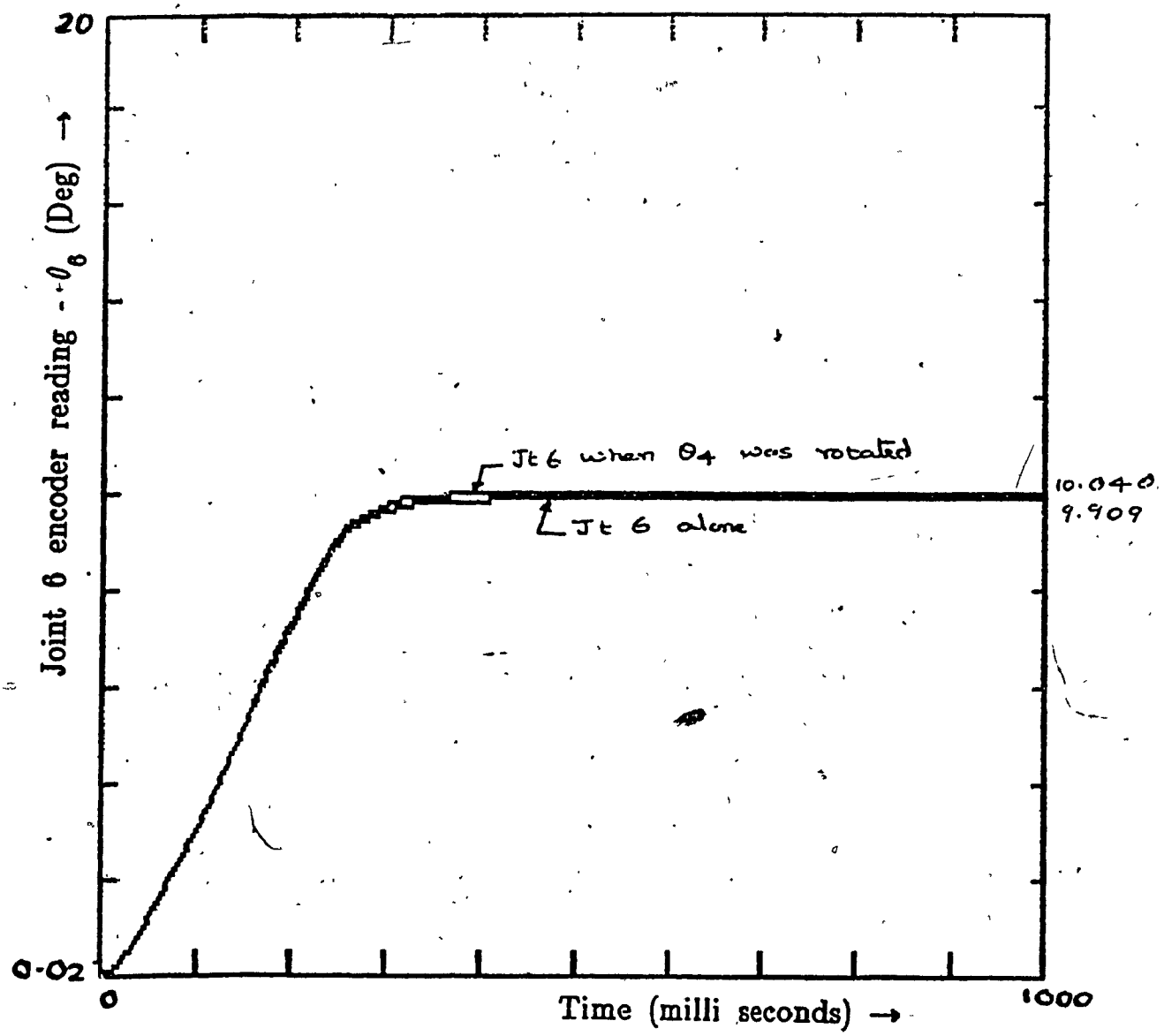

Fig.5.20. Experimental results for the cross coupling between joints 4 and 5 & 6

hence the correction factor σ_{56} is given by,

$$\sigma_{56} = \frac{\Delta}{\theta_5} = \frac{1.802}{10} = 0.1802 \text{ deg/unit rotation of joint 5.}$$

This indicates the joint 6 encoder may rotate through approximately 65 degrees when joint 5 makes 360 degrees. The magnitude of σ_{56} specified in [33,34] for this robot is 0.1806 deg and hence there is little error between the estimated value and the value prescribed by the robot manufacturer. Figure 5.20 shows the results from cross coupling effects in 5 and 6 due to joint 4. The σ_{45} and σ_{46} are evaluated below :

The joint 6 encoder reading with joint 4 rotation $\theta_{46} = 10.040$ deg

The joint 6 encoder reading without joint 4 rotation $\theta_6 = 9.909$ deg
The error $\Delta = 0.131$ deg for 10 degrees of joint 4 rotation.

hence the correction factor σ_{46} is given by,

$$\sigma_{46} = \frac{\Delta}{\theta_4} = \frac{0.131}{10} = 0.0131 \text{ deg/unit rotation of joint 4.}$$

The joint 5 encoder reading with joint 4 rotation $\theta_{45} = 10.073$ deg
The joint 5 encoder reading without joint 4 rotation $\theta_5 = 9.934$ deg
The error $\Delta = 0.141$ Deg for 10 degrees of joint 4 rotation.
hence the correction factor σ_{45} is given by,

$$\sigma_{45} = \frac{\Delta}{\theta_4} = \frac{0.141}{10} = 0.0141 \text{ deg/unit rotation of joint 4.}$$

the error between the magnitudes of these correction factors specified by [33] and those computed above are very small. The sign for the correction factor σ_{46} should be positive instead of being negative as indicated in [33].

5.7 Summary

It can be concluded from this Chapter that the process of evaluating the robot errors and the Denawit-Hartenberg parameters of the robot involves an error referred to as the estimation error in this thesis. This error is due to the readability of the instruments used for calibration and the accuracy associated with the process of measuring the reference distances and lengths. This estimation error can be computed by differentiating partially the mathematical expressions governing the experimental setup to evaluate the robot errors, joint angles, and the Denawit-Hartenberg parameters. This determines the confidence level that can be placed on the measured parameters. It is mandatory that these errors should be less than the repeatability of the robot and the joint encoder resolutions. Hence, it is necessary to minimize the estimation error.

From the results of the estimation error minimization presented here, it can be inferred that the parameters of the experimental setup greatly influences the magnitude of the estimation error for the same resolutions of the instruments and the measuring accuracies of the reference distances. By varying the magnitude of the parameters of the experimental setup, the estimation error can be reduced. The optimum set of experimental parameters of the experimental setup searched using the computerized minimization scheme are used to setup the experimental setups.

This section also presents results from the Puma 560 robot using the technique discussed in this thesis. The link parameters a_1, d_2, and

- d_3 of the Puma 560 robot shows little deviation from the values specified by the manufacturer whereas the parameters d_1, and a_2 exhibits considerable deviations. The joint misalignment analysis shows that there is very little joint misalignment between adjacent joints. Sample results are presented for the transmission errors and joint compliance analyses. Effect of link compliance was found to be negligible compared to the joint compliance. Cross coupling effects were observed between the joints 4, 5, and 6. The correction factor evaluated for this effect were found to be the same as that specified in the literature.

CHAPTER 6

ANOTHER APPROACH TO EVALUATE LINK LENGTHS AND OFFSET DISTANCES

6.1 Introduction

This chapter presents another approach to the process of evaluating the link lengths and the offset distances of robots. To estimate the link lengths and offset distances, the scheme outlined in Chapter 4 relies on a mathematical model which requires manipulation of 5 variables per link. On the other hand to achieve the same goal, the method to be discussed here relies on a mathematical model which manipulates a total of 6 variables for the entire robot(independent of number of links). However it requires the knowledge of the joint errors. It is also necessary to be able to tap the joint angles from the shaft encoders or resolvers. Alternatively, one could depend on the robot controllers to provide a readout of these angular positions.

To achieve better results in both methods, it is advisable to include the deviations from the design joint orientations. Present models of industrial robots usually have 0° or 90° for the joint orientations. Recognizing that the method described here requires joint errors and joint angles as the additional informations, nontheless is simpler mathematical approach compares favourably with the technique in method - 1 in terms of computing time and accumulation of estimation errors.

6.2 Kinematic Equations

This section provides the expressions to evaluate the link lengths and offset distances (a_j, d_j) from the measured tool positions, and tapped joint angles. Let ${}^{R_f}T_w$ be the transformation relating the reference frame R_f and the world frame of the robot given by,

$$
{}^{R_f}T_w = \mathrm{Trans}(X_{c1}, Y_{c1}, Z_{c1})\ \mathrm{Rot}(X, \delta\theta_x)\ \mathrm{Rot}(Y, \delta\theta_y)\ \mathrm{Rot}(Z, \delta\theta_z)
$$

$$
= \begin{bmatrix} 1 & -\delta\theta_z & \delta\theta_y & X_{c1} \\ \delta\theta_z & 1 & -\delta\theta_x & Y_{c1} \\ -\delta\theta_y & \delta\theta_x & 1 & Z_{c1} \\ 0 & 0 & 0 & 1 \end{bmatrix}
$$

where (X_{c1}, Y_{c1}, Z_{c1}) and ($\delta\theta_x$, $\delta\theta_y$, $\delta\theta_z$) are the position and orientation of the world frame of the robot with respect to R_f. Let (X_t, Y_t, Z_t) is the location of the tool with respect to the last (j^{th}) link.

It is shown latter in this section that the relations for the tool coordinates with respect to R_f, are linear functions of the link parameters to be estimated. By moving the robot end-effector to different locations in the workspace, one can generate sufficient number of equations to solve for the parameters applying linear regression techniques. This method uses the joint angle readings, the deviations in the Denawit-Hartenberg parameters α_i, and θ_i i.e., $\Delta\alpha_i$, and $\Delta\theta_i$. The joint angle readings of the robot controller are corrected for the

following joint errors: transmission errors, joint compliance, link compliance, cross coupling effects, and the backlash effects. The actual joint angle θ_{j_a} is given by,

$$\theta_{j_a} = \theta_j \left[1 + K_{t_j} + K_{jc_j} + K_{lc_j} + K_{b_j} \right] + \theta_{j+1} K_{\sigma_{jk}} \qquad (6.1)$$

where K_{t_j}, K_{jc_j}, K_{lc_j}, K_{b_j}, are the correction factors for the j^{th} joint angle for transmission errors, joint compliance, link compliance, and backlash respectively. The factor $K_{\sigma_{jk}}$ is attributed to the cross coupling between the j^{th} and the k^{th} joints.

The tool location is given by,

$${}^{w}T_E = A_1 \, A_2 \, A_3 \, \ldots \, \ldots \, A_j \, {}^{j}E$$

where A_j represents the A-matrices which describes the relationship between joints j and j-1 and ${}^{j}E$ is the fixed transformation between the link j and the end-effector. The link coordinate frames assigned, the link parameter table, and the A-matrices for the Puma 560 robot are given in Chapter 3. The process of computing the effect of deviations in the joint orientations on the A_j-matrices is given in §4.3.1.

The A_j matrices are replaced by the actual matrices $\bar{A}_j$ given as,

$$\bar{A}_j = A_j + dA_j = A_j \, (I + \delta A_j) \qquad (6.2)$$

The net transformation from joint 1 to j with respect to the world

frame is given by,

$$^{w}T_{j} = A_1 A_2 A_3 \ldots \ldots A_j$$

and that of the tool with respect to the world frame can be written as,

$$^{w}T_{E} = A_1 A_2 A_3 \ldots \ldots A_j \, ^{j}E \tag{6.3}$$

and finally the tool coordinates expressed with respect to the reference frame R_f,

$$^{R_f}T_{E} = {}^{R_f}T_{w} A_1 A_2 A_3 \ldots \ldots A_j \, ^{j}E \tag{6.4}$$

$$= \begin{bmatrix} N_x & O_y & A_x & X_e \\ N_y & O_y & A_y & Y_e \\ N_z & O_z & A_z & Z_e \\ 0 & 0 & 0 & 1 \end{bmatrix} \tag{6.5}$$

the matrices are multiplied and the coefficients of the parameters a_j, d_j, X_t, Y_t, Z_t, etc., are collected. The tool location (X_e, Y_e, Z_e) with respect to the reference frame R_f for any given location for the Puma 560 robot is written as,

$$X_e = A_1 d_1 + A_2 d_2 + A_3 d_3 + A_4 a_1 + A_5 a_2 + A_6 X_t + A_7 Y_t + A_8 Z_t + A_9 X_{c1} + A_{10} Y_{c1} + A_{11} Z_{c1}$$

$$Y_e = B_1 d_1 + B_2 d_2 + B_3 d_3 + B_4 a_1 + B_5 a_2 + B_6 X_t + B_7 Y_t + B_8 Z_t + B_9 X_{c1} + B_{10} Y_{c1} + B_{11} Z_{c1}$$

$$Z_e = C_1d_1 + C_2d_2 + C_3d_3 + C_4a_1 + C_5a_2 + C_6X_t + C_7Y_t + C_8Z_t + C_9X_{c1} + C_{10}Y_{c1} + C_{11}Z_{c1} \quad (6.6)$$

Where A_k, B_k, C_k, k=1,2,...11 are the coefficients computed for the location under consideration.

The tool coordinates (X_e,Y_e,Z_e) for the Puma 560 robot are given as,

Let,

$$R_f T_n = \begin{bmatrix} n_x & o_y & a_x & p_x \\ n_y & o_y & a_y & p_y \\ n_z & o_z & a_z & p_z \\ 0 & 0 & 0 & 1 \end{bmatrix}$$

$$X_e = P_x - \delta\theta_z P_y + \delta\theta_y P_z + X_{c1}$$
$$Y_e = P_y - \delta\theta_x P_z + \delta\theta_z P_x + Y_{c1}$$
$$Z_e = P_z - \delta\theta_y P_x + \delta\theta_x P_y + Z_{c1}$$

Where P_x, P_y, P_z are written as,

$$P_x = X_t n_x + Y_t o_x + Z_t a_x + p_x$$
$$P_y = X_t n_y + Y_t o_y + Z_t a_y + p_y$$
$$P_z = X_t n_z + Y_t o_z + Z_t a_z + p_z$$

The expressions for p_x, p_y, and p_z are given below :-

$$p_x = d_3\{C_1C_4C_5\cos(\theta_2-\theta_3) + C_1C_5\sin(\theta_3-\theta_2) + S_1S_4S_5\} +$$

$$d_2C_1\text{Sin}(\theta_3-\theta_2) + a_2C_1\text{Cos}(\theta_2-\theta_3) + a_1C_1C_2 - d_1S_1 -$$

$$X_t\{C_1\text{Cos}(\theta_2-\theta_3)\{C_4C_5C_6 - S_4S_6\} - C_1S_5C_6\text{Sin}(\theta_3-\theta_2) +$$

$$S_1S_4C_5C_6 + S_1C_4S_6\} - Y_t\{-C_1\text{Cos}(\theta_2-\theta_3)\{C_4C_5S_6+S_4C_6\} +$$

$$C_1S_5S_6\text{Sin}(\theta_3-\theta_2) - S_1S_4C_5S_6 + S_1C_4C_6\} + Z_t\{C_1C_4S_5\text{Cos}(\theta_2-\theta_3)$$

$$+ C_1C_4S_5\text{Sin}(\theta_3-\theta_2) + S_1S_4S_5\}$$

$$p_y = d_3\{-S_1C_4S_5\text{Sin}(\theta_2-\theta_3) + S_1C_5\text{Cos}(\theta_3-\theta_2) - C_1S_4S_5\} +$$

$$d_2S_1\text{Cos}(\theta_3-\theta_2) + a_2S_1\text{Cos}(\theta_2-\theta_3) + a_1S_1C_2 - d_1C_1 -$$

$$X_t\{S_1\text{Sin}(\theta_2-\theta_3)\{C_4C_5C_6 - S_4S_6\} - S_1S_5C_6\text{Cos}(\theta_3-\theta_2) -$$

$$C_1C_4C_5C_6 - C_1C_4S_6\} - Y_t\{-S_1\text{Sin}(\theta_2-\theta_3)\{C_4C_5S_6+C_4C_6\} +$$

$$-S_1S_5S_6\text{Cos}(\theta_3-\theta_2) + C_1S_4C_5S_6 - C_1C_4C_6\} +$$

$$Z_t\{-S_1C_4C_5\text{Sin}(\theta_2-\theta_3) + S_1C_4C_5\text{Cos}(\theta_3-\theta_2) - C_1S_4S_5\}$$

$$p_z = d_3\{-C_4S_5\text{Sin}(\theta_3-\theta_2) + C_5\text{Cos}(\theta_2-\theta_3)\} + d_2\text{Cos}(\theta_2-\theta_3) +$$

$$a_2\text{Sin}(\theta_2-\theta_3) + a_1S_2 - X_t\{\text{Sin}(\theta_2-\theta_3)\{C_4C_5S_6+S_4C_6\} -$$

$$S_5C_6\text{Cos}(\theta_2-\theta_3) - Y_t\{\text{Sin}(\theta_2-\theta_3)\{C_4C_5S_6+S_4C_6\} +$$

$$S_5S_6\text{Cos}(\theta_2-\theta_3)\} + Z_t\{-C_4S_5\text{Sin}(\theta_2-\theta_3) + C_5\text{Cos}(\theta_2-\theta_3)\} \quad (6.7)$$

Where the notations S_1, S_2, C_1, C_2, etc., represents $\text{Sin}\theta_1$, $\text{Sin}\theta_2$, $\text{Cos}\theta_1$, $\text{Cos}\theta_2$, etc.

6.3 Error Analysis, Design of Experiments and Discussions

From equation 6.6, it can be inferred that the accuracy of evaluating the link lengths and the offset distances a_j and d_j are functions of the accuracy associated with the process of estimating the the tool positions X_e, Y_e, Z_e. The relationship between a_j, d_j and the tool positions is given by,

$$(a_j, d_j) = G_2(X_e, Y_e, Z_e) \quad (6.8)$$

differentiating the expressions for the tool positions with respect to a_j, d_j, X_{c1}, Y_{c1}, Z_{c1}, X_t, Y_t, Z_t, the expression containing the differential quantities can be arrived as,

$$\begin{aligned}
\Delta X_e &= A_{11}\,\Delta a_1 + A_{12}\,\Delta a_2 + A_{13}\,\Delta d_1 + A_{14}\,\Delta d_2 + A_{15}\,\Delta d_3 \\
&\quad + A_{16}\,\Delta X_{c1} + A_{17}\,\Delta X_t + A_{18}\Delta Y_t \\
\Delta Y_e &= B_{11}\,\Delta a_1 + B_{12}\,\Delta a_2 + B_{13}\,\Delta d_1 + B_{14}\,\Delta d_2 + B_{15}\,\Delta d_3 \\
&\quad + B_{16}\,\Delta X_{c1} + B_{17}\,\Delta X_t + B_{18}\Delta Y_t \\
\Delta Z_e &= C_{11}\,\Delta a_1 + C_{12}\,\Delta a_2 + C_{13}\,\Delta d_1 + C_{14}\,\Delta d_2 + C_{15}\,\Delta d_3 \\
&\quad + C_{16}\,\Delta X_{c1} + C_{17}\,\Delta X_t + C_{18}\Delta Y_t
\end{aligned} \quad (6.9)$$

these simultaneous equations can be solved using linear regression techniques and the error quantities can be evaluated.

It can be seen that the tool position can be changed by varying the joint angles (θ_1 to θ_6), the location of the world coordinate frame with respect to R_f (X_{c1}, Y_{c1}, Z_{c1}) and the tool dimensions (X_t, Y_t, Z_t). As mentioned in the previous section, the estimation error can be minimized by changing the distances. The objective function can be defined as,

$$\begin{aligned} &\underset{(X_{cj},Y_{cj},Z_{cj},X_t,Y_t,Z_t)}{\text{Minimize}} && f_1(\Delta a_j) \\ &\underset{(X_{cj},Y_{cj},Z_{cj},X_t,Y_t,Z_t)}{\text{Minimize}} && f_2(\Delta d_j) \end{aligned} \qquad (6.10)$$

a. Effect of X_{c1} and X_t

The effect of X_{c1} and X_t on the estimated values of the link lengths and the offset distances (a_2, a_1, d_3, d_2, d_1) and the world frame location (X_{c1}, Y_{c1}, Z_{c1}) and the tool dimensions (X_t, Y_t) is shown in fig.5.10. At low values of X_{c1} distance, for d_2, X_{c1}, increase in the X-tool distance increases the estimation errors initially and thereafter exhibits less influence. For d_3, d_1, X_t, and Y_t, a similar change increases the errors monotonically. For a similar variation the estimation error decreases for a_2, and d_1. For all parameters, increase in the X_{c1} distance shows monotonic decrease in the errors.

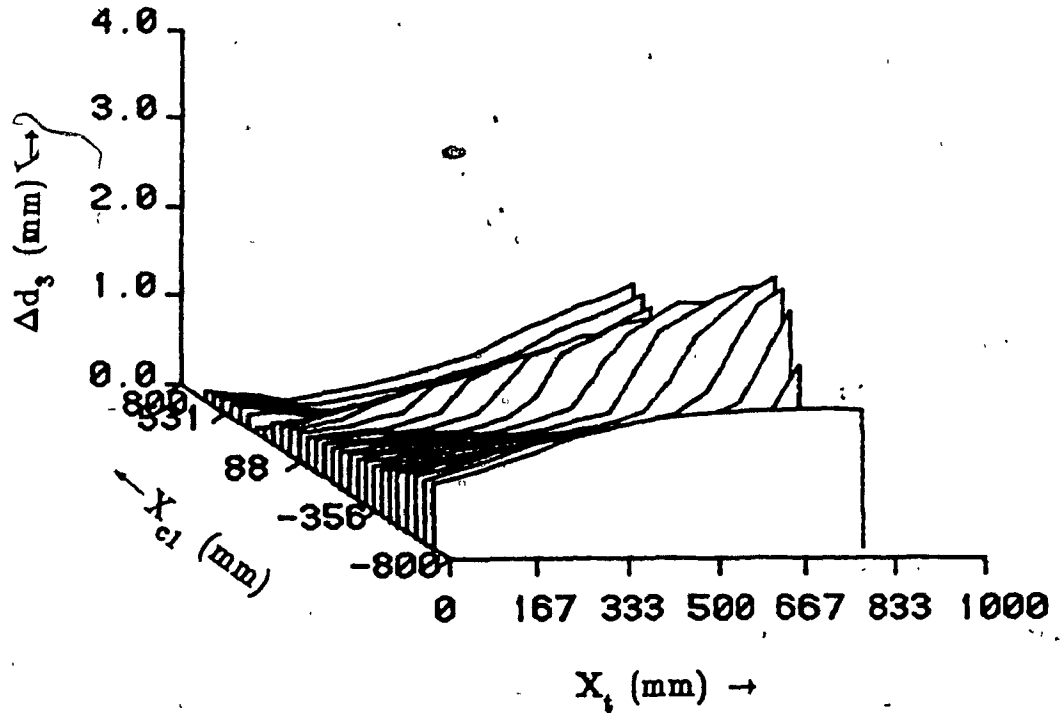

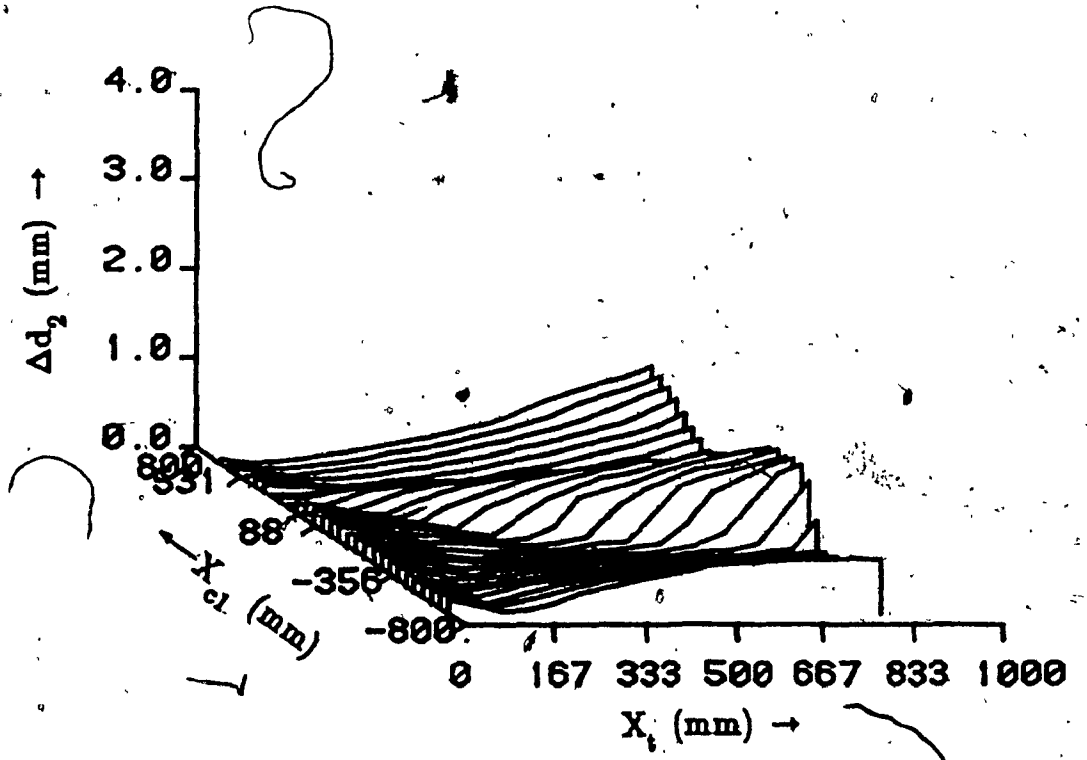

Fig.6.1. Effect of X_{c1} and X_t on the link lengths and the offset distances

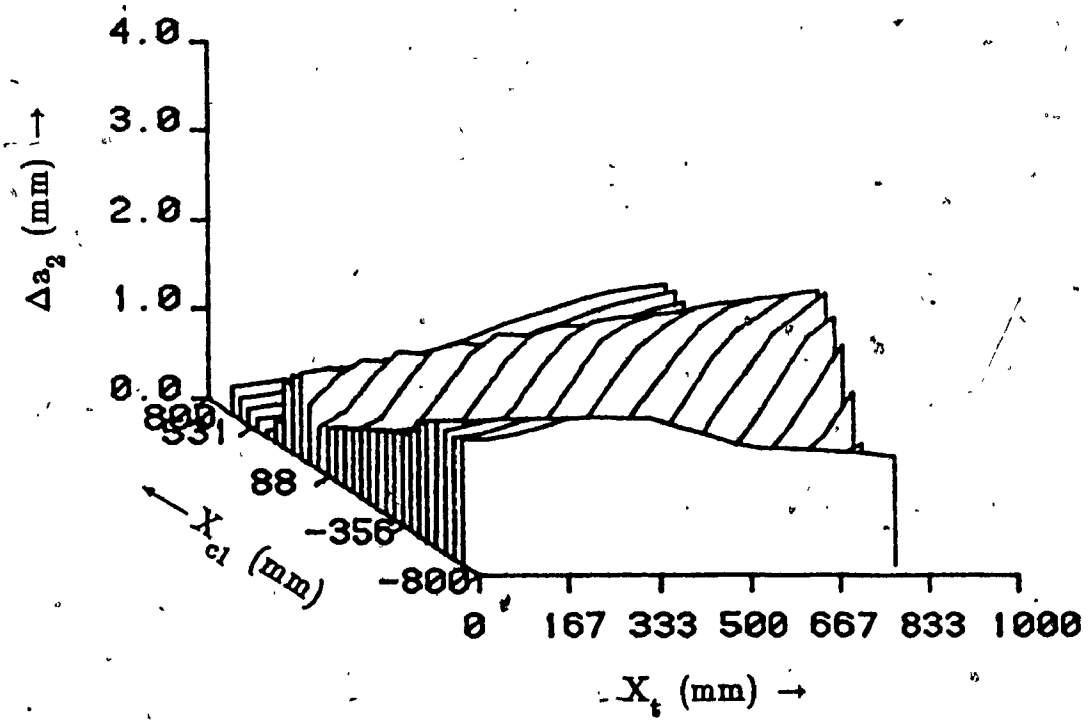

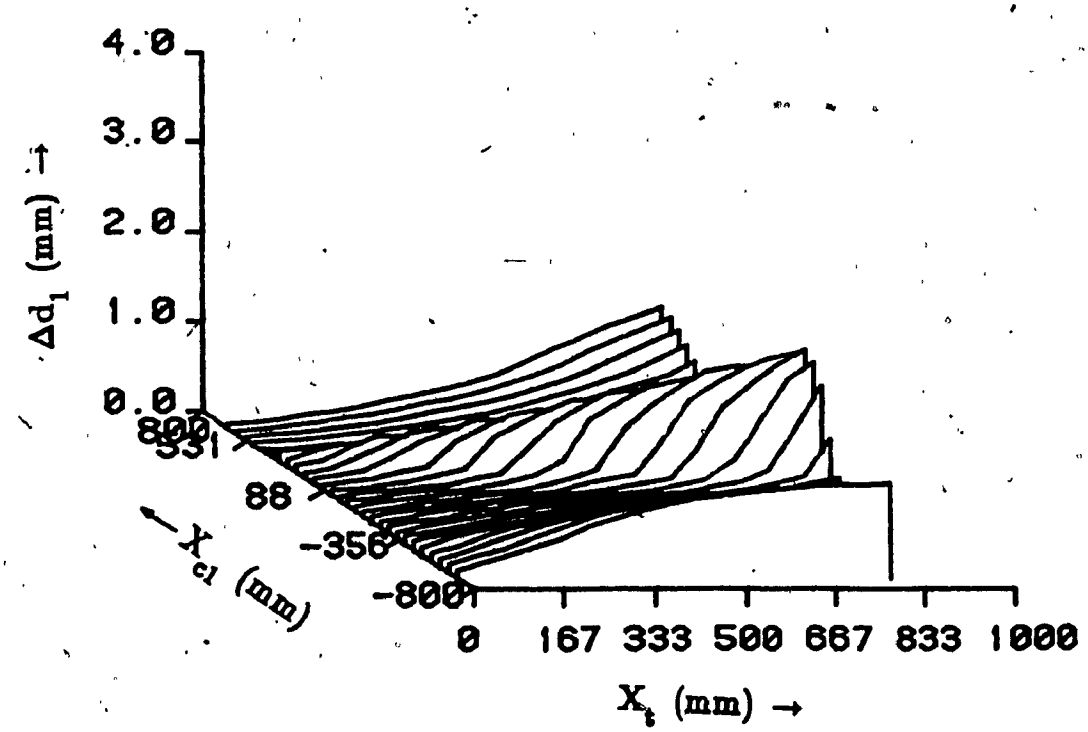

Fig.6.1. Effect of X_{c1} and X_t on the link lengths and the offset distances

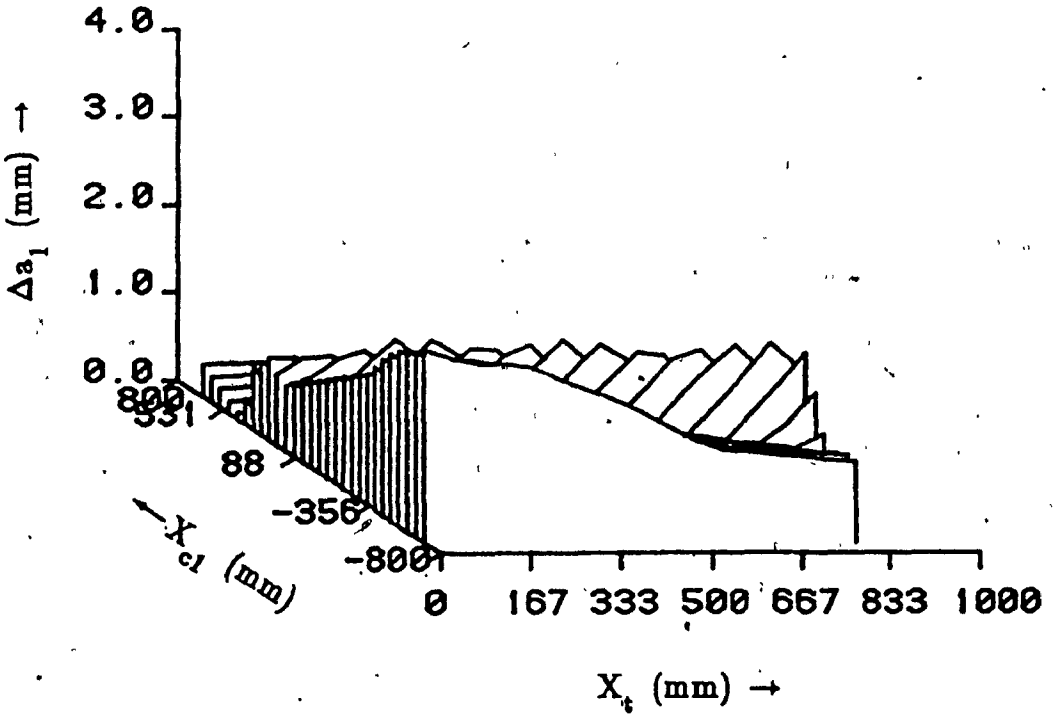

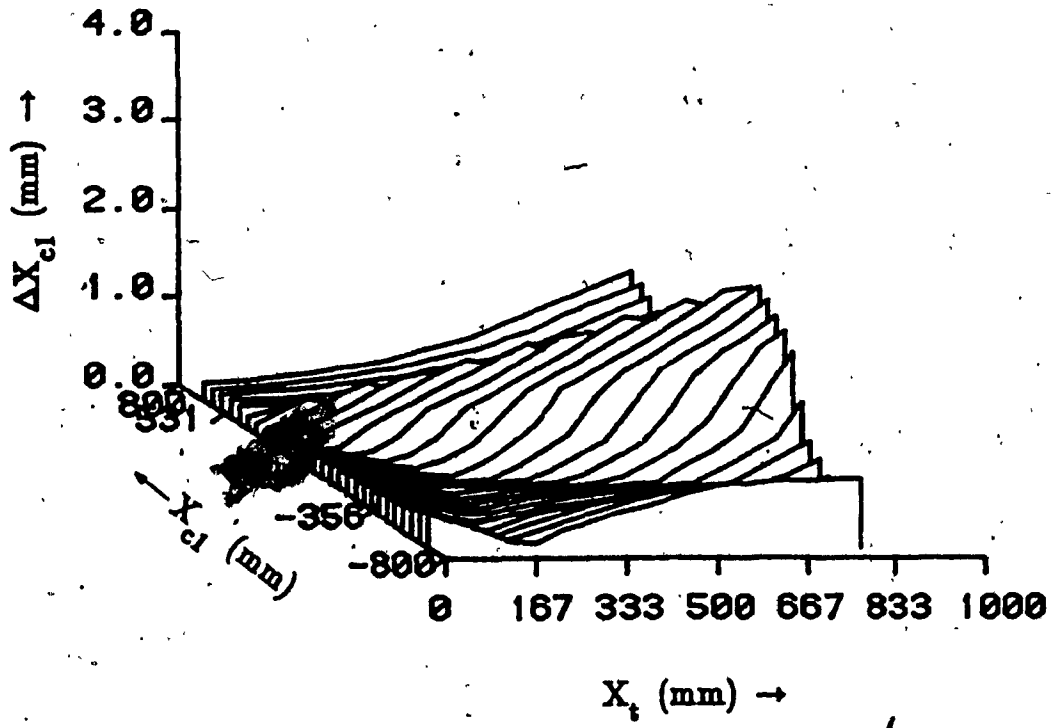

Fig.6.1. Effect of X_{c1} and X_t on the link lengths and the offset distances

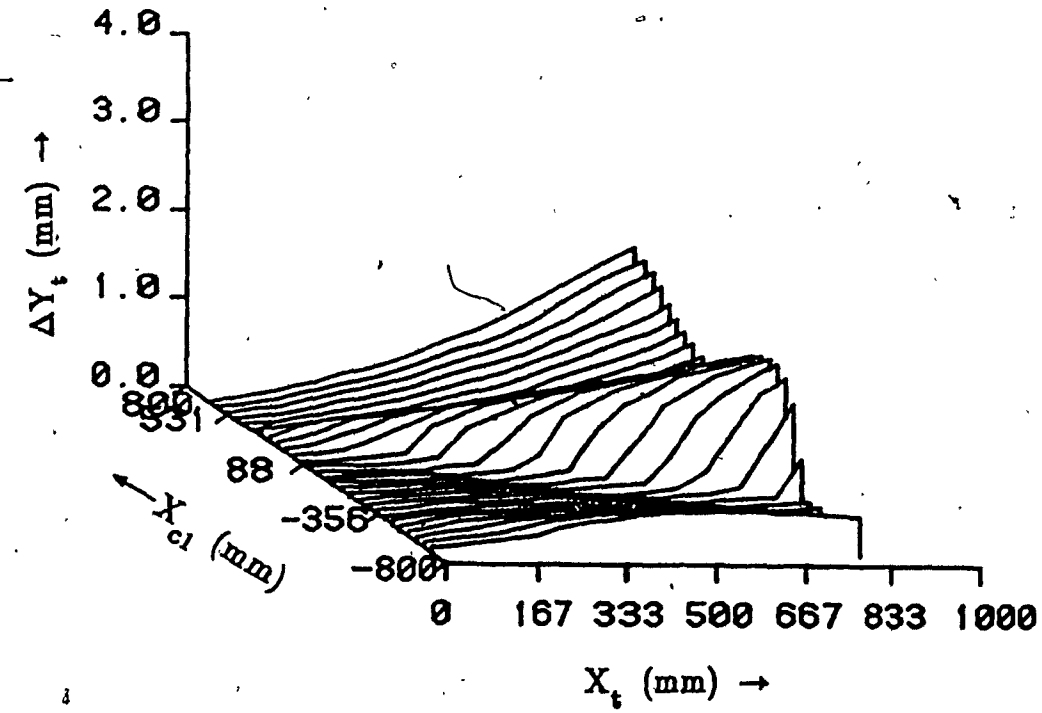

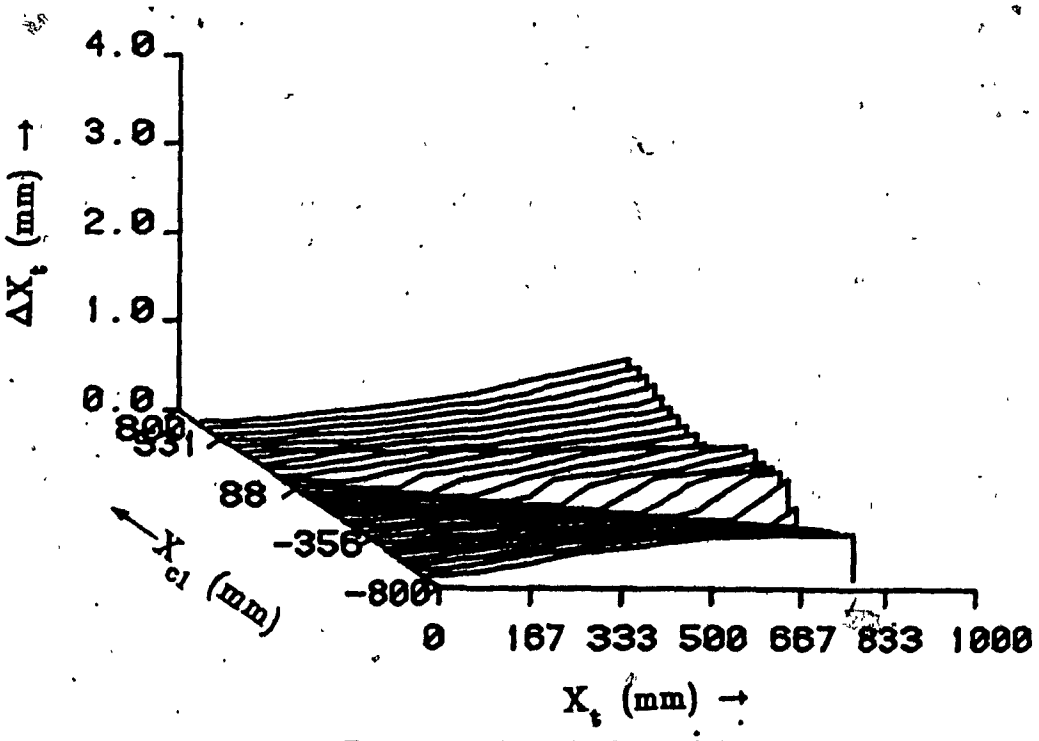

Fig.6.1. Effect of X_{c1} and X_t on the link lengths and the offset distances

b. Effect of X_{c1} and Y_t

Figure 5.11 presents the influence of X_{c1} and Y_t on the estimated values of the link lengths, offset distance, the location of the world frame, and the tool dimensions. For all parameters initially increase in the X_{c1} distance decreases the errors drastically and thereafter increases and decreases again and again. Hence the minima are only local in nature. For all parameters except a_1, an increase in the Y_t distance increases the estimation error monotonically. The error plot for a_1 exhibits monotonic decrease as Y_t is increased.

c. Effect of X_{c1}, and Z_t

The influence of X_{c1}, and Z_t on the estimated parameters is presented in fig.5.12. For variations in the X_{c1} distance, the error characteristics exhibited for all parameters is similar to that explained above for X_{c1}, and Y_t. For all parameters except a_2, a_1, and d_2, the estimation errors decreases when Z_t is increased. A similar change produces increase in the estimation errors for a_2, and a_1. For d_1, the estimation error initially decreases and increases monotonically thereafter.

6.4 Experimental Results

This chapter presents only the methodology of the approach to evaluate link lengths and offset distances. The experimental results are not included as they are beyond the scope of this thesis. However, to illustrate the correctness of the mathematical model, the manufacture's specifications for the link parameters, the joint angle informations provided by the robot controller, and the assumed tool location values

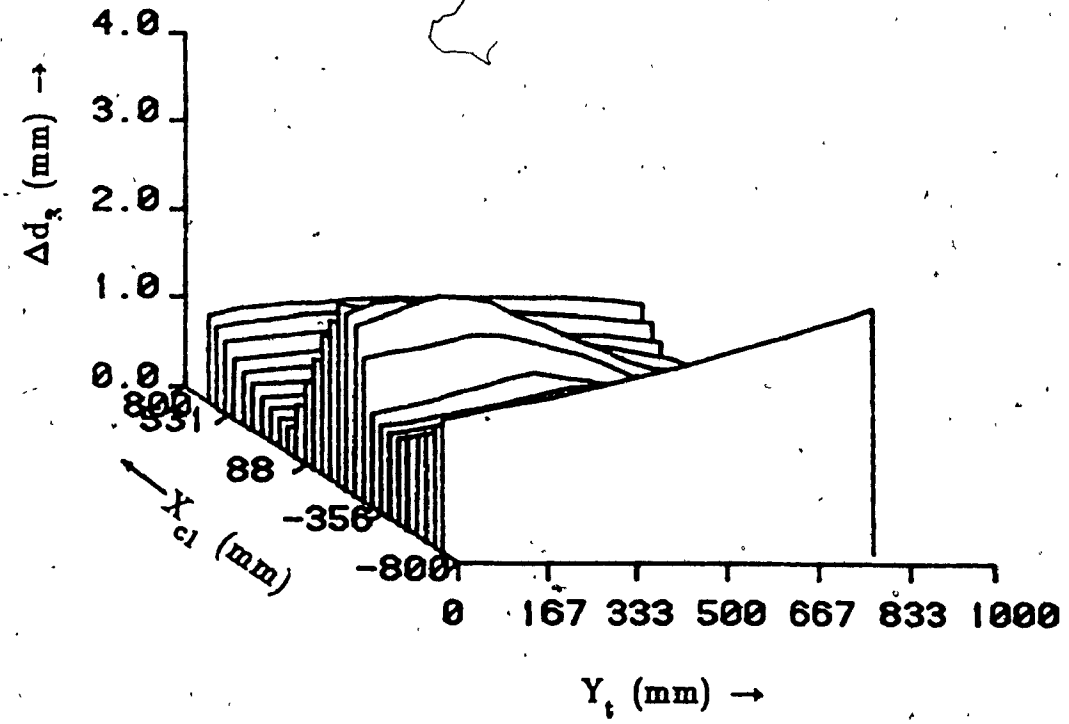

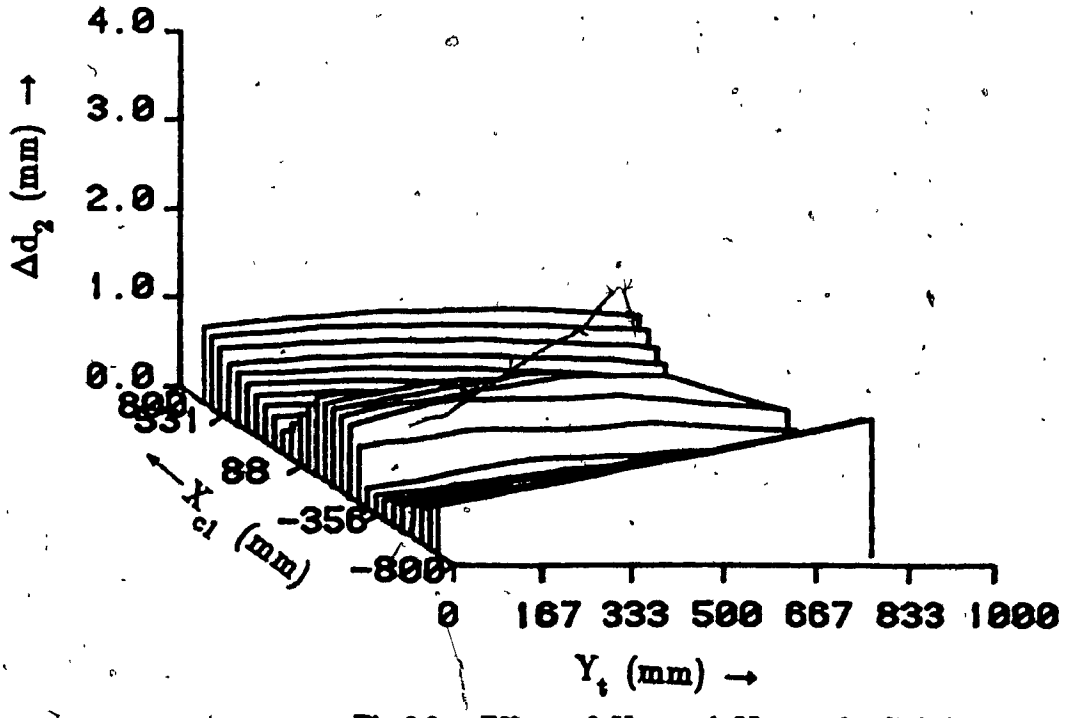

Fig.6.2. Effect of X_{c1} and Y_t on the link lengths and the offset distances

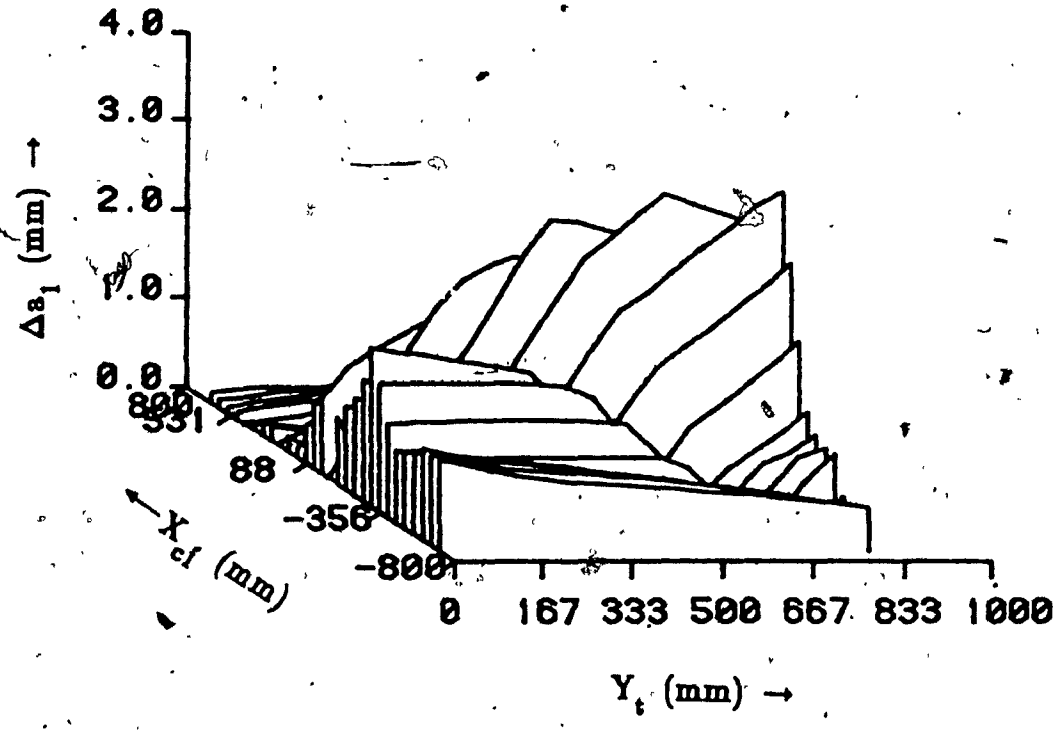

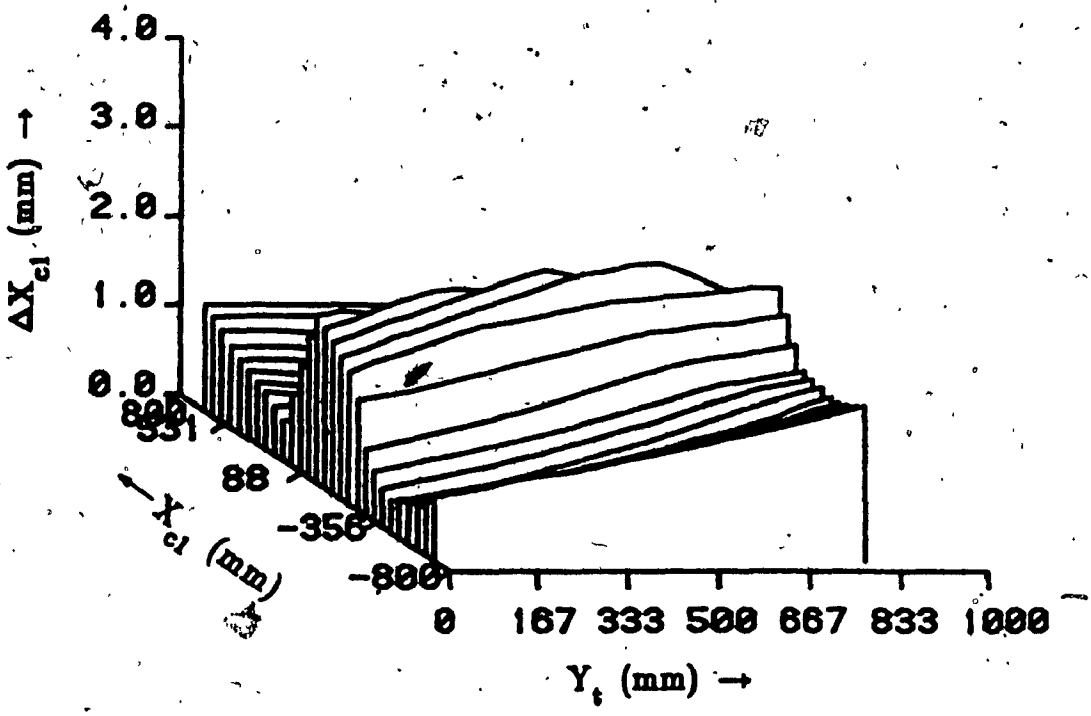

Fig.6.2. Effect of X_{c1} and Y_t on the link lengths and the offset distances

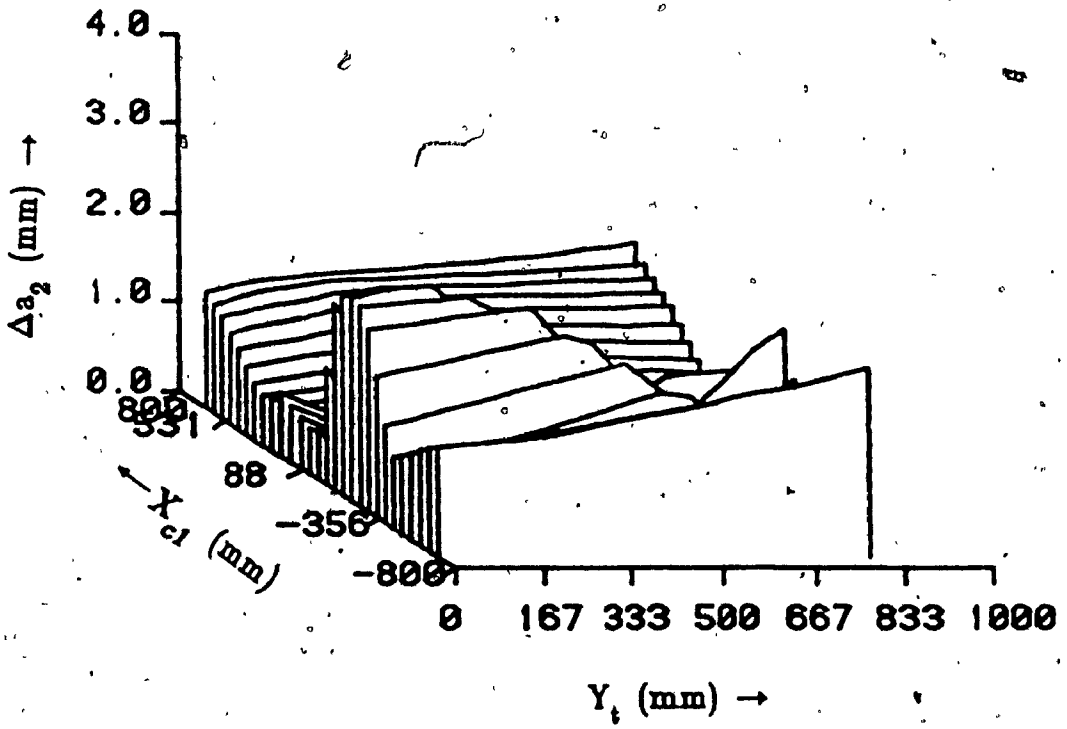

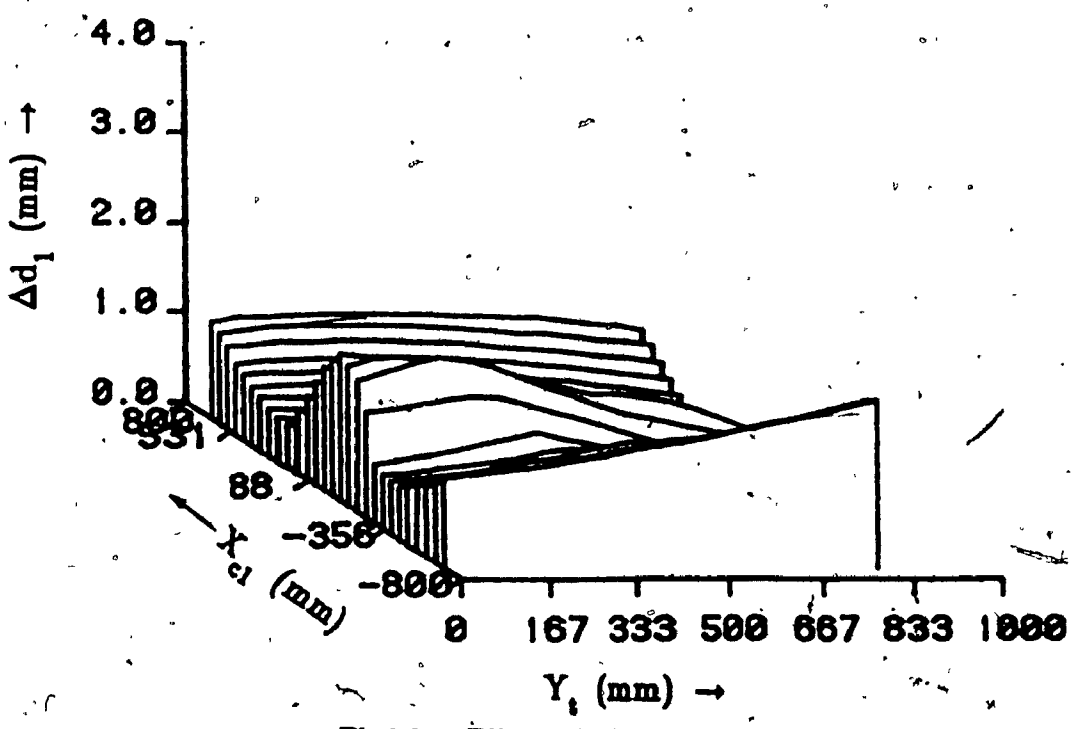

Fig.6.2. Effect of X_{c1} and Y_t on the link lengths and the offset distances

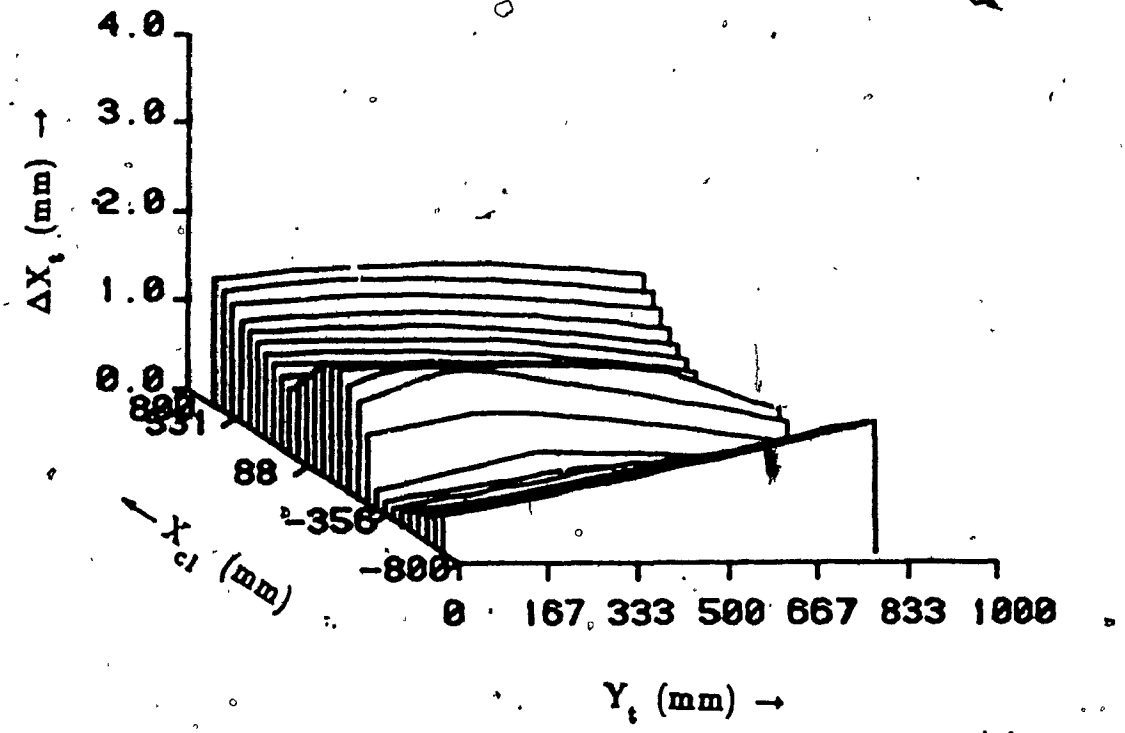

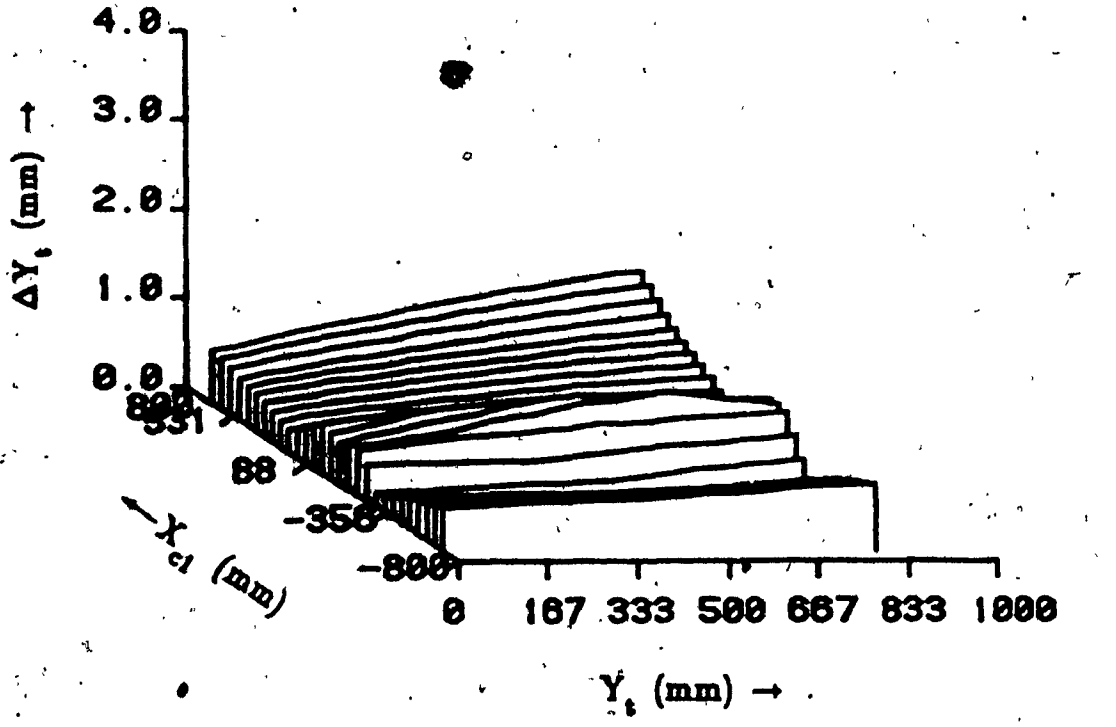

Fig.6.2. Effect of X_{c1} and Y_t on the link lengths and the offset distances

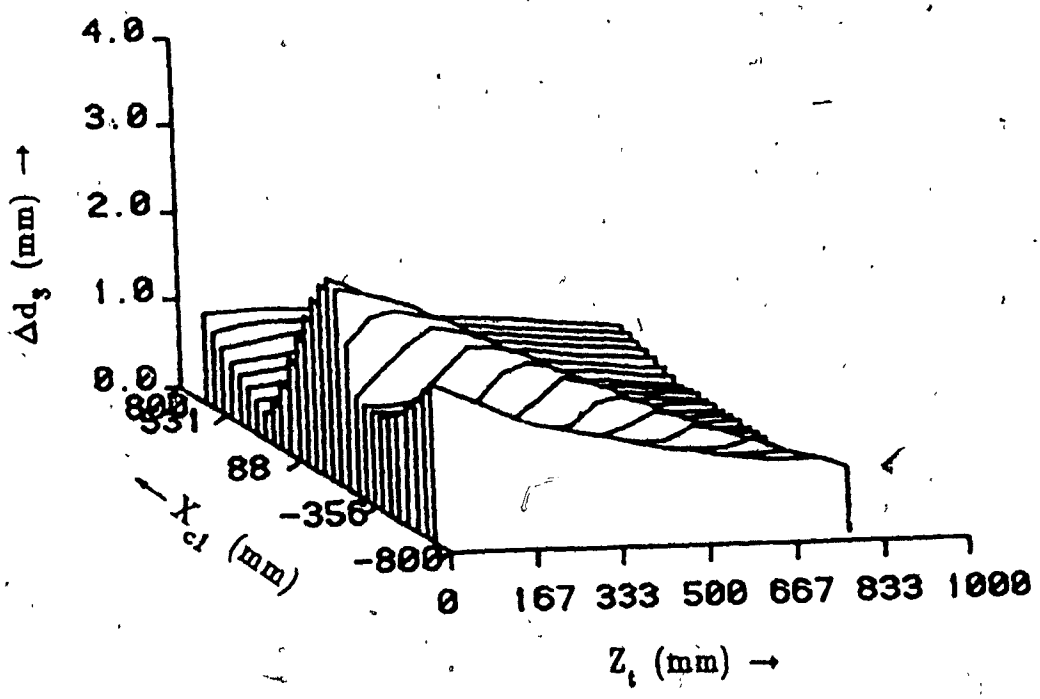

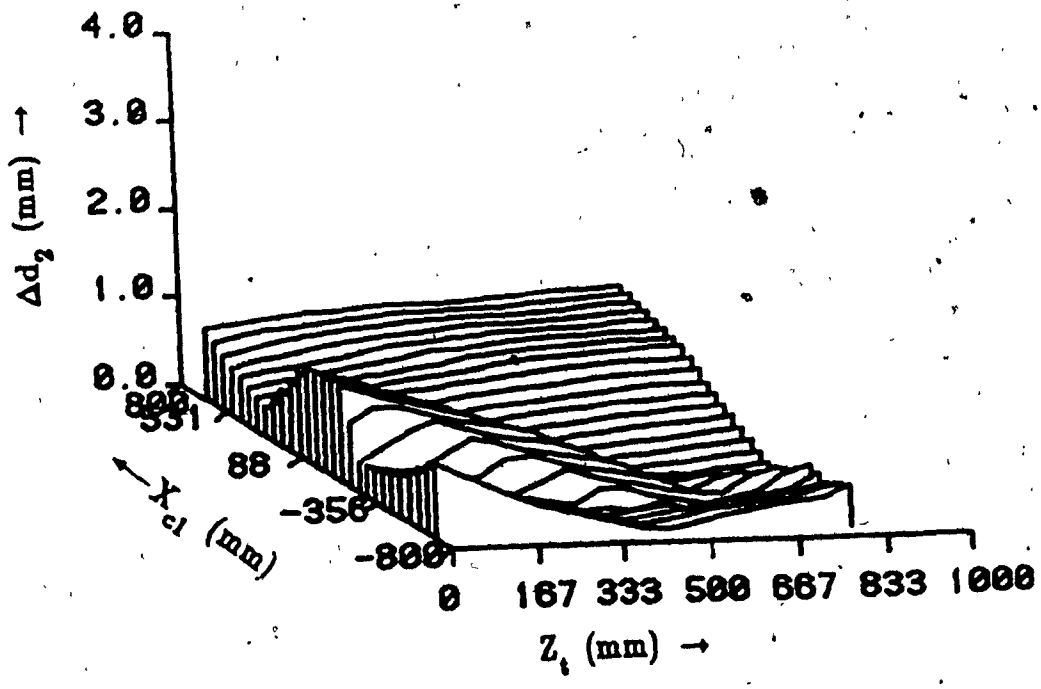

Fig.6.3. Effect of X_{c1} and Z_t on the link lengths and the offset distances

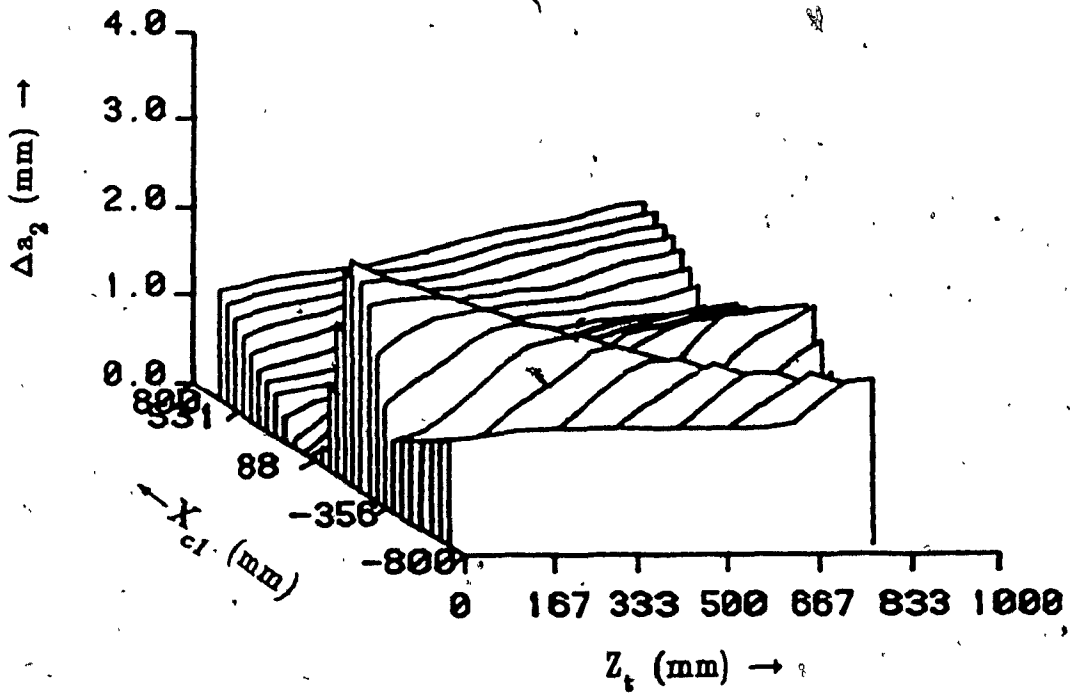

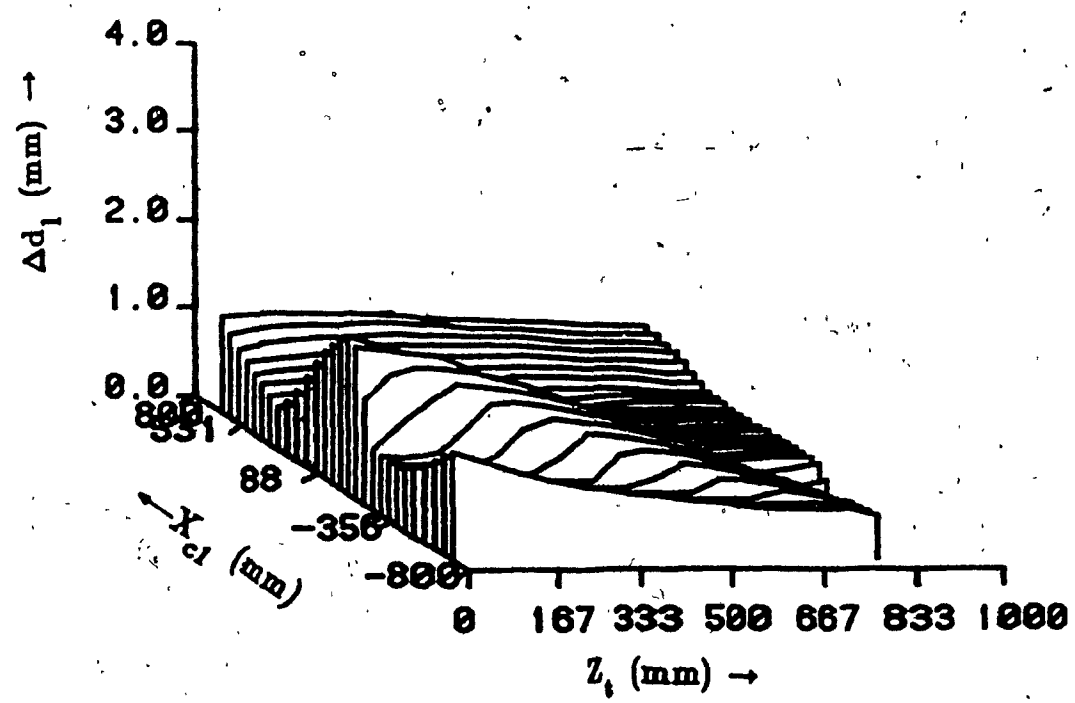

Fig.6.3. Effect of X_{c1} and Z_t on the link lengths and the offset distances

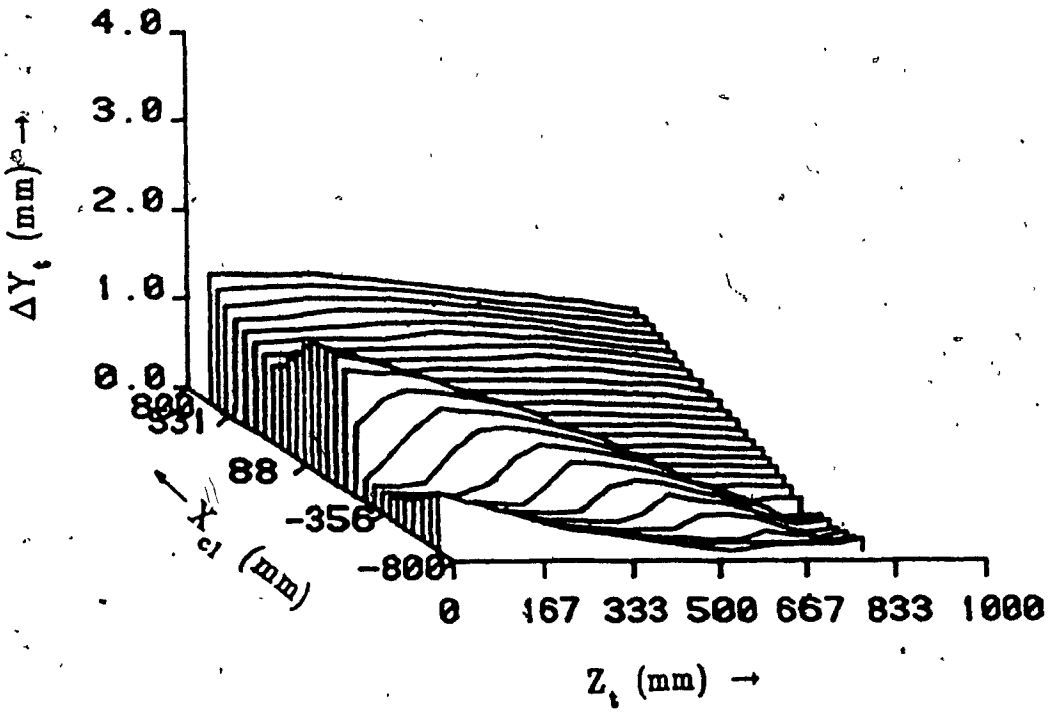

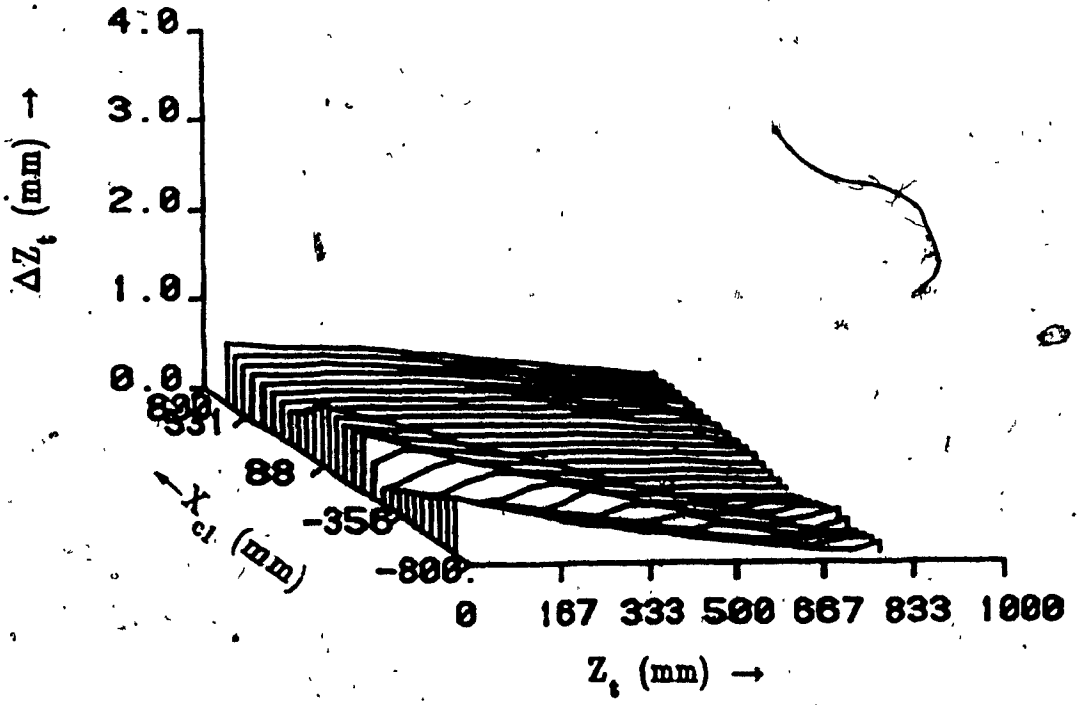

Fig.6.3. Effect of X_{c1} and Z_t on the link lengths and the offset distances

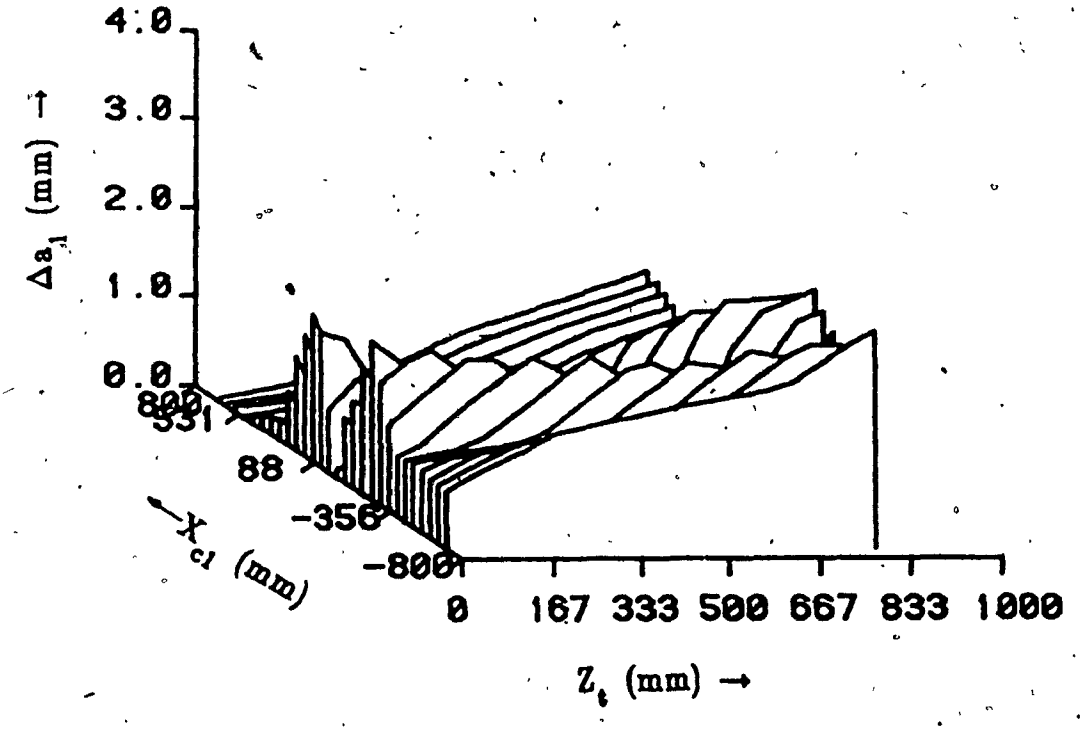

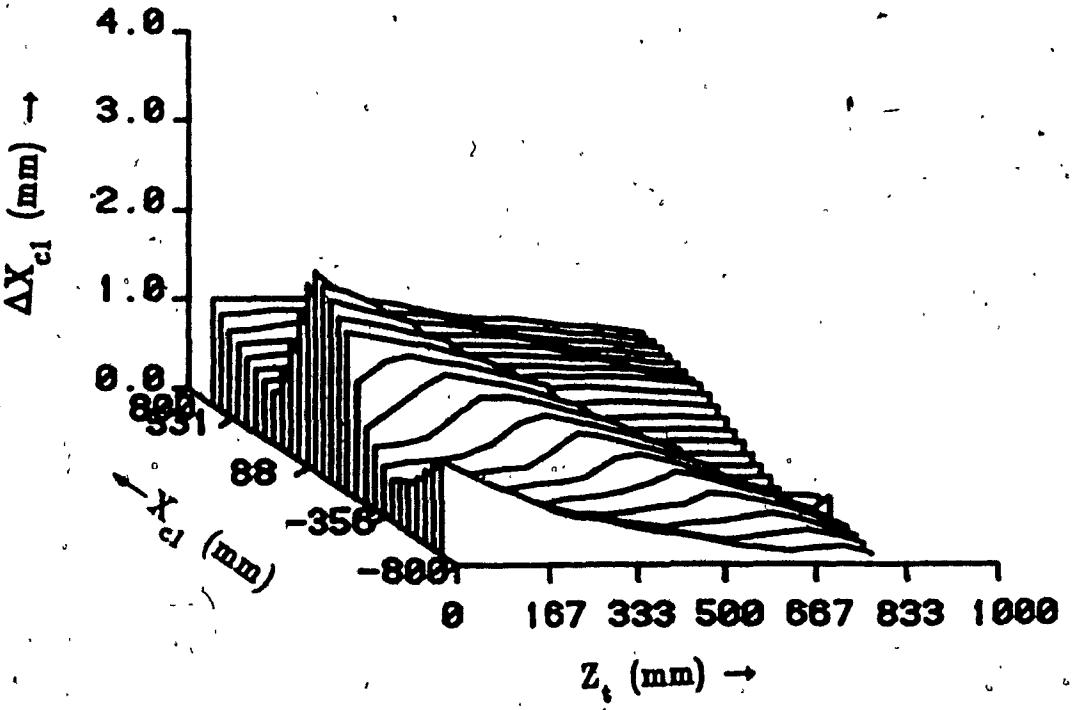

Fig.6.3. Effect of X_{c1} and Z_t on the link lengths and the offset distances

Using X-tool positions (X_t) :

$$0.27d_3 + 0.17d_2 - 0.04a_2 + 0.99d_1 + 0.17a_1 + 1.00X_{c1} - 0.15Y_t + 0.95X_t = 1065.95$$

$$0.46d_3 + 0.20d_2 - 0.04a_2 + 0.98d_1 + 0.19a_1 + 1.00X_{c1} - 0.05Y_t + 0.89X_t = 1059.01$$

$$0.62d_3 + 0.16d_2 + 0.01a_2 + 0.99d_1 + 0.11a_1 + 1.00X_{c1} + 0.39Y_t + 0.69X_t = 895.69$$

$$-0.18d_3 + 0.08d_2 + 0.12a_2 + 0.99d_1 + 0.13a_1 + 1.00X_{c1} + 0.88Y_t + 0.44X_t = 681.62$$

$$-0.05d_3 + 0.04d_2 - 0.11a_2 + 0.99d_1 + 0.11a_1 + 1.00X_{c1} + 0.66Y_t + 0.75X_t = 867.31$$

$$0.88d_3 - 0.04d_2 - 0.22a_2 + 0.98d_1 + 0.18a_1 + 1.00X_{c1} + 0.25Y_t + 0.40X_t = 641.34$$

$$0.67d_3 + 0.18d_2 - 0.03a_2 + 0.98d_1 + 0.18a_1 + 1.00X_{c1} - 0.30Y_t + 0.67X_t = 897.21$$

$$0.53d_3 + 0.01d_2 - 0.13a_2 + 0.99d_1 + 0.07a_1 + 1.00X_{c1} + 0.52Y_t + 0.66X_t = 800.34$$

$d_3 = 57.13$ mm ; $d_2 = 431.99$ mm ; $a_2 = 20.32$ mm ;
$d_1 = 149.31$ mm ; $a_1 = 432.04$ mm ; $X_{c1} = 99.78$ mm ;
$Y_t = 50.00$ mm ; $X_t = 700.00$ mm ;

Joint Angle readings from the Robot Controller :

θ_1(deg)	θ_2(deg)	θ_3(deg)	θ_4(deg)	θ_5(deg)	θ_6(deg)
-80.05	14.00	64.00	10.00	55.00	100.10
-78.05	23.00	56.00	25.00	45.00	82.00
-81.05	-46.00	140.00	60.00	35.00	10.00
-82.05	-14.00	160.00	-30.00	25.00	62.00
-83.05	-25.00	44.00	-10.00	75.00	52.00
-77.05	-38.00	27.00	50.00	85.00	43.00
-79.51	6.00	76.00	40.00	70.00	110.00
-82.51	-57.00	62.00	30.00	60.00	31.00

Fig.6.4 Sample results for the Denawit-Hartenberg parameters

are given as the inputs to the mathematical model to recompute the link lengths, and the offset distances. The joint angles are selected carefully to simulate the experimental conditions. This provides the informations on feasibility of the methodology for experimentation. Figure 6.4 presents the results of this exercise and is observed to be satisfactory.

6.5 Summary

This chapter describes a modified approach to evaluate link lengths and offset distances of robots using the kinematic model of the robots. This model relates the coordinates of the tool with respect to a reference coordinate frame R_f and the link parameters. It has been shown in this chapter that the relationship is linear and hence linear regression technique can be applied to solve for the unknown parameters from the measured tool coordinates. For illustration, the kinematics of the Puma 560 robot are used here. This method requires the knowledge of the joint errors and angles as the additional informations compared to the methodology discussed in chapter 4. The joint angles can be obtained either by tapping the joint encoders/resolvers or one could use the joint angle informations provided by the robot controller. Though this method requires additional informations compared to method discussed in chapter 4, nontheless is simpler mathematical approach compares favourably in terms of computing time, and accumulation errors. It can be inferred from the kinematic relationships for the tool coordinates, that the estimation errors can be changed by varying the distances X_{c1}, Y_{c1}, Z_{c1}, X_t, Y_t, and Z_t. Variations in the distance X_{c1}

results in large number of local minima. An increase in the X_t distance decreases the errors for most of the parameters initially and thereafter remains the same. Increase in the Y_t, Z_t distances increases the errors monotonically. Since in this chapter, experiments are not performed, the joint angles for the sample results are carefully chosen such that, the testing includes the feasibility of the methodology for actual experiments as one of the constraints.

CHAPTER 7

CONCLUSIONS AND RECOMMENDATIONS FOR FUTURE WORK

7.1 Conclusions

It can be concluded from this thesis that a procedure to calibrate robots is essential to measure the errors in robots and hence to improve the accuracy with which the tool is positioned and oriented at the desired location. It has been demonstrated here the presence of estimation errors due to instrument resolution and/or repeatability and human errors and the usefulness of the error analysis to evaluate these errors. It has been shown that the estimation errors can be controlled by the appropriate choice of the geometrical parameters of the experimental setup for a given values of the instrument resolution. Hence the importance of designing the experiements to search for the optimum set of geometrical parameters of the experimental setup that results minimum estimation errors.

The procedure outlined in this thesis has been applied to the Puma 560 robot and the contribution of some of the error sources are measured. It has been found that the estimated values of all link parameters except a_1 and d_1 were very close to the manufacturer's specification. The deviations in a_1 and d_1 may be attributed to the presence of a 1 degree misalignment in the XZ - plane between coordinate frames of the joints 2 and 5. The amplitude of the

transmission errors in the joints 4 and 6 are of the order of 0.08 and 0.06 degrees respectively. The experiments for the joint stiffness indicates that the joints 2 and 3 are nearly 10 times stiffer than the wrist joints. The wrist joint 4 and the joint 3 exhibits a deflection of 0.004 and 0.0005 deg/unit torque. Experiments on the cross coupling effects indicates the presence of cross coupling between the wrist joints. The magnitude of the correction factors are found to be the same as that specified by Vistnes[35]. The sign for the correction factor σ_{56} given by Vistnes[35] should be positive instead of being negative.

7.2 Suggestions for Future Work

The robot errors can be grouped under two classes namely, fixed errors and running errors. The fixed errors are the deviations in the Denawit-Hartenberg parameters of the robot from the nominal values, and the running errors are the errors due to the transmission errors, joint compliance, link compliance, cross coupling effects, and backlash effects. The magnitude of these errors changes with the joint angles and hence known as the running errors. It has been mentioned in section 1.2, since the joint encoders are normally mounted at the actuator end rather than at the joint end, the effect of running errors can not be sensed by the robot controller. These running errors can be eliminated completely if the joint encoders can be mounted at the joint end. Also, use of direct drive systems in robots eliminates some of the running errors. Hence the author recommends the use of direct drive systems and/or mounting the joint encoders/resolvers at the joint end as the changes for future robot designs.

The search technique described in the Chapter 6 to evaluate the link lengths and the offset distances uses the joint orientation informations and the joint errors computed using separate experiments. It can be modified to search for the joint orientations as well. This reduces the amount of experimentation involved but increases the number of unknown quantities to be searched mathematically to 23. If the joint encoders can not be mounted at the joint end, then this search technique can be made to include the running errors as well. This means the number of unknown parameters to be computed becomes 59. This method should be designed to protect against such problems as the presence of degenerate solutions, singularity, and non-linearity.

It is preferable to use optical instrument with digital readout to reduce reading errors and also to hasten the calibration process. The methodology discussed in this thesis can be applied to calibrate robots in static. There are number of industrial applications requiring accuracy in the tool trajectory of the robot under various load conditions. This calls for another area of research leading to the design of a technique for dynamic calibration of robots. This requires a completely automated calibration setup using laser/camera tracking systems. This also involves real time computation of robot errors and corrections for the same. Since this process will affect the robot controller computation time, it is preferable to use parallel processing to compute the tool trajectory and the errors concurrently.

REFERENCES

1. Kissam, P. Surveying For Civil Engineers, McGraw-Hill Book Company, 1956.
2. Uchiyama, M., "A Study of Control of Motion of a Mechanical Arm (1st Report, Calculation of Coordinative Motion Considering Singular Points)", Bulletin of the Japan Society of Mechanical Engineers, Vol. 22, No. 173, pp. 1640 - 1647, Nov. 1979.
3. Inagaki, S., "A Discussion on Positioning Accuracy on Industrial Robots", Proceedings of the 9th International Symposium on Industrial Robots, pp. 679 - 690, 1979.
4. Warnecke, H.J., Weck, W., Brodleck B., Engel, G., "Assesment of Industrial Robots", Annals of the International Institution for Production Engineering Research, Manufacturing Technology, Vol. 29, No. 1, pp. 391 - 396, 1980.
5. Morgan, C., "The Rationalisation of Robot Testing", Proceedings of the 10th International Symposium on Industrial Robots, 5th International Conference on Industrial Robot Technology, pp. 399 - 406, 1980.
6. Paul, R.P. Robot Manipulators : Mathematics, Programming, and Control, The MIT Press, 1981.
7. Anderson, R.H., Gillard, C.W., Huang, C.C., "Application of Laser Interferometry to Robotics", Proceedings of the Society of Photo-Optical Instrumentation Engineers, Robotics and Industrial Inspection, Vol. 359, pp. 207 - 213, 1981.
8. Scheffer, B., "Geometrical Control and Calibration Method of an Industrial Robot", Proceedings of the 12th Symposium on Industrial

Robots, 6th International Conference on Industrial Robot Technology, pp. 331 - 339, 1982.

9. Laurent P.F., Kelly, B.R., "Improving the Precision of a Robot", Proceedings of The Society of Photo-Optical Instrumentation Engineers, Robotics and Industrial Inspection, Vol. 360, pp. 62 - 67, Aug. 1982.
10. Fohanno, T., "Assessment of Mechanical Performance of Industrial Robots", Proceedings of the 12th International Symposium on Industrial Robots and 6th Conference on Industrial Robot Technology, pp. 349 - 358, 1982.
11. Warnecke, H.J., Schraft, R.D. Industrial Robots: Application Experience, IFS Publication, England, pp. 63 - 92, 1982.
12. Featherstone, R., "Position and Velocity Transformations between Robot End Effector Coordinates and Joint Angles", The International Journal of Robotics Research, Vol. 2, No. 2, pp. 35 - 45, Summer 1983.
13. Mooring, B.W., "The Effect of Joint Axis Misalignment on Robot Positioning Accuracy", Proceedings of the ASME Computers in Engineering Conference, pp. 151 - 155, Aug. 1983.
14. Grossman, D.D., Taylor, R.H., "Method and Apparatus for Calibration of Manipulator Axis", IBM Technical Disclosure Bulletin, Vol. 26, No. 4, pp. 1803 - 1807, Sep. 1983.
15. Martinez, P.L., Rex, D.K., "Video Test Tool for Robotics Accuracy/Repeatability", IBM Technical Disclosure Bulletin, Vol. 26, No. 4, pp. 1816 - 1817, Sep. 1983.
16. Furuya, N., Makino, H., "Calibration of Scara Robot Dimensions by Teaching", Journal of Japanese Society of Precision Engineering,

Vol. 49, No: 9, pp. 1223 - 1228, Sep. 1983.

17. Albertson, P., " Verifying Robot Performance", Robotics Today, pp. 33 - 36, Oct. 1983.
18. Kumar, A. and Sunil Prakash, "Analysis of Mechanical Errors in Manipulators", Proceedings of the 6th World Congress on the Theory of Machines and Mechanisms, Vol. II, pp. 960 - 963, Dec. 1983.
19. Lozinski, C.A., "Robot Calibration Method and Results", Masters' Thesis, MIT, June 1984.
20. Whitney, D.E., Lozinski, C.A., Rourke, J.M., "Industrial Robot Calibration Method and Results", Proceedings of the ASME Computers in Engineering Conference, pp. 92 - 100, Aug. 1984.
21. Mooring, B.W., "An Improved Method for Identifying the Kinematic Parameters in a Six Axis Robot", Proceedings of the ASME Computers in Engineering Conference, pp. 79 - 84, Aug. 1984.
22. Langmoen, R., Lien, T.K., Ramsli, E., "Testing of Industrial Robots", Proceedings of the 14th International Symposium on Industrial Robots, 7th International Conference on Industrial Robot Technology, pp. 201 - 207, 1984.
23. Lau, K., Hocken, R.J., "A Survey of Current Robot Metrology Methods", Annals of the International Institution for Production Engineering Research, Manufacturing Technology, Vol. 33, No. 2, pp. 485 - 488, 1984.
24. Kreamer, C.W., "Measuring Robot and Sensor Accuracy", Technical Paper, Society of Manufacturing Engineers, MS 84 - 1038, 1984.
25. Unimation Incorporation. Puma 500 Series Equipment, and Programming Manual, 1985.

26. Wu, Chi-Haur., Lee, C.C., "Estimation of the Accuracy of a Robot Manipulator", IEEE Transactions on Automatic Control, Vol. AC - 30, No. 3, pp. 304 - 306, March 1985.

27. Stauffer, N. R., "RT Special Report on Robot Accuracy", Robotics Today, pp. 43 - 49, April 1985.

28. Kirchner, H.O.K., Gurumoorthy, B., Prinz, F.B., "A Perturbation Approach to Robot Calibration", Technical Report, The Robotics Institute, Carnegie-Mellon University, No:CMU-RI-TR-85-9, 1985.

29. Hsu, T.W., Everett, L.J., "Identification of the Kinematic Parameters of a Robot Manipulator for Positional Accuracy Improvement", Proceedings of the ASME Computers in Engineering Conference, Vol. 1, pp. 263 - 267, 1985.

30. Benhabib, B., Fenton, R.G., Goldenberg, A.A., "Kinematic Error Analysis of Robots", Technical Report, University of Toronto, Sep. 1985.

31. Dagalakis, N.G., Myers, D.R., "Adjustment of Robot Joint Gears using Encoder Velocity and Position Information", Journal of Robotic Systems, 2(2), pp. 229 - 234, 1985.

32. Chao, L.M., Yang, J.C.S., "Development and Implementation of a Kinematic Parameter Identification Technique to Improve the Positional Accuracy of Robots", Robots 10, Conference Proceedings, pp. 11.69 - 11.81, April 1986.

33. Cheng, R.M.H., Ramesh Rajagopalan, Stepanenko, Y., "A Computer-aided Methodology for the Calibration of Industrial Robots Employing Optical Metrology, Part - 1 : Denawit-Hartenberg Parameters Estimation", Submitted to the International Journal of

Robotics and Computer-integrated Manufacturing, Oct. 1986.

34. Cheng, R.M.H., Ramesh Rajagopalan, "A Computer-aided Methodology for the Calibration of Industrial Robots Employing Optical Metrology, Part - 2 : Joint Errors", Submitted to the International Journal of Robotics and Computer-integrated Manufacturing, Oct. 1986.
35. Cheng, R.M.H., Ramesh Rajagopalan, "A Computer-aided Methodology to calibrate Link Lengths and Offset Distances of Robots Employing Optical Metrology", Submitted to the ASME Computers in Engineering Conference, Nov. 1986.
36. Vistnes, R., "Breaking Away from VAL or How to use your Puma without using VAL", Technical Report, Stanford University.
37. Library Unimation Incorporation., "Controlling the Puma Robot Arm without using VAL", Technical Report.

APPENDIX - A

APPENDIX A

MATHEMATICAL MODEL DERIVATIONS

A.1 Theodolite Parameters

As mentioned in §4.2, points A and B are the centers of the two theodolites. Points C, D, and E are marked on the reference ruler. L being the distance between A and B, r_1, r_2, and R are the distances CD, DE, and CE respectively. γ_1 and γ_2 are the offset angles. Referring to fig.4.1.b,

from $\triangle AED$ and $\triangle AEC$,

$$\frac{AE}{\sin\phi_1} = \frac{r_1}{\sin\alpha_1} = K_1 \quad \text{(say)}$$

$$\text{i.e.,} \quad AE = K_1 \sin\phi_1 \qquad \text{(A.1.1)}$$

$$\frac{AE}{\sin\theta_1} = \frac{r_2}{\sin\alpha_2} = K_2 \quad \text{(say)}$$

$$\text{i.e.,} \quad AE = K_2 \sin\theta_1 \qquad \text{(A.1.2)}$$

but $\phi_1 + \theta_1 + \alpha_1 + \alpha_2 = 180$

and hence $\phi_1 + \theta_1 = 180 - \alpha_1 - \alpha_2 = K_3$ (say)

from A.1.1 and A.1.2,

$$K_1 \, \mathrm{Sin}\phi_1 = K_2 \, \mathrm{Sin}\theta_1$$

replacing ϕ_1 by $K_3 - \theta_1$ we get,

$$K_1 \, \mathrm{Sin}(K_3-\theta_1) = K_2 \, \mathrm{Sin}\theta_1$$

after expanding and rearranging the quantities the expression for θ_1 is given as,

$$\tan\theta_1 = \frac{\mathrm{Sin}K_3}{\frac{K_2}{K_1} + \mathrm{Cos}K_3}$$

substituting K_1, K_2, and K_3 and using the following identities,

$$\mathrm{Sin}K_3 = \mathrm{Sin}(\alpha_1+\alpha_2) \; ; \; \mathrm{Cos}K_3 = - \mathrm{Cos}(\alpha_1+\alpha_2)$$

the final expressions for θ_1 and θ_2 are given below :

$$\left.\begin{aligned} \tan\theta_1 &= \frac{\mathrm{Sin}(\alpha_1+\alpha_2)}{\frac{r_1\mathrm{Sin}\alpha_1}{r_2\mathrm{Sin}\alpha_2} - \mathrm{Cos}(\alpha_1+\alpha_2)} \\ \tan\theta_2 &= \frac{\mathrm{Sin}(\beta_1+\beta_2)}{\frac{r_1\mathrm{Sin}\beta_1}{r_2\mathrm{Sin}\beta_2} - \mathrm{Cos}(\beta_1+\beta_2)} \end{aligned}\right\} \qquad \text{(A.1.3)}$$

from ΔADC,

$$\left.\begin{aligned} \frac{AC}{\text{Sin}\phi_1} &= \frac{R}{\text{Sin}(\alpha_1+\alpha_2)} \text{ i.e., } AC = \frac{R\ \text{Sin}\phi_1}{\text{Sin}(\alpha_1+\alpha_2)} \\ \frac{BC}{\text{Sin}\phi_2} &= \frac{R}{\text{Sin}(\beta_1+\beta_2)} \text{ i.e., } BC = \frac{R\ \text{Sin}\phi_2}{\text{Sin}(\beta_1+\beta_2)} \end{aligned}\right\} \quad (A.1.4)$$

from ΔABC,

$$\bar{V}_{cb} + \bar{V}_{ba} + \bar{V}_{ac} = 0$$

substituting the values of the components $\bar{V}_{cb}$, $\bar{V}_{ba}$, $\bar{V}_{ac}$,

$$CB\ \text{Cos}\theta_2\underline{i} + CB\ \text{Sin}\theta_2\underline{j} + \bar{V}_{ba} - AC\ \text{Cos}\theta_1\underline{i} - AC\ \text{Sin}\theta_1\underline{j} = 0$$

i.e.,

$$\bar{V}_{ba} = \sqrt{(AC\ \text{Cos}\theta_1 - BC\ \text{Cos}\theta_2)^2 + (AC\ \text{Sin}\theta_1 - BC\ \text{Sin}\theta_2)^2} \quad (A.1.5)$$

To compute γ_1 and γ_2

To compute γ_1, the triangle ABC is used. This is because since the angle CAB is small, the estimation error will be minimum. From ΔABC,

$$\frac{BC}{\text{Sin}\angle CAB} = \frac{AB}{\text{Sin}\angle ACB} \text{ i.e., } \frac{BC}{\text{Sin}\angle CAB} = \frac{AB}{\text{Sin}(\theta_2-\theta_1)}$$

$$\text{i.e., } \text{Sin}\angle CAB = \frac{BC}{AB}\ \text{Sin}(\theta_2-\theta_1)$$

$$\text{hence } \alpha'_{3c} = \text{Sin}^{-1}\left[\frac{R\ \text{Sin}\phi_2\ \text{Sin}(\theta_2-\theta_1)}{L\ \text{Sin}(\beta_1+\beta_2)}\right]$$

Let α_3' be the azimuth reading for the point C. The offset angle γ_1 is given by,

$$\gamma_1 = -\alpha_3' + \alpha'_{3c}$$

$$= -\alpha_3' + \text{Sin}^{-1}\left[\frac{R\ \text{Sin}\phi_2\ \text{Sin}(\theta_2-\theta_1)}{L\ \text{Sin}\ (\beta_1+\beta_2)}\right] \qquad \text{(A.1.6)}$$

To compute γ_2, the ΔBDA is used. From this triangle,

$$\frac{AD}{\text{Sin}\angle ABD} = \frac{AB}{\text{Sin}\ (\phi_1-\phi_2)}$$

$$\text{i.e., } \text{Sin}\angle ABD = \frac{AD}{AB}\ \text{Sin}(\phi_1-\phi_2)$$

$$\text{hence } \beta'_{1c} = \text{Sin}^{-1}\left[\frac{R\ \text{Sin}\theta_1\ \text{Sin}(\phi_1-\phi_2)}{L\ \text{Sin}(\alpha_1+\alpha_2)}\right]$$

Let β_1' be the theodolite reading for the point D. The offset angle γ_2 can be computed from the following expression :

$$\gamma_2 = -\beta_1' + \beta'_{1c}$$

$$= -\beta_1' + \text{Sin}^{-1}\left[\frac{R\ \text{Sin}\theta_1\ \text{Sin}(\phi_1-\phi_2)}{L\ \text{Sin}(\alpha_1+\alpha_2)}\right] \qquad \text{(A.1.7)}$$

A.2 Coordinates of a point P(X, Y, Z)

Let α_1 and β_1 be the azimuth readings of the theodolites 1 and 2 and ϕ_1 be the elevation angle of the theodolite 1 for any point chosen in the working envelope of the theodolites. As before, L is the center distance between the theodolites. Let R_f be the reference coordinate frame chosen with its origin at A. The X axis of this frame is directed along the distance L, the Y axis being perpendicular to it and the Z axis is parallel to the vertical axes of the theodolites. The X axis of the theodolites makes γ_1 and γ_2 with respect to the X_{R_f} axis respectively. Referring to fig.4.1.b, the coordinates of the point in space can be computed using the distance L and the theodolite angles α_1, β_1, and ϕ_1 as follows :

Let AD $= X_1$, CD $= Y_1$, and EC $= Z_1$. From $\triangle$ADC, and $\triangle$BDC,

$$CD = X_1 \tan(\alpha_1' - \gamma_1) = (L - X_1) \tan(\beta_1' - \gamma_2)$$

i.e., $$X_1 \tan(\alpha_1' - \gamma_1) = (L - X_1) \tan(\beta_1' - \gamma_2)$$

$$X_1 \{ \tan(\alpha_1' - \gamma_1) + \tan(\beta_1' - \gamma_2) \} = L \tan(\beta_1' - \gamma_2)$$

Let $\alpha_1 = \alpha_1' - \gamma_1$ and $\beta_1 = \beta_1' - \gamma_2$, we get

$$X_1 = \frac{L \tan\beta_1}{\tan\alpha_1 + \tan\beta_1} \qquad (A.2.1)$$

$$\text{and } CD = Y_1 = X_1 \tan\alpha_1 = \frac{L \tan\alpha_1 \tan\beta_1}{\tan\alpha_1 + \tan\beta_1} \qquad \text{(A.2.2)}$$

from ΔAEC,

$$Z_1 = CE = AC \tan\phi_1 = \sqrt{(X_1^2 + Y_1^2)} \tan\phi_1 \qquad \text{(A.2.3)}$$

A.3 Joint Center Coordinates

The equation for the circular path traced by a point P_j in the XY plane given by the equation 4.3.1.4 and is given as,

$$(X_{cj}-X_i)^2 + (Y_{cj}-Y_i)^2 = R_{pj}^2$$

substituting i = 1, 2, and 3, and then solving the three simultaneous equations, the expressions for the center of the circular path (X_{cj}, Y_{cj}) are given by,

$$X_{cj} = \left.\frac{\{X_2^2-X_1^2+Y_2^2-Y_1^2\}\{Y_3-Y_2\} - \{X_3^2-X_2^2+Y_3^2-Y_2^2\}\{Y_2-Y_1\}}{2\{(X_2-X_1)(Y_3-Y_2) - (X_3-X_2)(Y_2-Y_1)\}}\right\} \qquad \text{(A.3.1)}$$

$$= N_{r1}/(2 D_{r1}) \qquad \text{and}$$

$$Y_{cj} = \frac{\{X_2^2-X_1^2+Y_2^2-Y_1^2\} - \{X_2-X_1\}}{2\ (Y_2-Y_1)} \qquad \left.\right\} \text{(A.3.2)}$$

$$= N_{r2}/(2\ D_{r2})$$

for the circular path traced by the point P_j in the XZ plane, replace Y_i, and Y_{cj} by Z_i, and Z_{cj} respectively.

APPENDIX - B

APPENDIX B

ERROR ANALYSIS

B.1. Distance between the theodolites L

From equation 4.2.1, L can be written as,

$$L = R\sqrt{(AC\ Cos\theta_1 - BC\ Cos\theta_2)^2 + (AC\ Sin\theta_1 - BC\ Sin\theta_2)^2} \tag{B.1.1}$$

substituting AC and BC from equation 4.2.3, L can be rewritten as,

$$L = R\sqrt{\left[\frac{Sin\phi_1\ Cos\theta_1}{Sin\ (\alpha_1+\alpha_2)} - \frac{Sin\phi_2\ Cos\theta_2}{Sin\ (\beta_1+\beta_2)}\right] + \left[\frac{Sin\phi_1\ Sin\theta_1}{Sin\ (\alpha_1+\alpha_2)} - \frac{Sin\phi_2\ Sin\theta_2}{Sin\ (\beta_1+\beta_2)}\right]} \tag{B.1.2}$$

$$L = R\sqrt{K_1^2 + K_2^2} \tag{B.1.3}$$

from equation 5.2.2, ΔL is given by,

$$\Delta L = \frac{\partial L}{\partial R}\Delta R + \frac{\partial L}{\partial \theta_1}\Delta\theta_1 + \frac{\partial L}{\partial \theta_2}\Delta\theta_2 + \frac{\partial L}{\partial \phi_1}\Delta\phi_1 + \frac{\partial L}{\partial \phi_2}\Delta\phi_2 +$$

$$\frac{\partial L}{\partial \alpha_1}\Delta\alpha_1 + \frac{\partial L}{\partial \alpha_2}\Delta\alpha_2 + \frac{\partial L}{\partial \beta_1}\Delta\beta_1 + \frac{\partial L}{\partial \beta_2}\Delta\beta_2 \qquad \text{(B.1.3)}$$

$$\text{i.e., } \epsilon_L = \epsilon_1 + \epsilon_2 + \epsilon_3 + \epsilon_4 + \epsilon_5 + \epsilon_6 + \epsilon_7 + \epsilon_8 + \epsilon_9 \qquad \text{(B.1.4)}$$

To find ϵ_1 : Differentiating equation B.1.3 with respect to R,

$$\epsilon_1 = \sqrt{(K_1^2 + K_2^2)}\,\Delta R$$
$$= \frac{L}{R}\Delta R$$

To find ϵ_2 : Differentiating equation B.1.3 with respect to θ_1,

$$\epsilon_2 = -\frac{R^2}{L}\left[K_1\frac{\partial K_1}{\partial \theta_1} + K_2\frac{\partial K_2}{\partial \theta_1} \right]\Delta\theta_1$$

where

$$\frac{\partial K_1}{\partial \theta_1} = -\frac{\mathrm{Sin}\phi_1\mathrm{Sin}\theta_1}{\mathrm{Sin}(\alpha_1+\alpha_2)}\,; \qquad \frac{\partial K_2}{\partial \theta_1} = \frac{\mathrm{Sin}\phi_1\mathrm{Cos}\theta_1}{\mathrm{Sin}(\alpha_1+\alpha_2)}$$

$$K_1 = \frac{\mathrm{Sin}\phi_1\mathrm{Cos}\theta_1}{\mathrm{Sin}(\alpha_1+\alpha_2)} - \frac{\mathrm{Sin}\phi_2\mathrm{Cos}\theta_2}{\mathrm{Sin}(\beta_1+\beta_2)}$$

$$K_2 = \frac{\mathrm{Sin}\phi_1\mathrm{Sin}\theta_1}{\mathrm{Sin}(\alpha_1+\alpha_2)} - \frac{\mathrm{Sin}\phi_2\mathrm{Sin}\theta_2}{\mathrm{Sin}(\beta_1+\beta_2)}$$

To find ϵ_3 : Differentiating equation B.1.3 with respect to θ_2,

$$\epsilon_3 = \frac{R^2}{L}\left[K_1\frac{\partial K_1}{\partial \theta_2} + K_2\frac{\partial K_2}{\partial \theta_2} \right]\Delta\theta_2$$

where

$$\frac{\partial K_1}{\partial \theta_2} = -\frac{\mathrm{Sin}\phi_2 \mathrm{Sin}\theta_2}{\mathrm{Sin}(\beta_1+\beta_2)} \text{ and } \frac{\partial K_2}{\partial \theta_2} = -\frac{\mathrm{Sin}\phi_2 \mathrm{Cos}\theta_2}{\mathrm{Sin}(\beta_1+\beta_2)}$$

To find ϵ_4 : Differentiating equation B.1.3 with respect to ϕ_1,

$$\epsilon_4 = \frac{R^2}{L}\left[K_1 \frac{\partial K_1}{\partial \phi_1} + K_2 \frac{\partial K_2}{\partial \phi_1} \right] \Delta\phi_1$$

where

$$\frac{\partial K_1}{\partial \phi_1} = -\frac{\mathrm{Cos}\phi_1 \mathrm{Cos}\theta_1}{\mathrm{Sin}(\alpha_1+\alpha_2)} \text{ and } \frac{\partial K_2}{\partial \phi_1} = -\frac{\mathrm{Cos}\phi_1 \mathrm{Sin}\theta_1}{\mathrm{Sin}(\alpha_1+\alpha_2)}$$

To find ϵ_5 : Differentiating equation B.1.3 with respect to ϕ_2,

$$\epsilon_5 = \frac{R^2}{L}\left[K_1 \frac{\partial K_1}{\partial \phi_2} + K_2 \frac{\partial K_2}{\partial \phi_2} \right] \Delta\phi_2$$

where

$$\frac{\partial K_1}{\partial \phi_2} = -\frac{\mathrm{Cos}\phi_2 \mathrm{Cos}\theta_2}{\mathrm{Sin}(\beta_1+\beta_2)} \text{ and } \frac{\partial K_2}{\partial \phi_2} = -\frac{\mathrm{Cos}\phi_2 \mathrm{Sin}\theta_2}{\mathrm{Sin}(\beta_1+\beta_2)}$$

To find ϵ_6 : Differentiating equation B.1.3 with respect to α_1,

$$\epsilon_6 = \frac{R^2}{L}\left[K_1 \frac{\partial K_1}{\partial \alpha_1} + K_2 \frac{\partial K_2}{\partial \alpha_1} \right] \Delta\alpha_1$$

where

$$\frac{\partial K_1}{\partial \alpha_1} = -\frac{\mathrm{Sin}\phi_1 \mathrm{Cos}\theta_1 \mathrm{Cos}(\alpha_1+\alpha_2)}{\mathrm{Sin}^2(\alpha_1+\alpha_2)} \quad \text{and} \quad \frac{\partial K_2}{\partial \alpha_1} = -\frac{\mathrm{Sin}\phi_1 \mathrm{Sin}\theta_1 \mathrm{Cos}(\alpha_1+\alpha_2)}{\mathrm{Sin}^2(\alpha_1+\alpha_2)}$$

To find ϵ_7 : Differentiating equation B.1.3 with respect to α_2,

$$\epsilon_7 = \frac{R^2}{L}\left[K_1 \frac{\partial K_1}{\partial \alpha_2} + K_2 \frac{\partial K_2}{\partial \alpha_2} \right] \Delta\alpha_2$$

where

$$\frac{\partial K_1}{\partial \alpha_2} = \frac{\partial K_1}{\partial \alpha_1} \quad \text{and} \quad \frac{\partial K_2}{\partial \alpha_2} = \frac{\partial K_2}{\partial \alpha_1}$$

To find ϵ_8 : Differentiating equation B.1.3 with respect to β_1,

$$\epsilon_8 = \frac{R^2}{L}\left[K_1 \frac{\partial K_1}{\partial \beta_1} + K_2 \frac{\partial K_2}{\partial \beta_1} \right] \Delta\beta_1$$

where

$$\frac{\partial K_1}{\partial \beta_1} = -\frac{\mathrm{Sin}\phi_2 \mathrm{Cos}\theta_2 \mathrm{Cos}(\beta_1+\beta_2)}{\mathrm{Sin}^2(\alpha_1+\alpha_2)} \quad \text{and} \quad \frac{\partial K_2}{\partial \beta_1} = -\frac{\mathrm{Sin}\phi_2 \mathrm{Sin}\theta_2 \mathrm{Cos}(\beta_1+\beta_2)}{\mathrm{Sin}^2(\beta_1+\beta_2)}$$

To find ϵ_9 : Differentiating equation B.1.3 with respect to β_2,

$$\epsilon_9 = \frac{R^2}{L}\left[K_1 \frac{\partial K_1}{\partial \beta_2} + K_2 \frac{\partial K_2}{\partial \beta_2} \right] \Delta\beta_2$$

where

$$\frac{\partial K_1}{\partial \beta_2} = \frac{\partial K_1}{\partial \beta_1} \text{ and } \frac{\partial K_2}{\partial \beta_2} = \frac{\partial K_2}{\partial \beta_1}$$

To find $\Delta\theta_1$ and $\Delta\theta_2$:

$\Delta\theta_1$ can be evaluated by partially differentiating equation 4.2.2, with respect to α_1, α_2, r_1, and r_2 successively. This can be represented as,

$$\Delta\theta_1 = \frac{\partial\theta_1}{\partial\alpha_1}\Delta\alpha_1 + \frac{\partial\theta_1}{\partial\alpha_2}\Delta\alpha_2 + \frac{\partial\theta_1}{\partial r_1}\Delta r_1 + \frac{\partial\theta_1}{\partial r_2}\Delta r_2$$

$$\frac{\partial\theta_1}{\partial\alpha_1} = -2\,\frac{\text{Cos}\theta_1^{\,2}}{s_1^2}$$

$$\frac{\partial\theta_1}{\partial\alpha_2} = -\frac{\text{Cos}^2\theta_1}{s_1^2}\left[-1 + \frac{\text{Sin}\alpha_1}{\text{Sin}\alpha_2}\,\text{Sin}(\alpha_1+\alpha_2)\right]$$

$$\frac{\partial\theta_1}{\partial r_1} = -\frac{\text{Sin}(\alpha_1+\alpha_1)\text{Sin}\alpha_1\text{Cos}^2\theta_1}{r_2 s_1^2 \text{Sin}\alpha_2}$$

$$\frac{\partial\theta_1}{\partial r_2} = -\frac{r_1\text{Sin}(\alpha_1+\alpha_2)\text{Sin}\alpha_1\text{Cos}^2\theta_1}{r_2^2 s_1^2 \text{Sin}\alpha_2}$$

If equation 4.2.2 is partially differentiated with respect to β_1, β_2, r_1, and r_2, the estimation error $\Delta\theta_2$ can be computed as,

$$\Delta\theta_2 = \frac{\partial\theta_2}{\partial\beta_1}\Delta\beta_1 + \frac{\partial\theta_2}{\partial\beta_2}\Delta\beta_2 + \frac{\partial\theta_2}{\partial r_1}\Delta r_1 + \frac{\partial\theta_2}{\partial r_2}\Delta r_2$$

$$\frac{\partial\theta_2}{\partial\beta_1} = -2\,\frac{\mathrm{Cos}^2\theta_2}{s_2^2}$$

$$\frac{\partial\theta_2}{\partial\beta_2} = \frac{\mathrm{Cos}^2\theta_2}{s_2^2}\left[-1 + \frac{\mathrm{Sin}\beta_1}{\mathrm{Sin}\beta_2}\,\mathrm{Sin}(\beta_1+\beta_2)\right]$$

$$\frac{\partial\theta_2}{\partial r_1} = -\frac{\mathrm{Sin}(\beta_1+\beta_1)\ \mathrm{Sin}\beta_1\mathrm{Cos}^2\theta_2}{r_2\, s_2^2\, \mathrm{Sin}\beta_2}$$

$$\frac{\partial\theta_2}{\partial r_2} = \frac{r_1\mathrm{Sin}(\beta_1+\beta_2)\ \mathrm{Sin}\beta_1\mathrm{Cos}^2\theta_2}{r_2^2\, s_2^2\, \mathrm{Sin}\beta_2}$$

where,

$$s_1 = \frac{r_1\mathrm{Sin}\alpha_1}{r_2\mathrm{Sin}\alpha_2} - \mathrm{Cos}(\alpha_1+\alpha_2)$$

$$s_2 = \frac{r_1\mathrm{Sin}\beta_1}{r_2\mathrm{Sin}\beta_2} - \mathrm{Cos}(\beta_1+\beta_2)$$

B.2. The offset angles γ_1 and γ_2

From equation 4.2.5, γ_1 is given by,

$$\gamma_1 = -\alpha_3' + \text{Sin}^{-1}\left[\frac{R\ \text{Sin}\phi_2\ \text{Sin}(\theta_1-\theta_2)}{L\ \text{Sin}(\beta_1+\beta_2)}\right] \qquad \text{(B.2.1)}$$

where α_3' is the theodolite 1 azimuth reading for the reference point C. Equation B.2.1 can be rewritten as,

$$\text{Sin}(\gamma_1+\alpha_3') = \frac{R\ \text{Sin}\phi_2\ \text{Sin}(\theta_1-\theta_2)}{L\ \text{Sin}(\beta_1+\beta_2)} \qquad \text{(B.2.2)}$$

this indicates that γ_1 is a function of R, L, β_1, β_2, θ_1, θ_2, ϕ_2, and α_3'. The estimation error $\Delta\gamma_1$ is given by,

$$\Delta\gamma_1 = \frac{\partial\gamma_1}{\partial R}\Delta R + \frac{\partial\gamma_1}{\partial L}\Delta L + \frac{\partial\gamma_1}{\partial\beta_1}\Delta\beta_1 + \frac{\partial\gamma_1}{\partial\beta_2}\Delta\beta_2 + \frac{\partial\gamma_1}{\partial\theta_1}\Delta\theta_1$$

$$+ \frac{\partial\gamma_1}{\partial\theta_2}\Delta\theta_2 + \frac{\partial\gamma_1}{\partial\phi_2}\Delta\phi_2 + \frac{\partial\gamma_1}{\partial\alpha_3'}\Delta\alpha_3' \qquad \text{(B.2.3)}$$

To find ϵ_1 : Differentiating equation B.2.2 with respect to R,

$$\text{Cos}(\gamma_1+\alpha_3')\ \partial\gamma_1 = \Delta R\ \frac{\text{Sin}\phi_2\ \text{Sin}(\theta_1-\theta_2)}{L\ \text{Sin}\ (\beta_1+\beta_2)}$$

i.e., $$\epsilon_1 = \frac{\Delta R}{R}\tan(\gamma_1+\alpha_3')$$

To find ϵ_2 : Differentiating equation B.2.2 with respect to L,

$$\text{Cos}(\gamma_1+\alpha_3')\ \partial\gamma_1 = -\frac{\Delta L\ \text{Sin}\phi_2\text{Sin}(\theta_1-\theta_2)}{L^2\ \text{Sin}(\beta_1+\beta_2)}$$

i.e., $$\epsilon_2 = -\frac{\Delta L}{L} \tan(\gamma_1+\alpha_3')$$

To find ϵ_3 : Differentiating equation B.2.2 with respect to β_1,

$$\mathrm{Cos}(\gamma_1+\alpha_3')\ \partial\gamma_1 = -\frac{R\ \mathrm{Sin}\phi_2\mathrm{Sin}(\theta_1-\theta_2)\mathrm{Cos}(\beta_1+\beta_2)}{L\ \mathrm{Sin}^2(\beta_1+\beta_2)}\ \Delta\beta_1$$

i.e., $$\epsilon_3 = -\frac{\tan(\gamma_1+\alpha_3')}{\tan(\beta_1+\beta_2)}\ \Delta\beta_1$$

To find ϵ_4 : Differentiating equation B.2.2 with respect to β_2,

$$\epsilon_4 = -\frac{\tan(\gamma_1+\alpha_3')}{\tan(\beta_1+\beta_2)}\ \Delta\beta_2$$

To find ϵ_5 : Differentiating equation B.2.2 with respect to θ_1,

$$\mathrm{Cos}(\gamma_1+\alpha_3')\ \partial\gamma_1 = -\frac{R\ \mathrm{Sin}\phi_2\mathrm{Cos}(\beta_1+\beta_2)}{L\ \mathrm{Sin}(\beta_1+\beta_2)}\ \Delta\theta_1$$

i.e., $$\epsilon_5 = \frac{\tan(\gamma_1+\alpha_3')}{\tan(\beta_1+\beta_2)}\ \Delta\theta_1$$

To find ϵ_6 : Differentiating equation B.2.2 with respect to θ_2,

$$\epsilon_6 = -\frac{\tan(\gamma_1+\alpha_3')}{\tan(\beta_1+\beta_2)}\ \Delta\theta_2$$

To find ϵ_7 : Differentiating equation B.2.2 with respect to ϕ_2,

$$\text{Cos}(\gamma_1+\alpha_3')\ \partial\gamma_1 = \frac{R\ \text{Cos}\phi_2\text{Sin}(\theta_1-\theta_2)}{L\ \text{Sin}(\beta_1+\beta_2)}\ \Delta\phi_2$$

i.e., $$\epsilon_7 = \frac{\tan\ (\gamma_1+\alpha_3')}{\tan\phi_2}\ \Delta\phi_2$$

To find ϵ_8 : Differentiating equation B.2.2 with respect to α_3',

$$\epsilon_8 = -\Delta\alpha_3'$$

From equation 4.2.5, γ_2 is given by,

$$\gamma_2 = -\beta_3' + \text{Sin}^{-1}\left[\frac{R\ \text{Sin}\theta_1\ \text{Sin}(\phi_2-\phi_1)}{L\ \text{Sin}(\alpha_1+\alpha_2)}\right] \qquad \text{(B.2.1)}$$

where β_3' is the theodolite 1 azimuth reading for the reference point C. Equation B.2.1 can be rewritten as,

$$\text{Sin}(\gamma_2+\beta_3') = \frac{R\ \text{Sin}\theta_1\ \text{Sin}(\phi_2-\phi_1)}{L\ \text{Sin}(\alpha_1+\alpha_2)} \qquad \text{(B.2.2)}$$

this indicates that γ_2 is a function of R, L, α_1, α_2, ϕ_1, ϕ_2, θ_1, and β_3'. The estimation error $\Delta\gamma_2$ is given by,

$$\Delta\gamma_2 = \frac{\partial\gamma_2}{\partial R}\Delta R + \frac{\partial\gamma_2}{\partial L}\Delta L + \frac{\partial\gamma_2}{\partial\alpha_1}\Delta\alpha_1 + \frac{\partial\gamma_2}{\partial\alpha_2}\Delta\alpha_2$$

$$+ \frac{\partial\gamma_2}{\partial\phi_1}\Delta\phi_1 + \frac{\partial\gamma_2}{\partial\phi_2}\Delta\phi_2 + \frac{\partial\gamma_2}{\partial\theta_1}\Delta\theta_1 + \frac{\partial\gamma_2}{\partial\beta_3'}\Delta\beta_3' \qquad \text{(B.2.3)}$$

To find ϵ_1 : Differentiating equation B.2.2 with respect to R,

$$\text{Cos}(\gamma_2+\beta_3') \; \partial\gamma_2 = \Delta R \; \frac{\text{Sin}\theta_1 \; \text{Sin}(\phi_2-\phi_1)}{L \; \text{Sin} \; (\alpha_1+\alpha_2)}$$

i.e., $$\epsilon_1 = \frac{\Delta R}{R} \tan(\gamma_2+\beta_3')$$

To find ϵ_2 : Differentiating equation B.2.2 with respect to L,

$$\text{Cos}(\gamma_2+\beta_3') \; \partial\gamma_2 = - \frac{\Delta L \; \text{Sin}\theta_1 \text{Sin}(\phi_2-\phi_1)}{L^2 \; \text{Sin}(\alpha_1+\alpha_2)}$$

i.e., $$\epsilon_2 = -\frac{\Delta L}{L} \text{Tan}(\gamma_2+\beta_3')$$

To find ϵ_3 : Differentiating equation B.2.2 with respect to α_1,

$$\text{Cos}(\gamma_2+\beta_3') \; \partial\gamma_2 = - \frac{R \; \text{Sin}\theta_1 \text{Sin}(\phi_2-\phi_1)\text{Cos}(\alpha_1+\alpha_2)}{L \; \text{Sin}^2(\alpha_1+\alpha_2)} \Delta\alpha_1$$

i.e., $$\epsilon_3 = -\frac{\tan \; (\gamma_2+\beta_3')}{\tan \; (\alpha_1+\alpha_2)} \Delta\alpha_1$$

To find ϵ_4 : Differentiating equation B.2.2 with respect to α_2,

$$\epsilon_4 = -\frac{\tan \; (\gamma_2+\beta_3')}{\tan \; (\alpha_1+\alpha_2)} \Delta\alpha_2$$

To find ϵ_5 : Differentiating equation B.2.2 with respect to ϕ_1,

$$\text{Cos}(\gamma_2+\beta_3')\ \partial\gamma_2 = -\frac{R\ \text{Sin}\theta_1\text{Cos}(\alpha_1+\alpha_2)}{L\ \text{Sin}(\alpha_1+\alpha_2)}\ \Delta\phi_1$$

$$\text{i.e.,} \qquad \epsilon_5 = \frac{\tan(\gamma_2+\beta_3')}{\tan(\alpha_1+\alpha_2)}\ \Delta\phi_1$$

To find ϵ_6 : Differentiating equation B.2.2 with respect to ϕ_2,

$$\epsilon_6 = -\frac{\tan(\gamma_2+\beta_3')}{\tan(\alpha_1+\alpha_2)}\ \Delta\phi_2$$

To find ϵ_7 : Differentiating equation B.2.2 with respect to θ_1,

$$\text{Cos}(\gamma_2+\beta_3')\ \partial\gamma_2 = \frac{R\ \text{Cos}\theta_1\text{Sin}(\phi_2-\phi_1)}{L\ \text{Sin}(\alpha_1+\alpha_2)}\ \Delta\theta_1$$

$$\text{i.e.,} \qquad \epsilon_7 = \frac{\tan(\gamma_2+\beta_3')}{\tan\theta_1}\ \Delta\theta_1$$

To find ϵ_8 : Differentiating equation B.2.2 with respect to β_3',

$$\epsilon_8 = -\Delta\beta_3'$$

B.3. Error Analysis for the Coordinates of a point P (X,Y,Z)

From equation 4.3.1, the coordinates of a point P (X,Y,Z) is given by,

$$\left.\begin{aligned} X &= L \tan\beta \,/\, (\tan\alpha + \tan\beta) \\ Y &= X \tan\alpha \\ Z &= \sqrt{(X^2 + Y^2)}\,\tan\phi \end{aligned}\right\} \quad \text{(B.3.1)}$$

this can be rewritten as,

$$\left.\begin{aligned} X &= g_1 (L, \alpha, \beta) \\ Y &= g_2 (X, \alpha) \\ Z &= g_3 (X, Y, \phi) \end{aligned}\right\} \quad \text{(B.3.2)}$$

differentiating B.3.2, with respect to L, α, β, X, Y, and ϕ, the estimation errors ΔX, ΔY, ΔZ can be computed as follows :

$$\left.\begin{aligned} \Delta X &= \frac{\partial g_1}{\partial L}\Delta L + \frac{\partial g_1}{\partial \alpha}\Delta\alpha + \frac{\partial g_1}{\partial \beta}\Delta\beta \\ \Delta Y &= \frac{\partial g_2}{\partial X}\Delta X + \frac{\partial g_2}{\partial \alpha}\Delta\alpha \\ \Delta Z &= \frac{\partial g_3}{\partial X}\Delta X + \frac{\partial g_3}{\partial Y}\Delta Y + \frac{\partial g_3}{\partial \phi}\Delta\phi \end{aligned}\right\} \quad \text{(B.3.3)}$$

the errors ∂g_1, ∂g_2, and so on can be computed by partially differentiating B.3.1 with respect to L, α, β, X, Y, and ϕ. This is

given by;

$$\frac{\partial g_1}{\partial L} = \frac{\tan\beta}{\tan\alpha+\tan\beta} = X/L$$

$$\frac{\partial g_1}{\partial \alpha} = -\frac{L \tan\beta \sec^2\alpha}{(\tan\alpha+\tan\beta)^2} = -\frac{X \sec^2\alpha}{\tan\alpha+\tan\beta}$$

$$\frac{\partial g_1}{\partial \beta} = \frac{L \tan\alpha \sec^2\beta}{\tan\alpha+\tan\beta}$$

$$\frac{\partial g_2}{\partial \alpha} = X \sec^2\alpha \; ; \quad \frac{\partial g_2}{\partial X} = \tan\alpha = Y/X$$

$$\frac{\partial g_3}{\partial \phi} = \sqrt{(X^2+Y^2) \sec^2\phi}$$

$$\frac{\partial g_2}{\partial X} = \frac{X \tan\phi}{\sqrt{(X^2+Y^2)}} \text{ and } \frac{\partial g_3}{\partial Y} = \frac{Y \tan\phi}{\sqrt{(X^2+Y^2)}}$$

hence the expressions for the estimation errors can be obtained by substituting these expressions in B.3.2 and is given as,

$$\Delta X = \frac{X}{L}\Delta L - \frac{X \sec^2\alpha \, \Delta\alpha}{\tan\alpha+\tan\beta} + \frac{L \tan\alpha \sec^2\beta \, \Delta\beta}{\tan\alpha+\tan\beta}$$

$$\Delta Y = \frac{Y}{X}\Delta X + X \sec^2\alpha \, \Delta\alpha$$

$$\Delta Z = \frac{X \tan\phi \, \Delta X}{\sqrt{(X^2+Y^2)}} + \frac{Y \tan\phi \, \Delta Y}{\sqrt{(X^2+Y^2)}} + \sqrt{(X^2+Y^2)} \, \mathrm{Sec}^2\phi' \, \Delta\phi$$

B.4 Joint Orientations

From equation 4.3.2, the joint orientations θ_{xj}, θ_{yj}, θ_{zj}, are given by,

$$\theta_{xj} = \mathrm{Sin}^{-1}\left[\frac{X_{P4} - X_{P1}}{X_{P2} - X_{P3}}\right] ; \quad \theta_{yj} = \tan^{-1}\left[\frac{Z_{P2} - Z_{P3}}{X_{P2} - X_{P3}}\right]$$

$$\theta_{zj} = \tan^{-1}\left[\frac{Y_{P2} - Y_{P3}}{X_{P2} - X_{P3}}\right] \qquad \text{(B.4.1)}$$

and the estimation errors $\Delta\theta_{xj}$, $\Delta\theta_{yj}$, $\Delta\theta_{zj}$ are given as,

$$\Delta\theta_{xj} = \frac{\partial\theta_{xj}}{\partial Y_{P4}} \Delta Y_{P4} + \frac{\partial\theta_{xj}}{\partial Y_{P1}} \Delta Y_{P1} + \frac{\partial\theta_{xj}}{\partial X_{P2}} \Delta X_{P2} + \frac{\partial\theta_{xj}}{\partial X_{P3}} \Delta X_{P3}$$

$$\Delta\theta_{yj} = \frac{\partial\theta_{yj}}{\partial Z_{P3}} \Delta Z_{P3} + \frac{\partial\theta_{yj}}{\partial Z_{P2}} \Delta Z_{P2} + \frac{\partial\theta_{yj}}{\partial X_{P2}} \Delta X_{P2} + \frac{\partial\theta_{yj}}{\partial X_{P3}} \Delta X_{P3}$$

$$\Delta\theta_{zj} = \frac{\partial\theta_{zj}}{\partial Y_{P3}} \Delta Y_{P3} + \frac{\partial\theta_{zj}}{\partial Y_{P2}} \Delta Y_{P2} + \frac{\partial\theta_{zj}}{\partial X_{P2}} \Delta X_{P2} + \frac{\partial\theta_{zj}}{\partial X_{P3}} \Delta X_{P3}$$

the terms $\frac{\partial\theta_{xj}}{\partial Y_{P4}}$, $\frac{\partial\theta_{xj}}{\partial Y_{P1}}$ and so on can be evaluated by partially

differentiating equation B.4.1 with respect to Y_{P4}, Y_{P1} and so on.. The final expressions are given below :

$$\frac{\partial\theta_{xj}}{\partial Y_{P2}} = \frac{1}{(X_{P2}-X_{P3})Sec^2\theta_{xj}} ; \frac{\partial\theta_{xj}}{\partial Y_{P3}} = -\frac{1}{(X_{P2}-X_{P3})Sec^2\theta_{xj}}$$

$$\frac{\partial\theta_{xj}}{\partial X_{P2}} = -\frac{1}{(X_{P2}-X_{P3})^2Sec^2\theta_{xj}} ; \frac{\partial\theta_{xj}}{\partial Y_{P3}} = \frac{1}{(X_{P2}-X_{P3})^2Sec^2\theta_{xj}}$$

$$\frac{\partial\theta_{yj}}{\partial Z_{P2}} = \frac{1}{(X_{P2}-X_{P3})Sec^2\theta_{yj}} ; \frac{\partial\theta_{yj}}{\partial Z_{P3}} = -\frac{1}{(X_{P2}-X_{P3})Sec^2\theta_{yj}}$$

$$\frac{\partial\theta_{yj}}{\partial X_{P2}} = -\frac{1}{(X_{P2}-X_{P3})^2Sec^2\theta_{yj}} ; \frac{\partial\theta_{yj}}{\partial Y_{P3}} = \frac{1}{(X_{P2}-X_{P3})^2Sec^2\theta_{yj}}$$

$$\frac{\partial\theta_{xj}}{\partial Y_{P4}} = \frac{1}{(X_{P2}-X_{P3})Cos\theta_{xj}} ; \frac{\partial\theta_{xj}}{\partial Y_{P1}} = -\frac{1}{(X_{P2}-X_{P3})Cos\theta_{xj}}$$

$$\frac{\partial\theta_{xj}}{\partial X_{P2}} = -\frac{1}{(X_{P2}-X_{P3})^2Cos\theta_{xj}} ; \frac{\partial\theta_{xj}}{\partial Y_{P3}} = \frac{1}{(X_{P2}-X_{P3})^2Cos\theta_{xj}}$$

and the errors ΔX_{Pi}, ΔY_{Pi}, and ΔZ_{Pi} are given by equation 5.3.4, in the previous section can be used here to compute the estimation errors.

B.5 Joint Center Coordinates

The coordinates of the j^{th} joint center C (X_{cj}, Y_{cj}, Z_{cj}) with respect to the reference frame R_f is given by the equation as,

$$X_{cj} = \frac{\left[X_2^2-X_1^2+Y_2^2-Y_1^2\right]\left[Y_3-Y_2\right] - \left[X_3^2-X_2^2+Y_3^2-Y_2^2\right]\left[Y_2-Y_1\right]}{2\left[(X_2-X_1)(Y_3-Y_2) - (X_3-X_2)(Y_2-Y_1)\right]} \quad \text{(B.5.1)}$$

$$= N_{r1}/(2\ D_{r1}) \qquad \text{and}$$

$$Y_{cj} = \frac{\left[X_2^2-X_1^2+Y_2^2-Y_1^2\right] - \left[X_2-X_1\right]}{2\ (Y_2-Y_1)} \quad \text{(B.5.2)}$$

$$= N_{r2}/(2\ D_{r2})$$

these relationships are valid for the axis of rotation perpendicular to the XY plane of R_f. For axis of rotation parallel to the XY plane, replace Y by Z.

The estimation errors ΔX_{cj}, ΔY_{cj}, and ΔZ_{cj} are given by,

$$\Delta X_{cj} = \frac{\partial X_{cj}}{\partial X_3}\Delta X_3 + \frac{\partial X_{cj}}{\partial X_2}\Delta X_2 + \frac{\partial X_{cj}}{\partial X_1}\Delta X_1 +$$

$$\frac{\partial X_{cj}}{\partial Y_3}\Delta Y_3 + \frac{\partial X_{cj}}{\partial Y_2}\Delta Y_2 + \frac{\partial X_{cj}}{\partial Y_1}\Delta Y_1$$

$$\Delta Y_{cj} = \frac{\partial Y_{cj}}{\partial X_2}\Delta X_2 + \frac{\partial Y_{cj}}{\partial X_1}\Delta X_1 + \frac{\partial Y_{cj}}{\partial Y_2}\Delta Y_2 +$$

$$\frac{\partial Y_{cj}}{\partial Y_1}\,\Delta Y_1 + \frac{\partial Y_{cj}}{\partial X_{cj}}\,\Delta X_{cj}$$

the terms $\frac{\partial X_{cj}}{\partial X_i}$, $\frac{\partial X_{cj}}{\partial X_i}$ can be computed by partially differentiating equations B.5.1 and B.5.2 with respect to X_i, Y_i respectively and are given below :

$$\frac{\partial X_{cj}}{\partial X_1} = \frac{(Y_3-Y_2)[N_{r1}-2X_1\,D_{r1}]}{2\,D_{r1}^2}$$

$$\frac{\partial X_{cj}}{\partial X_2} = \frac{(Y_3-Y_1)[2\,X_2D_{r1}-N_{r1}]}{2\,D_{r1}^2}$$

$$\frac{\partial X_{cj}}{\partial X_3} = -\frac{(Y_2-Y_1)[N_{r1}+2\,X_3D_{r1}]}{2\,D_{r1}^2}$$

$$\frac{\partial X_{cj}}{\partial Y_1} = \frac{D_{r1}\left[-2Y_1(Y_3-Y_2)+(X_3^2-X_2^2+Y_3^2-Y_2^2)\right] - N_{r1}\left[X_3-X_2\right]}{2\,D_{r1}^2}$$

$$\frac{\partial X_{cj}}{\partial Y_2} = \frac{D_{r1}\left[X_3^2-X_2^2+Y_3^2-Y_2^2\right] - N_{r1}\left[X_1-X_3\right]}{2\,D_{r1}^2}$$

$$\frac{\partial X_{cj}}{\partial Y_3} = \frac{D_{r1}\left[-2Y_3(Y_2-Y_1)+(X_1^2-X_3^2+Y_1^2-Y_3^2)\right] - N_{r1}\left[X_2-X_1\right]}{2\,D_{r1}^2}$$

$$\frac{\partial Y_{cj}}{\partial X_1} = \frac{(X_{cj}-X_1)}{D_{r2}} \quad ; \quad \frac{\partial Y_{cj}}{\partial X_2} = \frac{(X_2-X_{cj})}{D_{r2}}$$

$$\frac{\partial Y_{cj}}{\partial Y_1} = \frac{N_{r2}-2Y_1 D_{r2}}{2D_{r2}^2} \quad ; \quad \frac{\partial Y_{cj}}{\partial Y_2} = \frac{2D_{r2}Y_2-N_{r2}}{2D_{r2}^2}$$

$$\frac{\partial Y_{cj}}{\partial X_{cj}} = \frac{X_1-X_2}{D_{r2}}$$

B.6 Link lenghts and offset distances

The expressions to evaluate the link lengths and the offset distances (a_j and d_j) of the Puma 560 robot are given by the equation 4.3.15, and is reproduced below :

$$a_1 = \sqrt{(X_{c2}-X_{c3})^2 + (Z_{c2}-Z_{c3})^2}$$

$$a_2 = X_{c6}-X_{c1} \quad ; \quad d_1 = Y_{c6}-Y_{c1}$$

$$d_2 = \sqrt{(X_{c3}-X_{c5})^2 + (Z_{c3}-Z_{c5})^2}$$

$$d_3 = \sqrt{(Z_p-Z_{c6})^2 + (X_p-X_{c6})^2} - L_p$$

the estimation errors Δa_j, and Δd_j are obtained by partially

differentiating these equations with respect to X_{cj}, Y_{cj}, and Z_{cj} and are given by the equation 5.3.7, as given below :

$$\Delta a_1 = \frac{\partial a_1}{\partial X_{c2}} \Delta X_{c2} + \frac{\partial a_1}{\partial X_{c3}} \Delta X_{c3} + \frac{\partial a_1}{\partial Z_{c2}} \Delta Z_{c2} + \frac{\partial a_1}{\partial Z_{c3}} \Delta Z_{c3}$$

$$\Delta a_2 = \frac{\partial a_2}{\partial X_{c6}} \Delta X_{c6} + \frac{\partial a_2}{\partial X_{c1}} \Delta X_{c1}$$

$$\Delta d_1 = \frac{\partial d_1}{\partial Y_{c6}} \Delta Y_{c6} + \frac{\partial d_1}{\partial Y_{c1}} \Delta Y_{c1}$$

$$\Delta d_2 = \frac{\partial d_2}{\partial X_{c3}} \Delta X_{c3} + \frac{\partial d_2}{\partial X_{c5}} \Delta X_{c5} + \frac{\partial d_2}{\partial Z_{c3}} \Delta Z_{c3} + \frac{\partial d_2}{\partial Z_{c5}} \Delta Z_{c5}$$

$$\Delta d_3 = \frac{\partial d_3}{\partial Z_p} \Delta Z_p + \frac{\partial d_3}{\partial Z_{c6}} \Delta Z_{c6} + \frac{\partial d_3}{\partial X_p} \Delta X_p +$$

$$\frac{\partial d_3}{\partial X_{c6}} \Delta X_{c6} - \frac{\partial d_3}{\partial L_p} \Delta L_p$$

the errors $\frac{\partial a_1}{\partial X_{cj}}$, $\frac{\partial d_1}{\partial X_{cj}}$ and so on can be obtained by partially differentiating the expression B.6.1 with respect to X_{cj}, Y_{cj} and so on. They are given below :

$$\frac{\partial a_1}{\partial X_{c2}} = \frac{X_{c2}-X_{c3}}{a_1} \quad ; \quad \frac{\partial a_1}{\partial X_{c3}} = \frac{X_{c3}-X_{c2}}{a_1}$$

$$\frac{\partial a_1}{\partial Z_{c2}} = \frac{Z_{c2}-Z_{c3}}{a_1} \quad ; \quad \frac{\partial a_1}{\partial Z_{c3}} = \frac{Z_{c3}-Z_{c2}}{a_1}$$

$$\frac{\partial a_2}{\partial X_{c6}} = 1.0 \; ; \quad \frac{\partial a_2}{\partial X_{c1}} = -1.0 \; ; \quad \frac{\partial d_1}{\partial Y_{c6}} = 1.0 \; ; \quad \frac{\partial d_1}{\partial Y_{c1}} = -1.0$$

$$\frac{\partial d_2}{\partial X_{c3}} = \frac{X_{c3}-X_{c5}}{d_2} \quad ; \quad \frac{\partial d_2}{\partial X_{c5}} = \frac{X_{c5}-X_{c3}}{d_2}$$

$$\frac{\partial d_2}{\partial Z_{c3}} = \frac{Z_{c3}-Z_{c5}}{d_2} \quad ; \quad \frac{\partial d_2}{\partial X_{c5}} = \frac{Z_{c5}-Z_{c3}}{d_2}$$

$$\frac{\partial d_3}{\partial Z_p} = \frac{Z_p-Z_{c6}}{d_3} \quad ; \quad \frac{\partial d_3}{\partial Z_{c6}} = \frac{Z_{c6}-Z_p}{d_3}$$

$$\frac{\partial d_3}{\partial X_p} = \frac{X_p-X_{c6}}{d_3} \quad ; \quad \frac{\partial d_3}{\partial X_{c6}} = \frac{X_{c6}-X_p}{d_3}$$

$$\frac{\partial d_3}{\partial L_p} = \frac{-1}{2\ d_3}$$

the errors ΔX_{cj}, ΔY_{cj}, and ΔZ_{cj} are derived in §B.5 and can be used here to compute the estimation errors.

B.7 Joint angle Estimation

From equation 4.4.1, the jont angle θ_{mj} for the transmission error analysis is given by,

$$ {}^{t_{fj}}\theta_{mj} = \tan^{-1}\left[\frac{{}^{t_{fj}}(Z_{a1}-Z_{a2})}{\sqrt{{}^{t_{fj}}(X_{a1}-X_{a2})^2 + {}^{t_{fj}}(Y_{a1}-Y_{a2})^2}}\right] \qquad \text{(B.7.1)} $$

hence ${}^{t_{fj}}\theta_{mj}$ is a function of distances and this relation can be written as,

$$ {}^{t_{fj}}\theta_{mj} = f\,(X_{a1},\ X_{a2},\ Y_{a1},\ Y_{a2},\ Z_{a1},\ Z_{a2}) \qquad \text{(B.7.2)} $$

from the error analysis for the transmission errors presented in Chapter 5, $\Delta\,{}^{t_{fj}}\theta_{mj}$ is given by,

$$ \Delta\,{}^{t_{fj}}\theta_{mj} = \frac{\partial f}{\partial X_{a1}}\Delta X_{a1} + \frac{\partial f}{\partial X_{a2}}\Delta X_{a2} + \frac{\partial f}{\partial Y_{a1}}\Delta Y_{a1} + \frac{\partial f}{\partial Y_{a2}}\Delta Y_{a2} + \frac{\partial f}{\partial Z_{a1}}\Delta Z_{a1} + \frac{\partial f}{\partial Z_{a2}}\Delta Z_{a2} \qquad \text{(B.7.3)} $$

the terms $\frac{\partial f}{\partial X_{a1}}$, $\frac{\partial f}{\partial Z_{a2}}$ etc., are obtained by partially differentiating B.7.1 with respect to X_{a1}, Z_{a2} and so on. The derivatives are given below :

$$ \frac{\partial f}{\partial X_{a1}} = \frac{{}^{t_{fj}}(X_{a1}-X_{a2})}{\left[{}^{t_{fj}}(X_{a1}-X_{a2})^2 + {}^{t_{fj}}(Y_{a1}-Y_{a2})^2\right]^{3/2}} \frac{1}{\text{Sec}^2\,{}^{t_{fj}}\theta_{mj}} $$

$$\frac{\partial f}{\partial X_{a2}} = \frac{{}^{t_{fj}}(X_{a1}-X_{a2})}{\left[{}^{t_{fj}}(X_{a1}-X_{a2})^2 + {}^{t_{fj}}(Y_{a1}-Y_{a2})^2 \right]^{3/2}} \frac{1}{\mathrm{Sec}^2\, {}^{t_{fj}}\theta_{mj}}$$

$$\frac{\partial f}{\partial Y_{a1}} = \frac{{}^{t_{fj}}(Y_{a1}-Y_{a2})}{\left[{}^{t_{fj}}(X_{a1}-X_{a2})^2 + {}^{t_{fj}}(Y_{a1}-Y_{a2})^2 \right]^{3/2}} \frac{1}{\mathrm{Sec}^2\, {}^{t_{fj}}\theta_{mj}}$$

$$\frac{\partial f}{\partial Y_{a2}} = \frac{-{}^{t_{fj}}(Y_{a1}-Y_{a2})}{\left[{}^{t_{fj}}(X_{a1}-X_{a2})^2 + {}^{t_{fj}}(Y_{a1}-Y_{a2})^2 \right]^{3/2}} \frac{1}{\mathrm{Sec}^2\, {}^{t_{fj}}\theta_{mj}}$$

$$\frac{\partial f}{\partial Z_{a1}} = \frac{1}{\left[{}^{t_{fj}}(X_{a1}-X_{a2})^2 + {}^{t_{fj}}(Y_{a1}-Y_{a2})^2 \right]^{3/2}} \frac{1}{\mathrm{Sec}^2\, {}^{t_{fj}}\theta_{mj}}$$

$$\frac{\partial f}{\partial Z_{a2}} = \frac{1}{\left[{}^{t_{fj}}(X_{a1}-X_{a2})^2 + {}^{t_{fj}}(Y_{a1}-Y_{a2})^2 \right]^{3/2}} \frac{1}{\mathrm{Sec}^2\, {}^{t_{fj}}\theta_{mj}}$$

the expressions for ΔX_{a1}, ΔZ_{a2} etc., are derived in §B.3. Substituting these expressions in B.7.3, the estimation error $\Delta\, {}^{t_{fj}}\theta_{mj}$ can be computed.